SRNL-STI-2012-00018
Revision 1

Glycolic-Nitric Acid Flowsheet Demonstration of the DWPF Chemical Process Cell with Sludge and Supernate Simulants

D.P. Lambert
M.E. Stone
J.D. Newell
D.R. Best
J.R. Zamecnik

August 2012

Savannah River National Laboratory
Savannah River Nuclear Solutions, LLC
Aiken, SC 29808

Prepared for the U.S. Department of Energy under contract number DE-AC09-08SR22470.

SRNL
SAVANNAH RIVER NATIONAL LABORATORY

DISCLAIMER

Printed in the United States of America

Prepared for
U.S. Department of Energy

SRNL-STI-2012-00018
Revision 1

Keywords: *Alternative Reductant, DWPF, CPC, glycolic acid, hydrogen*

Retention: *Permanent*

Glycolic-Nitric Acid Flowsheet Demonstration of the DWPF Chemical Process Cell with Sludge and Supernate Simulants

D.P. Lambert
M.E. Stone
J.D. Newell
D.R. Best
J.R. Zamecnik

August 2012

Savannah River National Laboratory
Savannah River Nuclear Solutions, LLC
Aiken, SC 29808

Prepared for the U.S. Department of Energy under contract number DE-AC09-08SR22470.

REVIEWS AND APPROVALS

AUTHORS:

D.P. Lambert, Process Technology Programs Date

M.E. Stone, Process Technology Programs Date

J.D. Newell, Process Technology Programs Date

D.R. Best, Engineering Process Development Date

J.R. Zamecnik, Process Technology Programs Date

TECHNICAL REVIEW:

D.C. Koopman, Process Technology Programs Date

APPROVAL:

C.C. Herman, Manager Date
Process Technology Programs

S.L. Marra, Manager Date
Environmental & Chemical Process Technology Research Programs

J.E. Occhipinti, Manager Date
Waste Solidification Engineering

EXECUTIVE SUMMARY

Testing was completed to demonstrate the viability of the newly developed glycolic/nitric flowsheet for processing in the Defense Waste Processing Facility's (DWPF) Chemical Process Cell (CPC). The Savannah River National Laboratory (SRNL) initiated a sludge matrix study to evaluate the impact on CPC processing. Four sludge simulants were designed to cover a broad insoluble solid composition range to bracket future sludge batches. The first pair of sludge parameters was high iron/low aluminum versus low iron/high aluminum (referred to as HiFe or LoFe in this report). The second pair of sludge parameters was high calcium-manganese/low nickel, chromium, and magnesium versus low calcium-manganese/high nickel, chromium, and magnesium (referred to as HiMn or LoMn in this report). In addition, a simple supernate simulant was prepared to match the composition of the matrix simulants.

Ten experiments (GF34 to GF37 and GF34b, GF34c, GF36b, GF36c, GF37b and GF38) were completed to demonstrate the glycolic-nitric flowsheet viability using the sludge matrix simulants at a nominal 1M Na washing endpoint. In addition, two experiments were performed with less washed simulants (GF40, 1.6 M Na and GF41, 1.9 M Na endpoints) to demonstrate the viability of processing these sludges. Five supernate experiments (GF39a-GF39e) were performed to better understand the reaction sequence, particularly the reduction and stripping of mercury.

Composition and physical property measurements were made on the Sludge Receipt and Adjustment Tank (SRAT) and Slurry Mix Evaporator (SME) products. Composition measurements were made on the composited condensates from the Mercury Water Wash Tank (MWWT), and Formic Acid Vent Condenser (FAVC), on the ammonia scrubber solution, and on SRAT samples pulled throughout the SRAT cycle. Updated values for glycolate and formate loss, nitrite-to-nitrate conversion, and oxalate formation were found that can be used in the acid calculations for future process simulations with the glycolic-nitric flowsheet.

Preliminary results of the initial testing indicate:

- Hydrogen generation rate was below detection limits (<1.4E-3 lb/hr) DWPF-scale or <0.005 vol%) throughout all SRAT cycles with matrix simulants. Hydrogen generation rate was above detection limits for the less washed simulants (3.2E-3 lb/hr DWPF-scale or 0.009 vol%) due to the higher acid stoichiometry and the lower offgas purge.
- Hydrogen generation rate was below 0.0258 lb/hr DWPF-scale (11.6% of DWPF SME limit) throughout all SME cycles with matrix simulants. The small amount of generated hydrogen with the nominal washing endpoint is attributed to formic acid added with the frit. When formic acid was not added with the frit in the underwashed sludge runs (GF40 and GF41), the maximum hydrogen seen was 1.8E-3 lb/hr DWPF scale (0.81% of DWPF SME limit).
- Mercury was both reduced and stripped without formic acid. The mercury concentration of the SRAT product was below the 0.8 wt % target in eight of the runs and below 0.92 wt %in the other four runs.
- Nitrite in the SRAT product was <100 mg/kg slurry for all runs.
- Foaminess was not an issue using the nominal antifoam addition strategy or with reduced antifoam in these tests.

- High wt % total solids were achieved while staying within rheological limits which makes the glycolic acid/nitric acid flowsheet an improvement for processing more viscous sludges. However, there may be a tradeoff between excessive dissolution of metals and thinner rheology.
- The pH remained steady throughout processing (i.e. no pH rebound) potentially leading to more consistent processing during the CPC. The SRAT and SME products pH varied from 3.5-5.0 for the 100% and 130% acid stoichiometry runs, significantly lower than is typical of the Baseline (nitric acid/formic acid) flowsheet.
- The testing apparatus has been significantly modified to improve processing with high viscosity slurries. Testing of the old style and new style rig identified no differences in CPC processing, including steam stripping of Hg.
- The SRAT lower air purge was demonstrated in Run GF34c and adapted in GF40 and GF41. Based on these results, the SRAT purge can be reduced from 190 scfm to 93.7 scfm without negatively impacting processing.
- Runs GF40 and 41 demonstrated that processing of less washed sludges is viable with this flowsheet. However, this flowsheet has not been demonstrated with ARP, MCU or actual waste.
- Several processing improvements were demonstrated in these runs including adding acid during heat-up, adding both acids at higher volumetric flowrates than are currently used in DWPF, and concentrating the SRAT during acid addition. Each of these improvements has the potential to shorten CPC processing time.

Recommendations Applying to Glycolic-Nitric Acid Flowsheet

The glycolic-nitric flowsheet is recommended as a viable flowsheet alternative to the Baseline DWPF flowsheet. In the testing that has been performed to date, this flowsheet meets or outperforms the current flowsheet in minimizing off-gas generation, removing mercury, and producing a rheologically thinner product. Previous testing with glycolic/formic acid mixtures demonstrated a wide processing window regarding both the glycolic-formic ratio and acid stoichiometry. The addition of glycolic acid leads to SRAT and SME products that are rheologically less viscous which means that more concentrated products can be produced, leading to potentially higher waste throughput per batch. In addition, the combination of lower pH processing and the complexing power of glycolic acid leads to the dissolution of more metals, which may minimize deposits in the CPC processing vessels and prevent the fouling of steam coils. Follow up testing is recommended in the following areas:

- Improve glycolate and oxalate analyses. The majority of the glycolate results reported were correct. However, there are issues with anion and cation deposition on the column of the Ion Chromatograph (IC), causing higher than expected glycolate and oxalate in blanks and some samples. Both Process Science and Analytical Laboratory (PSAL) and Analytical Development (AD) have reported results that have varied significantly from expectations. Modification to the sample preparation method is likely needed to improve analytical accuracy and minimize the cleaning and replacement of the IC column. An alternative to the IC measurement of glycolate should also be considered.
- Determine the appropriate REDOX model for the glycolic-nitric flowsheet. The REDOX model may need more terms due to the more extensive reduction of some metals, including Mn and Fe. In addition, accurate measurement of glycolate (and possibly oxalate) and nitrate is needed to accurately predict REDOX. REDOX testing

of the matrix sludges should be repeated using acceptable frits that meet Product Composition Control System (PCCS).

- Test the glycolic-nitric flowsheet at acid stoichiometries of less than 100%. Demonstration of this flowsheet at an acid stoichiometry of <100% is recommended and might be useful for mercury stripping.
- Demonstrate the glycolic-nitric flowsheet (previously demonstrated in SRAT cycle with 80:20 glycolic:formic acid blend) with actual waste in SRNL Shielded Cells SRAT and SME processing, to include periodic slurry sampling throughout the SRAT and SME processing along with a glass REDOX measurement.
- Add the nitric and glycolic acid flowrate at the same scaled molar flowrate as formic acid to minimize glycolic-nitric flowsheet batch time. This has been demonstrated in these tests.
- The nitric acid can be added during heat-up to decrease the SRAT cycle time. The nitric acid primarily neutralizes soluble base species in the slurry with little offgas generation.
- Improve understanding of process chemistry, the decomposition of glycolate and the production of oxalate which are important to REDOX.
- Improve understanding of mercury reduction, stripping and accumulation during processing. Determine whether alternative equipment or processing changes are needed to maximize the collection of mercury in the Mercury Water Wash Tank.
- If confirmed by actual waste testing and larger scale testing with simulants, the antifoam addition can be reduced for this flowsheet. The addition of 100 mg/kg prior to glycolic acid addition, 100 mg/kg prior to boiling and 100 mg/kg each 12 hours of processing was adequate during simulant testing.
- More rigorous data collection is needed to validate the OLI aqueous model's solubility predictions with sample results. The methodology is summarized in the discussion.

Recommendations Applying to both Baseline and Glycolic-Nitric Acid Flowsheet

- Testing should be completed with alternate forms of ruthenium to determine whether the elimination of the chloride added as ruthenium chloride would improve the reduction and stripping of the mercury. Testing should be completed with the Baseline and glycolic-nitric flowsheets.

TABLE OF CONTENTS

LIST OF TABLES

LIST OF FIGURES

LIST OF ABBREVIATIONS

AD	Analytical Development
CPC	Chemical Process Cell
DWPF	Defense Waste Processing Facility
GC	Gas Chromatograph
FAVC	Formic Acid Vent Condenser
FTIR	Fourier Transform InfraRed
HMDSO	Hexamethyldisiloxane
HM	H-Canyon Modified (PUREX)
IC	Ion Chromatography
ICP-AES	Inductively Coupled Plasma-Atomic Emission Spectroscopy
MS	Mass Spectrometer
MWWT	Mercury Water Wash Tank
NM	Not Measured
PSAL	Process Science Analytical Laboratory
PUREX	Plutonium - URanium Extraction
REDOX	Reduction/Oxidation
SME	Slurry Mix Evaporator
SMECT	Slurry Mix Evaporator Condensate Tank
SRAT	Sludge Receipt and Adjustment Tank
SRNL	Savannah River National Laboratory
SRR	Savannah River Remediation
SRS	Savannah River Site
TOC	Total Organic Carbon Analysis
TT&QAP	Task Technical and Quality Assurance Plan
XRD	X-ray Diffraction
XRF	X-ray Fluorescence

1.0 **Introduction**

Savannah River Remediation (SRR) is evaluating changes to its current DWPF flowsheet to improve processing cycle times. This will enable the facility to support higher canister production while maximizing waste loading. Higher throughput is needed in the CPC since the installation of the bubblers into the melter has increased melt rate. Due to the significant maintenance required for the DWPF gas chromatographs (GC) and the potential for production of flammable quantities of hydrogen, reducing or eliminating the amount of formic acid used in the CPC is being developed. Earlier work at Savannah River National Laboratory has shown that replacing formic acid with an 80:20 molar blend of glycolic and formic acids has the potential to remove mercury in the SRAT without any significant catalytic hydrogen generation.[1,2,3] This report summarizes the research completed to determine the feasibility of processing without formic acid.

In earlier development of the glycolic-formic acid flowsheet, one run (GF8) [2] was completed without formic acid. It is of particular interest that mercury was successfully removed in GF8, no formic acid at 125% stoichiometry. Glycolic acid did not show the ability to reduce mercury to elemental mercury in initial screening studies, which is why previous testing focused on using the formic/glycolic blend.

The objective of the testing detailed in this document is to determine the viability of the nitric-glycolic acid flowsheet in processing sludge over a wide compositional range as requested by DWPF.[4] This work was performed under the guidance of Task Technical and Quality Assurance Plan (TT&QAP).[5] The details regarding the simulant preparation and analysis have been documented previously.[6]

2.0 **Experimental Procedure**

The experimental apparatus used in these experiments is typical for DWPF SRAT/SME testing. The four experiments were performed in 4-L kettles. The test equipment included a GC to measure off-gas composition, an ammonia scrubber, and a pH meter. In all runs, the SRNL acid calculation spreadsheet[7] used the Koopman equation[8] to determine acid addition quantities and dewater targets.

2.1 CPC Simulation Details

The SRAT 4-L rigs were assembled following the guidelines of SRNL-3100-2011-00127.[9] The intent of the equipment is to functionally replicate the DWPF processing vessels. Each glass kettle is used to replicate both the SRAT and SME, and it is connected to the SRAT Condenser, the MWWT, and the FAVC. The Slurry Mix Evaporator Condensate Tank (SMECT) is represented by a sampling bottle that is used to remove condensate through the MWWT. For the purposes of this paper, the condensers and wash tank are referred to as the off-gas components. A sketch of the experimental setup is given in Figure 2-1.

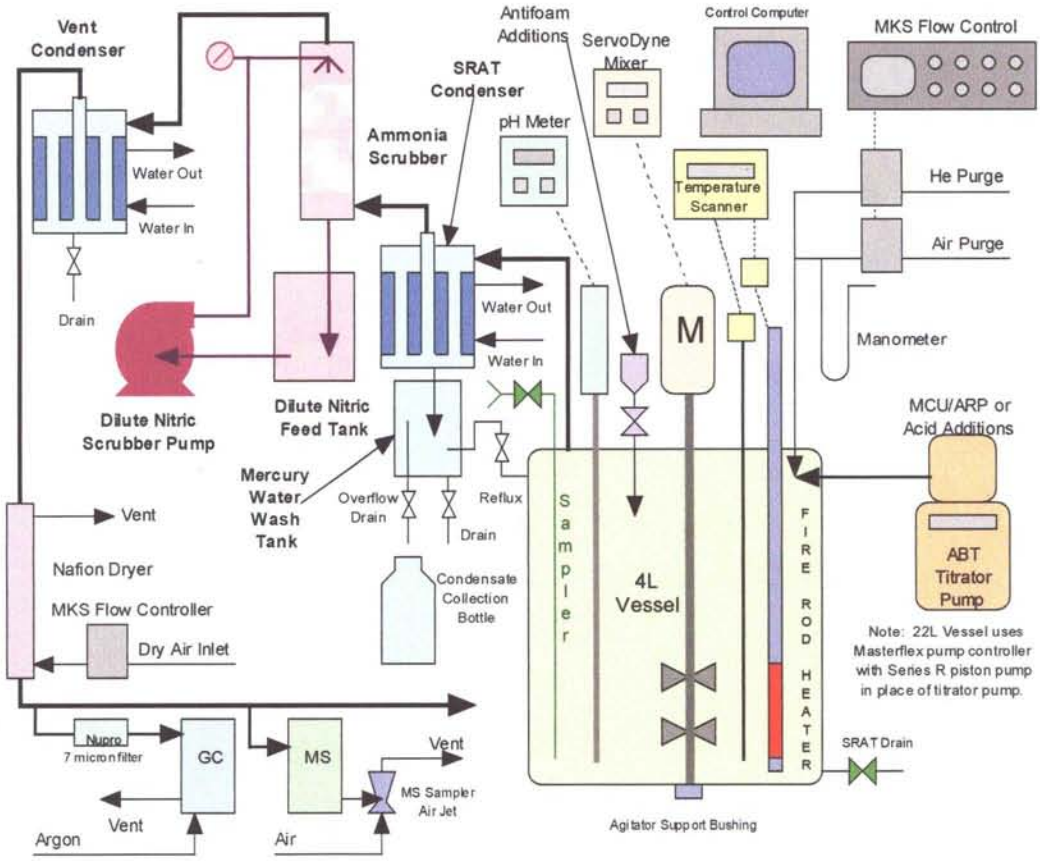

Figure 2-1. Schematic of CPC Equipment Set-Up

There were several notable changes to the CPC equipment set-up:

1. Used two heating rods to better simulate the steam coils instead of a heating mantle
2. Used Series R piston pump instead of titrator pump
3. The control system was modified to control the heating rod so that it could not reach a temperature of >160°C, the approximate maximum temperature of the DWPF steam coils

The runs were performed using the guidance of Procedure ITS-0094[10] ("Laboratory Scale Chemical Process Cell Simulations") of Manual L29. Off-gas hydrogen, oxygen, nitrogen, nitrous oxide, and carbon dioxide concentrations were measured during the experiments using in-line instrumentation. Helium was introduced at a concentration of 0.5% of the total air purge as an inert tracer gas so that total amounts of generated gas and peak generation rates could be calculated. This approach eliminates the impact of fugitive gas losses through small leaks on the calculated outlet gas flowrates. During the runs, the kettle was visually monitored to observe process behavior including foaming, air entrainment, rheology changes, loss of heat transfer capabilities, and off-gas carryover. Observations were recorded on data sheets and pasted into laboratory notebooks.[11]

Quality control measures were in place to qualify the data in this report. Helium and air purges were controlled using mass flow controllers calibrated by the SRNL Standards Lab using traceable standards and methods. Thermocouples were calibrated using a calibrated dry block calibrator. The

GCs were calibrated with standard calibration gases before and after the runs and the data reprocessed based on these data. The pH probes were calibrated with pH 4 and pH 10 buffer solutions and rechecked at the conclusion of each run using pH 4, 7 and 10 buffer solutions.

The automated data acquisition system developed for the 4-L SRAT rigs was used to collect data electronically. Data included SRAT temperature, bath temperatures for the cooling water to the SRAT condenser and FAVC, slurry pH, heating rod temperature and watts, SRAT mixer speed and torque, and air and helium purge flows. Cumulative acid addition flowrate and volume data are calculated from the acid pump rotation speed. Raw GC data were acquired on a computer dedicated to the GCs.

Dual column Agilent 3000A micro GC's were used on both runs. The GC's were baked out before and between runs. Column-A can collect data related to He, H_2, O_2, N_2, NO, and CO, while column-B can collect data related to CO_2, N_2O, and water. Calibrations were performed using a standard calibration gas containing 0.499 vol% He, 1.000 vol% H_2, 20.00 vol% O_2, 51.0 vol% N_2, 25.0 vol% CO_2 and 2.50 vol% N_2O. Instrument calibration was verified prior to starting the SRAT cycle. Room air was used to give a two point calibration for N_2. Calibration status was rechecked following the SRAT cycle.

Concentrated nitric acid (~50 wt %) and glycolic acid (~70 wt %) were used to acidify the sludge and perform neutralization and reduction reactions during processing. The total amount of acid (in moles) to add for each run was determined using the Koopman acid equation[8]. The Koopman minimum acid equation was used with a 100% stoichiometric factor for all tests except GF38 (125%), GF40 (134%) and GF41 (130%).

The acid mix was partitioned between nitric and glycolic acid by utilizing the latest REDOX equation[12] with a term added for glycolate ion (see below). A coefficient of 6 was used on the glycolate term based on electron equivalence.[13] The REDOX target ($Fe^{2+}/\Sigma Fe$) was 0.1. Process assumptions were made to predict SME product anion concentrations. In addition to the standard assumptions needed for formate and oxalate loss and nitrite to nitrate conversion, a factor was added to the acid calculation for glycolate loss. Process assumptions for the stoichiometric window testing were adjusted based on results from earlier testing.

$$REDOX=0.2358+0.1999*((2*C_{formate}+4*C_{oxalate}+4*C_{Carbon}+6*C_{glycolate}-5*(C_{Nitrate}+C_{Nitrite})-5*C_{Mn}))*(45/TS)$$

Where C_x = species concentration of component x, g-mole/kg melter feed, TS = total solids in melter feed in wt %, and REDOX is a molar ratio of $Fe^{2+}/\Sigma Fe$

A standard 4-L SRAT/SME apparatus with an ammonia scrubber was used for these simulations. The scrubber solution consisted of 749 g of de-ionized water and 1 g of 50 wt% nitric acid. The solution was recirculated through the column by a MasterFlex pump at 300 mL/min through a spray nozzle at the top of the packed section. Glass rings were used as packing and did not significantly add to the back pressure on the SRAT vessel as has been seen in earlier tests with different packing. The SRAT condenser was maintained at 25 °C during the run, while the vent condenser was maintained at 4 °C.

In the initial experiments with sludge simulants, 200 ppm antifoam was added prior to acid addition, 100 ppm was added after nitric acid addition, 500 ppm was added before boiling and 100 ppm was added before the SME cycle and every 12 hours during boiling. In later experiments the 200 and 500 ppm antifoam additions were reduced to 100 ppm.

In supernate experiments, no antifoam was added. SRAT processing was abbreviated to include a two hour dewater time and about three hours at reflux.

2.2 Sludge Preparation

SRNL produced four matrix sludge simulants in order to improve the understanding of how changing sludge composition impacts DWPF waste processing. These simulants have been used in other SRNL studies, and the composition has been previously measured.[14] These simulants were used to demonstrate the flowsheet across a broad compositional range. In addition, two less washed simulants (1.6 and 1.9 M Na) were produced to study the impact of less washing on CPC processing.

There are many elements in the insoluble solids. The two major insoluble elements in Savannah River Site (SRS) high activity waste slurries are iron and aluminum, corresponding to Plutonium - URanium EXtraction (PUREX) and H-Canyon Modified (HM) wastes respectively. The first solids concentration parameter was chosen to reflect variations between these two elements. There are a number of elements that occur at about an order of magnitude lower concentration than Al and Fe in SRS waste slurries including Ca, Hg, Mg, Mn, Ni, and Si (also U, but that is outside the scope of this study). These can be defined as the semi-major elements. Creating high-low pairs from all of these elements in addition to Al and Fe would have led to a prohibitively large study. The size of the study was controlled by grouping some of the semi-major elements into two sets. Manganese was paired with Ca, and Mg was paired with Ni. This defined the second concentration parameter in the study. Silicon, as SiO_2, was seen as essentially inert and not included in the pairings with the other semi-major elements.

Mercury has been studied in other contexts. Therefore, mercury was held at 1.5 wt% in the starting sludge total solids in all tests in the sludge matrix study. The noble metals were added at the same concentrations as were used in previous high noble metal tests of the matrix sludges.[15] Cr is typically at least an order of magnitude lower in concentration than the semi-major elements. It was considered potentially significant, however, due to its several oxidation states and was added to the Mg-Ni pair. Another constraint on handling the semi-major elements was that the oxides must sum to 100%. Suppressing or enhancing the concentrations of all of the semi-major elements simultaneously would have led to unreasonably high or low concentrations of either Al or Fe. Conceptually, the second concentration parameter represents reasonable compositional variations within each of the two main waste types, PUREX or HM (Figure 2-2).

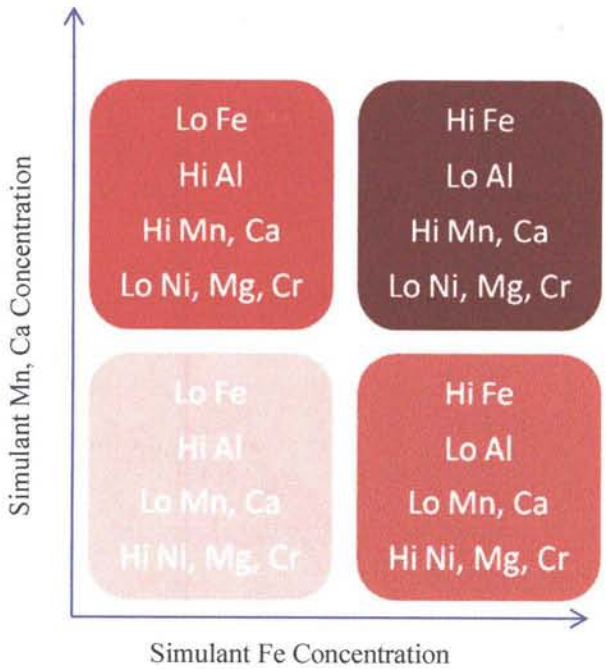

Figure 2-2. Definition of Sludge Matrix Simulants

The three primary parameter groups drawn from the insoluble solids are summarized below:

1. High iron or high aluminum (representing PUREX and HM wastes respectively). This parameter is referred to as either Hi Fe or Lo Fe in the discussion below.
2. High Mn and Ca or high Mg, Ni, and Cr (representing the semi-major insoluble species). This parameter is referred to as either Hi Mn or Lo Mn below.
3. The other (minor) sludge species, such as Ba, Zn, Zr, Cu, La, etc., were to be held in constant relative proportions in the simulants.

The measured slurry composition is summarized in Table 2-1. The supernate compositions of the matrix sludge simulants were maintained nearly constant.

The sludge simulations had identical mercury and noble metal targets, given in Table 2-2 as wt% in the total solids of the trimmed slurry. The noble metals concentrations are comparable to the high noble metal case in the Rh-Ru-Hg matrix study, while mercury was held constant during this study at the midpoint value of the Rh-Ru-Hg matrix study.[15]

Table 2-1. Composition of Sludge Simulants

Result	GF34 HiFeHiMn	GF35 SB7An	GF36 HiFeLoMn	GF37/38 LoFeLoMn	GF40 1.6 M Na	GF41 1.9 M Na	Units
Total Solids	23.70	18.02	22.81	23.07	24.14	25.43	wt%
Calcined Solids	17.81	13.61	16.95	16.00	17.01	17.85	wt%
Insoluble Solids	16.70	12.57	16.35	16.05	16.51	16.97	wt%
Soluble Solids	7.00	5.45	6.47	7.01	7.63	8.46	wt%
Slurry Density	1.185	1.142	1.189	1.176	1.174	1.215	kg / L slurry
Filtrate Density	1.057	1.053	1.055	1.057	1.076	1.091	kg / L supernate
Aluminum	9.000	15.65	9.130	23.8	14.8	13.9	wt % calcined basis
Boron	<0.100	<0.100	<0.100	<0.100	NM	NM	wt % calcined basis
Barium	0.077	0.102	0.101	0.0705	0.085	0.0802	wt % calcined basis
Calcium	3.83	0.836	2.22	1.97	0.565	0.288	wt % calcined basis
Cadmium	<0.010	NM	<0.010	<0.010	NM	NM	wt % calcined basis
Cerium	0.104	0.148	0.108	0.0965	NM	NM	wt % calcined basis
Chromium	0.015	0.0455	0.285	0.244	0.027	0.0260	wt % calcined basis
Copper	0.045	0.033	0.045	0.048	0.040	0.0350	wt % calcined basis
Iron	32.4	19.2	31.5	12.2	14.8	13.7	wt % calcined basis
Potassium	0.120	0.125	0.0905	0.0955	0.369	0.392	wt % calcined basis
Magnesium	0.396	0.366	2.69	2.42	0.317	0.302	wt % calcined basis
Manganese	4.04	4.37	0.721	0.661	4.86	4.53	wt % calcined basis
Sodium	12.9	15.3	13.1	14.2	22.8	24.4	wt % calcined basis
Nickel	0.213	3.37	2.6345	2.31	2.10	1.95	wt % calcined basis
Phosphorus	<0.100	<0.100	<0.100	<0.100	0.032	<0.010	wt % calcined basis
Lead	0.071	0.025	0.047	0.0715	<0.010	<0.010	wt % calcined basis
Sulfur	0.289	0.371	0.340	0.374	0.276	0.333	wt % calcined basis
Silicon	1.580	1.91	1.52	1.32	1.52	1.369	wt % calcined basis
Tin	<0.010	0.013	0.106	0.0925	NM	NM	wt % calcined basis
Titanium	<0.010	0.025	<0.010	<0.010	0.025	0.0230	wt % calcined basis
Zinc	0.065	0.047	0.0775	0.0705	0.049	0.0452	wt % calcined basis
Zirconium	0.054	0.252	0.1175	0.049	0.027	0.195	wt % calcined basis
Nitrite	17,900	9,140	17,800	13,300	13,500	15,800	mg/kg slurry
Nitrate	13,550	6,470	13,400	13,300	7,895	9,940	mg/kg slurry
Formate	<100	<100	<100	<100	<100	<100	mg/kg slurry
Sulfate	1,770	1,460	1,575	1,590	1,980	2,610	mg/kg slurry
Chlorine	116	<100	131	127	<100	<100	mg/kg slurry
Phosphate	0	<100	<100	<100	<100	<100	mg/kg slurry
Oxalate	300	8,500	275	295	18,750	20,000	mg/kg slurry
Glycolate	<100	NM	<100	<100	<100	<100	mg/kg slurry
Slurry TIC	2,751	1,066	2,492	2,400	1,840	1,730	mg/kg slurry
Supernate TIC	1,080	664	1,310	1,280	1,790	1760	mg/L supernate
Total Base pH 7	0.590	0.580	0.562	0.522	0.838	0.879	moles/L

Table 2-2. Mercury and Noble Metal Composition Added to Sludge Simulants, wt% Total Solids Basis

Noble Metal	Runs GF34-GF38	GF40-41
Target Hg	1.5000	1.500
Target Ag	0.0014	0.0144
Target Pd	0.0790	0.0033
Target Rh	0.0380	0.0192
Target Ru	0.2170	0.0877

An additional supernate simulant was prepared to supplement the four slurry simulants above. The purpose of this simpler simulant was to improve understanding of the mercury reduction chemistry. The simulant was similar to the supernate used in the matrix slurry preparation. The only soluble species added were sodium hydroxide, sodium nitrite, sodium nitrate, sodium sulfate, sodium oxalate, sodium carbonate and potassium nitrate. The resulting concentration is summarized in Table 2-3. The added noble metal and mercury target of these runs is summarized in Table 2-4. Note that because of the lower total solids of the supernate, the added mass of noble metals and mercury is approximately one-third that added in the slurry experiments.

Table 2-3. Composition of Supernate Simulant

Anion or Cation	GF39a-d	GF39e
Nitrite, mg/kg	21,561	0
Nitrate, mg/kg	15,784	16,311
Carbonate, mg/kg	6,051	6,253
Oxalate, mg/kg	351	363
Sulfate, mg/kg	1,888	1,951
Free Hydroxide, M	3,556 (0.221 M)	0.221
Na, mg/kg	27,067	27,067
K, mg/kg	153	153

Table 2-4. Mercury and Noble Metal Composition Added to Supernate Simulants, wt% Total Solids Basis

Noble Metal	GF39a	GF39b	GF39c	GF39d	GF39e
Target Hg	1.5000	1.5000	1.5000	1.5000	2.5717
Target Ag	0.0000	0.0014	0.0014	0.0014	0.0000
Target Pd	0.0000	0.0790	0.0790	0.0790	0.0000
Target Rh	0.0000	0.0297	0.0297	0.0297	0.0000
Target Ru	0.0000	0.2170	0.0000	0.2170	0.0000

2.3 CPC Run Details

The twelve nitric-glycolic acid flowsheet tests with slurry and five tests with supernate were performed at the ACTL using the four-liter kettle setup. Table 2-5 identifies each run and its corresponding assumptions.

Table 2-5. CPC Simulation Process Assumptions

Run	Sludge	Cycles	Date	% Koopman Acid Stoichiometry	% Hsu Acid Stoichiometry	Labware
GF34	HiFeHiMn	SRAT/SME	16-Nov-11	104.0	108.0	New
GF34b	HiFeHiMn	SRAT/SME	16-Nov-11	104.0	108.0	New
GF34c	HiFeHiMn	SRAT/SME	16-Nov-11	104.0	108.0	New
GF35	SB7A	SRAT/SME	17-Nov-11	100.0	102.2	New
GF36	HiFeLoMn	SRAT/SME	16-Nov-11	106.1	125.1	New
GF36b	HiFeLoMn	SRAT	25-Jan-12	106.1	125.1	New
GF36c	HiFeLoMn	SRAT	25-Jan-12	106.1	125.1	Old
GF37	LoFeLoMn	SRAT/SME	2-Feb-12	100.0	112.3	New
GF37b	LoFeLoMn	SRAT	17-Nov-11	100.0	112.3	New
GF38	LoFeLoMn	SRAT	2-Feb-12	125.0	140.4	New
GF39A	Supernate	SRAT	22-Feb-12	100.0	73.9	New
GF39B	Supernate	SRAT	22-Feb-12	100.0	73.9	New
GF39C	Supernate	SRAT	29-Feb-12	100.0	73.9	New
GF39D	Supernate	SRAT	29-Feb-12	80.0	59.1	New
GF39E	No Nitrite Supernate	SRAT	8-May-12	100.0	73.4	New
GF40	1.6M Na	SRAT	24-May-12	133.9	133.1	New
GF41	1.9 M Na	SRAT	24-May-12	130.0	131.1	New

DWPF design basis processing conditions were scaled down and used for most processing parameters including SRAT/SME air purges and boil-up rate. SRAT product total dried solids were targeted at 27 wt% for the slurry simulant runs. Final SME total dried solids were targeted at 45% at 36% waste loading.

Because nitric and glycolic acid are more dilute acids than formic acid, both acids were added at the same molar flowrate as formic acid. Thus nitric acid was added at a DWPF scaled flowrate of 4.572 gallons per minute and glycolic acid was added at a DWPF scaled flowrate of 3.948 gallons per minute to maintain acid addition times. It is recommended that DWPF modify the acid feed pumps to deliver the higher flow rates before implementing the glycolic flowsheet.

The following constraints must be met by the current DWPF CPC flowsheet:

- SRAT hydrogen <0.65 lb/hr
- SME hydrogen <0.223 lb/hr
- Reduce mercury to elemental form
- Steam strip mercury below 0.8 wt% in the SRAT product dried solids
- SRAT product less than 1000 mg nitrite/kg product slurry
- SRAT product rheology* design basis 1.5 to 5 Pa yield stress and 5 to 12 cP consistency
- SME product rheology* 2.5 to 15 Pa yield stress and 10 to 40 cP consistency
- Glass REDOX of 0.09-0.33 $Fe^{2+}/\Sigma Fe$
- Minimize water in SME product (55 wt% typical)
- Minimal foaming

* Processing limits are the same for both SRAT and SME as agitator and drive are identical

Twelve to fifteen samples were taken during each SRAT cycle to monitor the progress of the main chemical reactions. Major cations and anions were checked immediately after acid addition. Samples were taken during boiling to monitor suspended and dissolved mercury in the SRAT slurry. These samples were transferred directly into digestion vials to eliminate potential segregation of mercury during sub-sampling/aliquoting steps. The SRAT and SME product slurries were sampled similarly once they had cooled to 90° C while the vessel contents were still mixing.

Additional SRAT product samples were taken for compositional and solids analyses after the product had cooled further. The MWWT and FAVC were drained and the condensates weighed after both the SRAT and SME cycles. Elemental mercury was separated from the aqueous phase in the post-SRAT MWWT sample, and the mass of the mercury-rich material determined. Beads of elemental mercury were also recovered from a few of the SME dewatering condensates and weighed (depending on how big or numerous the bead(s) appeared to be).

Data are presented in Section 3 showing how the nitric-glycolic flowsheet met or exceeded the processing constraints in the list above with the possible exception of mercury removal and REDOX.

2.4 Analytical Methods

Process samples were analyzed by various methods. Slurry and supernate elemental compositions were measured by inductively coupled plasma-atomic emission spectroscopy (ICP-AES) at PSAL. Soluble anion concentrations were measured by IC. Mercury concentration was measured by ICP-AES. Ammonium ion concentration on selected samples was measured by cation chromatography by SRNL AD. Slurry and supernate densities were measured using an Anton-Parr instrument at PSAL. Dewater and condensate samples were submitted to PSAL for IC. A gradient method using the Dionex AG-11HC and AS-11HC, 2mm microbore columns was used to analyze fluoride, glycolate, formate, chloride, nitrite, nitrate, sulfate, oxalate and phosphate on SRAT/SME samples.[16]

SME product samples were vitrified in nepheline sealed crucibles, and the resulting glasses were measured for REDOX ($Fe^{2+}/\Sigma Fe$).[17] The REDOX target for all the simulations in this study was 0.1. The target is achieved by predicting the SME product anion concentrations and adjusting the split of acids between nitric and glycolic. Therefore the ability to control REDOX at the target value is highly dependent on being able to accurately predict anion behavior in the SRAT and SME cycles. Inserting the actual SME product data into the latest REDOX correlation gave a "predicted" REDOX that was different than the target. It should be noted that frit 418 was used for all runs. No attempt was made to produce a frit that was optimized for each of the four sludges. The glass produced was nonhomogeneous and this likely impacted the redox results.

Agilent® 3000A micro GC's were used for all runs. The GC's were baked out before and between runs. Column-A can collect data related to He, H_2, O_2, N_2, NO, and CO, while column-B can collect data related to CO_2, N_2O, and water. GC's were calibrated with a standard calibration gas containing 0.510 vol% He, 1.000 vol% H_2, 20.10 vol% O_2, 50.77 vol% N_2, 25.1 vol% CO_2 and 2.52 vol% N_2O. The calibration was verified prior to starting the SRAT cycle and after completing the SME cycle. Room air was used to give a two point calibration for N_2. No evidence for CO generation was obtained while examining the region of the chromatogram where it would elute. The chilled off-gas leaving the FAVC was passed through a Nafion® dryer in counter-current flow with a dried air stream to reduce the moisture content at the GC inlet. The dried, chilled off-gas stream was sampled by a GC from the beginning of heat-up to temperature to start the SRAT cycle through most of the cool down following the SME cycle.

Gas chromatograph off-gas data were scaled to DWPF flow rates. The calculation methodology has been previously documented.[18] An internal standard flow is usually established with helium. Other gas flow rates are determined relative to helium by taking the ratio of the two gas volume percentages times the helium standard flow. The result is scaled by the ratio of 6,000 gallons of fresh sludge divided by the volume of fresh sludge in the simulant SRAT charge.

Two new instruments were used in the last four slurry-fed sludge runs. An Extrel® MAX300LG Mass Spectrometer (MS) was used in runs GF34b, GF34c, GF40 and GF41. In addition, an MKS MG2030 Fourier Transform InfraRed (FTIR) Analyzer was used during runs GF40 and GF41.

The Extrel® MS was used to alternate between measuring the gas composition of both experiments. The MS uses a multiport switching valve to select the sample stream. The samples were pulled through the MS using a single diaphragm sample pump on the outlet of the MS sampling port. When not being sampled by the MS, the other sample stream still flowed continuously through a bypass port so the sample would always be fresh. The two sample streams were alternately analyzed for approximately 2.87 minutes with a 30 second delay during switching to purge out the previous sample stream. The MS was calibrated with a series of calibration gases as described in the next paragraph. The MS measured the composition of the sample approximately every 7 seconds (or 24 sample results during the 2.87 minute period).

Process mass spectrometry measures the intensity of ion signals and converts these signals to concentrations using the calibration data. Because some gases have interfering ions (e.g., N_2 is measured at mass/charge (m/z) of 28 (N_2^+); CO_2 is measured at m/z 44, and has an interfering ion fragment at m/z of 28 from CO^+ that must be subtracted from the total signal at m/z 28 to give the correct signal for N_2. This 'fragment' calibration is done using a calibration gas, in this case CO_2 in Ar. The gases NO_2, NO, N_2O, and CO_2 all have fragments that interfere at other m/z values. The signals are calibrated with calibration gases; the calibration factors determined are termed "sensitivity". Background signals at each measurement m/z were measured in pure N_2 and Ar. The calibration gases used are summarized in Table 2-6.

Table 2-6. Mass Spectrometer Calibration Gases

Gas	Purpose
Ar	background signals at m/z 28 & 30
N_2	background signals at m/z 2, 4, 32, 40, 44, 46
20% CO_2 in Ar	CO_2 fragment at m/z 28
5% NO_2 in N_2 + O_2	NO_2 fragment at m/z 30, calibration for NO_2 m/z 46
2% H_2, 1% He, 20% O_2, 10% CO_2, 1% Ar, 66% N_2	calibration of each gas (m/z 2, 4, 32, 44, 40, respectively); N_2 sensitivity = 1.000 by definition)
2% NO in Ar	calibration for NO at m/z 30

The presence of N_2O in the process gas introduces error in the measurements of CO_2, NO, and N_2 because it has fragments with m/z at the measurement masses of each of these gases. The MS cannot be calibrated for N_2O because the relative amount of N_2O to the other gases is too small to give a reliable calibration. The presence of 1.2% N_2O (the highest measured by GC) would result in the measurement of N_2 being high by about 0.12%, NO being high by about 0.24%, and CO_2 being high by about 0.86%.

About twice per hour, the MS was set to scan the mass spectrum from 48 to 250 to detect any larger species. The purpose of this was to search of components that weren't being measured by the GCs. The ion CF_3^+ was consistently found, but this was due to the turbomolecular pump seal oil. The presence of hexamethyldisiloxane (HMDSO) was seen in several of the mass spectra. No other species were detected.

The FTIR was used to measure the gas composition of one of the two SRAT rigs during each concurrent run. The sample location was the same as used for the GC and MS. The FTIR uses factory calibration data for the infrared spectra and does not need to be calibrated; it automatically adjusts for changes in signal strength. The gases measured by the FTIR were CO_2, N_2O, NO, NO_2, and HMDSO. It also had the ability to detect CO, NH_3, nitric acid, formic acid, and water, but no significant amounts were detected. Low ppm amounts of nitric and formic acids were detected during nitric and glycolic acid additions, but these values may have been due to interferences.

In general, the FTIR values matched the GC and MS values reasonably well. Note that the concentrations in the process for NO, NO_2, and CO_2 significantly exceeded the calibration data, so the FTIR values are extrapolations of the calibration curves. The raw spectral data will be analyzed for the presence of species not in the calibration library at a future date. Antifoam breakdown products such as trimethylsilanol and siloxanes larger than six carbons are possible species that could be found from the spectra by further analysis.

3.0 Results and Discussion

Four SRAT simulations with supernate and eight SRAT/SME process simulations with slurry feeds were completed to demonstrate the feasibility of using only glycolic acid as the reducing acid in SRAT processing. The elimination of formic acid has the potential to eliminate the catalytic generation of hydrogen, which could lead to the reduction of the air purge in the DWPF CPC. The main concern in eliminating formic acid[1] is that the mercury won't be effectively reduced, and won't be removed by steam stripping to meet the DWPF SRAT mercury target and minimize the mercury sent to the melter. The discussion begins with the supernate results followed by the slurry results.

3.1 Supernate Testing

Four SRAT process simulations were completed with a simple supernate solution with added mercury and noble metals. A fifth run was completed with a nitrite free supernate solution to determine whether nitrite is needed to reduce mercury. These runs were performed after the slurry runs in order to better understand the processing chemistry. In particular, it was important to understand when the mercury is reduced in processing. Samples were pulled during glycolic acid addition and for several hours during the dewater and reflux phases to better understand the process chemistry using a simpler mixture than sludge simulants.

3.1.1 *Mercury Reduction and Stripping*

Approximately 3.4 g of mercury were added to each simulation. The mercury recovery results are summarized in Table 3-1.

Table 3-1. Supernate Testing with Mercury and Noble Metals

Run	GF39a	GF39b	GF39c	GF39d	GF39e
Hg, wt %	1.5	1.5	1.5	1.5	1.5
Rh, wt %	0	0.0297	0.0297	0.0297	0
Pd, wt %	0	0.079	0.079	0.079	0
Ag, wt%	0	0.0014	0.0014	0.0014	0
Ru, wt %	0	0.3358	0	0.3358	0
% Koopman Acid Stoichiometry	100	100	100	80	100
% Hsu Acid Stoichiometry	74	74	74	60	58
Hg Collected, g	0.62*	None	0.43#	None	0.98

* Found 1.455 g of elemental Hg in kettle
# Found 1.939 g of black solids in kettle

The runs demonstrated that the mercury could be reduced and stripped with only glycolic acid (no formic acid). The exception to this is that in the runs with added ruthenium chloride (GF39b, GF39d), no mercury was recovered. Based on the obvious color changes (see photos below), the mercury was likely reduced in all the supernate runs. In runs with added ruthenium, 0.765 g Ru was added as $RuCl_3 \cdot 1.93H_2O$ (1.832 g or 0.0227 g-moles of Cl). In all runs, 3.689 g of HgO were added (0.0170 g-moles of Hg). In previous testing, the presence of Cl led to the production of calomel (Hg_2Cl_2), which is not steam stripped. It is recommended that these runs should be repeated with another form of Ru such as ruthenium oxide hydrate to see if adding the Ru without Cl has the same impact on mercury stripping.

The mercury (II) contained in the starting slurry as mercuric oxide was reduced during the glycolic acid addition at a pH of approximately 4.5. The photographs below (Figure 3-1) show the slurry both before and after the run from Run GF39a (mercury was added but no noble metals). The kettle contents quickly changed from the orange HgO slurry to a transparent silver colored solution over a period of several minutes. The silver color slowly disappeared during boiling when the mercury was being steam stripped and recovered in the MWWT.

Figure 3-1. Photographs of GF39a before and after SRAT cycle (Supernate plus HgO)

In the runs with added noble metals and mercury, the slurry looked very much like sludge. The photographs below (Figure 3-2) show the slurry both before and after the run from Run GF39b (mercury and noble metals were added). The kettle contents quickly changed from the brown slurry to a transparent brown colored solution over a period of several minutes at a pH of 4.3. No mercury was recovered in the MWWT.

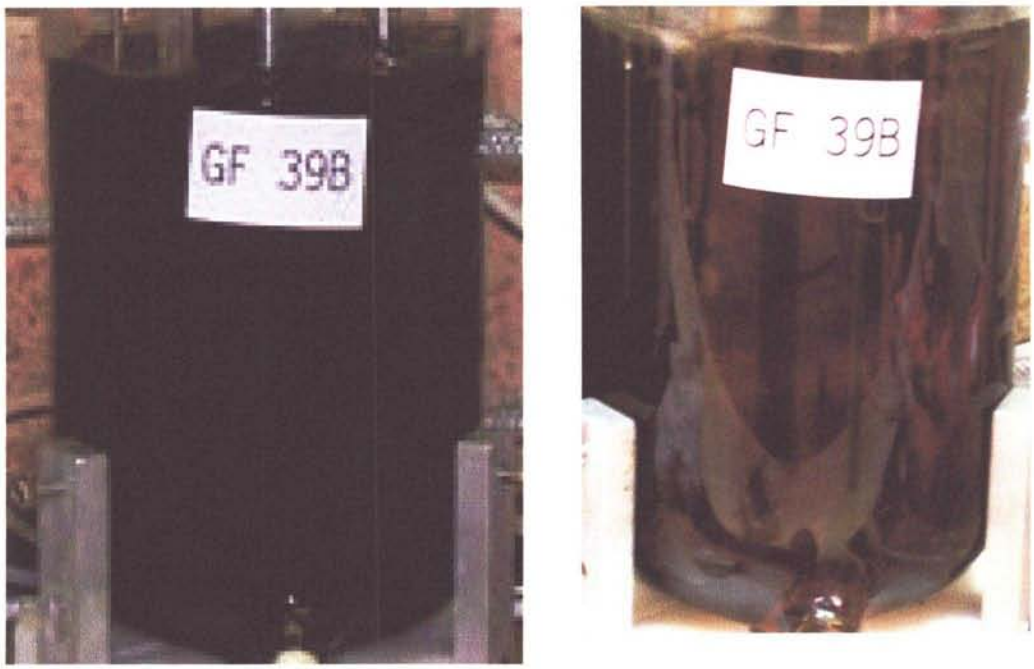

Figure 3-2. Photographs of GF39b before and after SRAT cycle (Supernate plus HgO and noble metals)

A mass balance was performed for each run to predict the concentration of all cations and anions throughout the run. In run GF39b (100% Koopman Stoichiometry, added noble metals and mercury), there was an apparent mass loss of 986 g (expected mass loss 151 g). This was calculated to match the final sodium concentration measured in the SRAT product sample. Using this mass loss, the predicted mercury concentration in the SRAT product is 2,306 mg/L and the measured mercury concentration was 2,315 mg/L. In other words, the mercury was completely soluble in the SRAT product and no mercury was recovered (not reduced, not stripped) in the MWWT. In contrast, run GF39a (100% Koopman stoichiometry, add mercury only), the final mercury concentration in the SRAT product was 14.9 mg/L compared to a predicted concentration of 1,433 mg/L (1.04% of the mercury was soluble). In addition, of the 3.4 g of mercury added initially on an elemental basis, 0.6 g was collected in the MWWT and 1.5 g was found in the SRAT product slurry as elemental mercury.

3.1.2 *Nitrite and Carbonate Destruction*

Nitrite and carbonate were below detection limits by the first hour of reflux in supernate testing. The results are summarized in Table 3-2.

Table 3-2. Nitrite Data, mg/L

Anion	GF39a	GF39b	GF39c	GF39d	**GF39e**
Post Nitric Acid	20,000	19,700	21,800	21,700	<500
Mid Glycolic Acid	10,800	6,560	4,540	11,700	<500
Post Glycolic Acid	<100	1,070	1,150	2,615	<500
1 hour dewater	<100	<100	<100	224	<500
Post Dewater	<100	<100	<100	<100	<500
Post Run	<100	<100	<100	<100	<500

3.1.3 *Anion and Cation Mass Balance*

Anions and cations were measured (solid lines in graphs below) throughout the supernate runs. A mass balance was completed for each run based on the known amounts added in preparing the supernate and the mass of added noble metals and mercury. These predictions (dotted lines), calculated by mass balance, were plotted along with the measured result in Figure 3-3 and Figure 3-4 (GF39b is presented as an example of this data). It should be noted that the PSAL measured nitrate agrees well with the nitrate prediction and the PSAL measured glycolate is approximately 20% higher than the prediction. In addition, oxalate is also much higher than predicted. It is likely that some oxalate is produced from glycolate decomposition. The measured nitrate is greater than predicted during glycolic acid addition due to the oxidation of nitrite to nitrate but is lower than predicted during reflux and boiling due to nitrate destruction. The sulfate concentration as measured by IC was very different than predicted. However, the measured sulfate, as calculated from ICP-AES S, was approximately 30% higher than predicted.

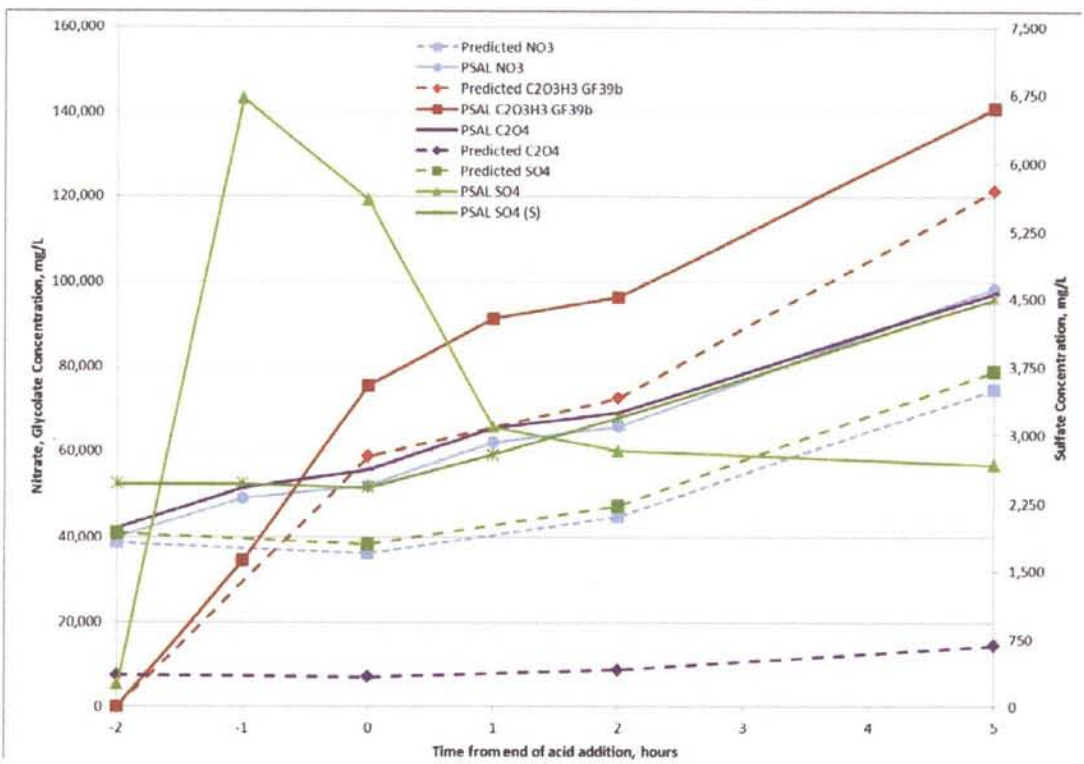

Figure 3-3. Supernate Run GF39b Predicted and Measured Anion Concentration

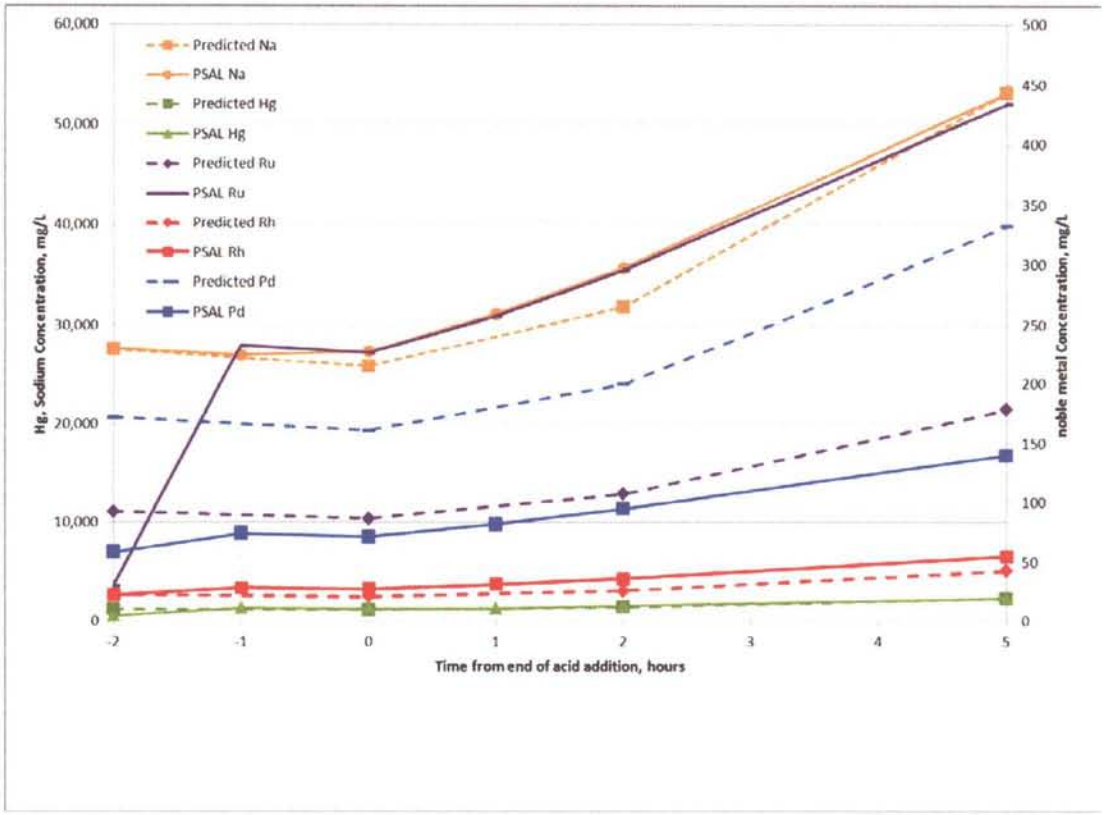

Figure 3-4. Supernate Run GF39b Predicted and Measured Cation Concentration

The measured sodium and mercury concentrations agreed well with predictions throughout run GF39b. The concentration of Pd and Ru were higher than predicted in Run GF39b. The Rh was approximately 80% of the predicted value and the Ag was below the detection limit. In Run GF39a (no added noble metals), the noble metals were all below detection limits.

3.1.4 *Nitrite-free Supernate Test*

One question that has always bothered our research team is whether glycolic acid is able to reduce mercury, allowing the elemental mercury to be removed by steam stripping. One theory was that glycolic acid needed a more reducing form such as glyoxylic acid to reduce the mercury. Glyoxylic acid, a better reducing agent than glycolic acid, could be produced by the reduction of glycolic acid by nitrite. As a result, a run was completed with a nitrite free simulant. This run was noble metal free, only mercury was added to the supernate. The result was that the mercury was completely reduced, a virtual duplication of Run GF39a. It appears that glycolic acid is fully capable of reducing mercury with or without nitrite present.

3.1.5 *Conclusions from Supernate Testing*

The new SRAT apparatus is capable of keeping the noble metals and mercury suspended prior to acid addition. In runs with all noble metals (GF39b, GF39d), no mercury was reduced or collected. In runs without ruthenium chloride (GF39a, GF39c, GF39e), mercury was collected in the MWWT and mercury was found in the SRAT product as an insoluble mercury compound. Run GF39e demonstrated that mercury could be reduced with or without nitrite present.

The concentrations of Pd and Ru were higher than predicted in Run GF39b. The Rh was approximately 80% of predicted and the Ag was below the detection limit. In Run GF39a (no added noble metals), the noble metals were all below detection limits.

Another interesting observation is that although the runs had no added Al, Ca, Cu, Fe, Mn, Mg, Ni or Si, these compounds were detected in samples throughout the runs (most of these have concentrations of approximately 10 mg/L, although Si was 40-80 mg/L). Although the glassware and agitator is cleaned by soaking in 8 M nitric acid overnight, the runs cleaned the equipment by dissolving these metals. This is further demonstration that the glycolic-nitric flowsheet will help to keep the DWPF processing vessels cleaner than the current flowsheet.

3.2 Slurry Testing

Twelve SRAT and six SME process simulations were completed to demonstrate the Glycolic-Nitric Flowsheet. Ten SRAT and four SME process simulations utilized the matrix sludges with added mercury and noble metals. Runs GF34, GF35, GF36 and GF37 were completed first and also included SME cycles. Runs 36b and 36c were duplicates of the GF36 SRAT cycle to compare the old and new processing rigs and determine whether the changes had impacted process chemistry. Run 37b was a duplicate of GF37 and GF38 was a higher acid stoichiometry repeat of GF37. The main reason for the four repeat runs was to better track mercury as the mercury recovery in the first four runs was poor. Runs 34b and 34c were duplicates of the GF34 SRAT cycle to determine whether lowering the purge impacted process chemistry. In addition, runs GF40 and GF41 were SRAT and SME process simulations designed to determine whether the Glycolic-Nitric Acid flowsheet could successfully process the less washed simulants. Some data from the supernate runs is included in this section for completeness if they were not reported in Section 3.1.

3.2.1 *Off-gas*

Besides essentially eliminating hydrogen generation, the glycolic acid flowsheet also appears to stop or significantly slow down other off-gas generating reactions. Data is presented to summarize the results of these analyses. More detailed data is included in Appendix B.

3.2.1.1 Hydrogen

A main objective of this testing was to show that hydrogen generation could be mitigated or eliminated by the use of the glycolic/nitric flowsheet. Hydrogen was detected only in the GF40 and 41 SRAT cycles. These two runs had the "new lower purge" which led to higher measured hydrogen concentrations for a given generation rate. The GC hydrogen quantitation limit is 0.005 volume %. The maximum hydrogen detected in these runs was 0.009 volume %, which would have been below detection limits with the current DWPF scaled purge. Note that these runs were completed at approximately 130% stoichiometry and produced approximately 1% of the hydrogen compared to essentially identical runs with the Baseline flowsheet. Table 3-3 compares SRAT and SME cycle hydrogen on a DWPF scale. (Figure 3-5) summarizes the SRAT cycle hydrogen generation.

In the first four SME cycles (GF34, GF35, GF36, and GF37), formic acid was added with the frit in the SME cycle. In these runs, measurable hydrogen was generated, on the order of 0.05 volume percent. No formic acid was added in the GF40 and GF41 SME cycles. The GF41 hydrogen generation was just above quantitation limits in the GF40 SME cycle. In essentially identical runs with the Baseline flowsheet, the SME hydrogen limit was exceeded in runs at 125 and 130% acid stoichiometry.

Table 3-3. Peak Hydrogen Generation

Run	Sludge Composition	SRAT H_2, lb/hr	SME H_2, lb/hr
DWPF	Current Limit	0.65	0.223
GF34	HiFeHiMn	<0.0014	0.00556
GF34b	HiFeHiMn	<0.0014	No SME
GF34c	HiFeHiMn	<0.0014	No SME
GF35	SB7A	<0.0014	0.00398
GF36	HiFeLoMn	<0.0014	0.0111
GF37b	HiFeLoMn	<0.0014	No SME
GF37c	HiFeLoMn	<0.0014	No SME
GF37	LoFeLoMn	<0.0014	0.0157
GF37b	LoFeLoMn	<0.0014	No SME
GF38	LoFeLoMn	<0.0014	No SME
GF39a, b, c, d, e	Supernate	<0.0014	No SME
GF40	1.6 M Na	0.00287	0.00184
GF41	1.9 M Na	0.00324	<0.0012

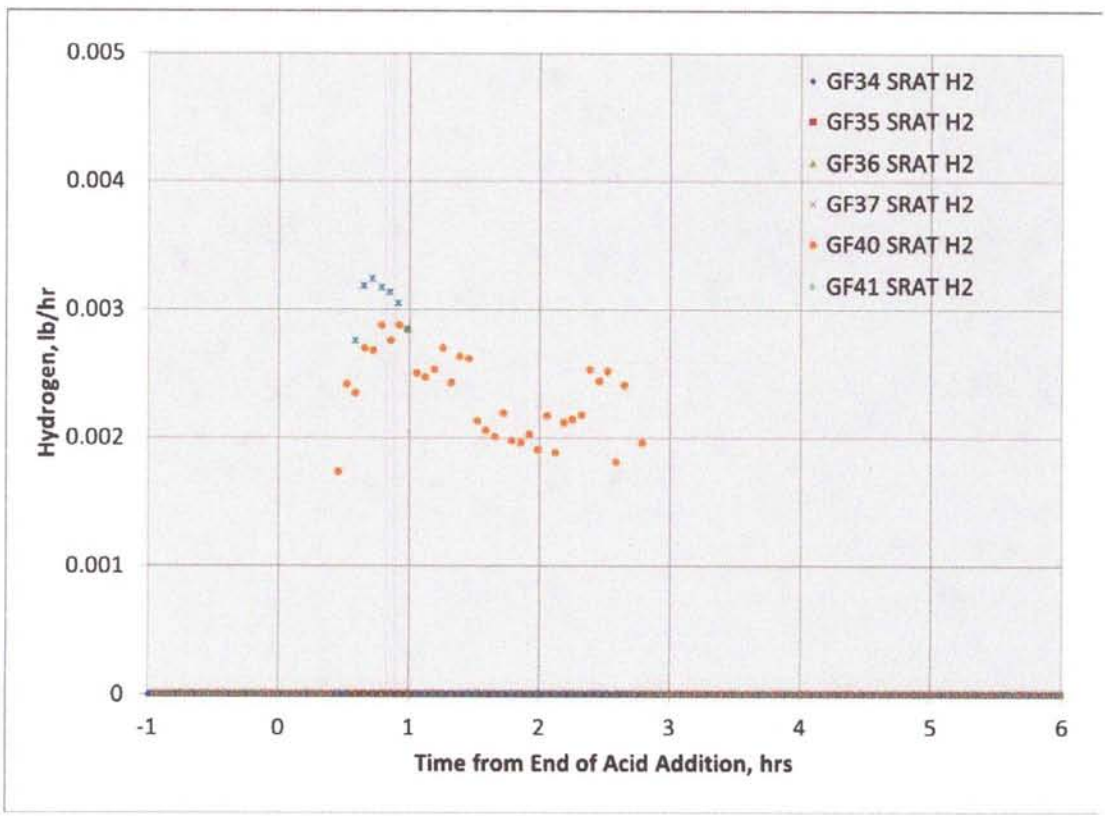

Figure 3-5. SRAT Cycle Hydrogen Generation

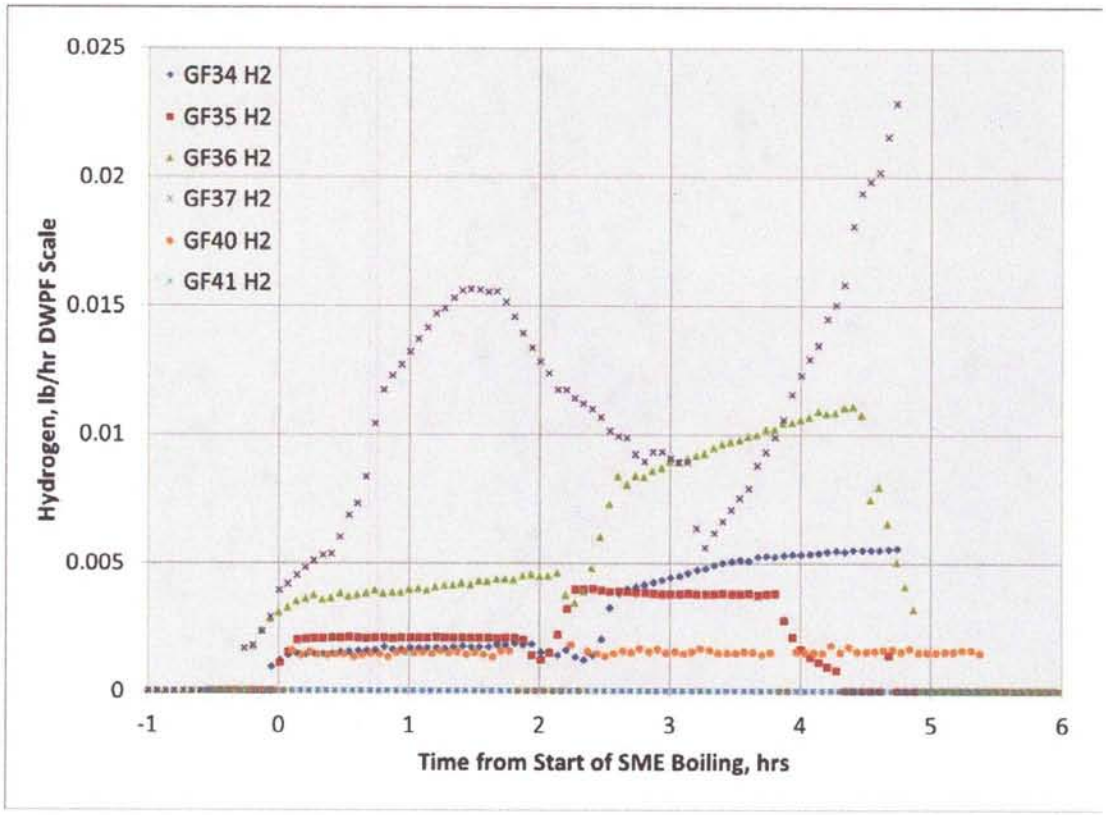

Figure 3-6. SME Cycle Hydrogen Generation

The MS was also used to measure hydrogen during Runs GF40 and GF41. The MS hydrogen peak was 0.025 volume % in both the GF40 and GF41 SRAT cycles. This is almost three times the maximum detected by the GC. Although the potential detection limit is significantly lower for the MS (10 ppb) than the GC (10 ppm), quantification at these low concentrations is difficult due to variations in the background signal intensity. Therefore, the MS values can be considered qualitative at best. Both peaks occurred at boiling as is often the case in runs with low offgas generation (H_2 accumulated during frit slurry addition and was purged out as boiling was initiated). The comparison graph for Run GF40 is below (Figure 3-7).

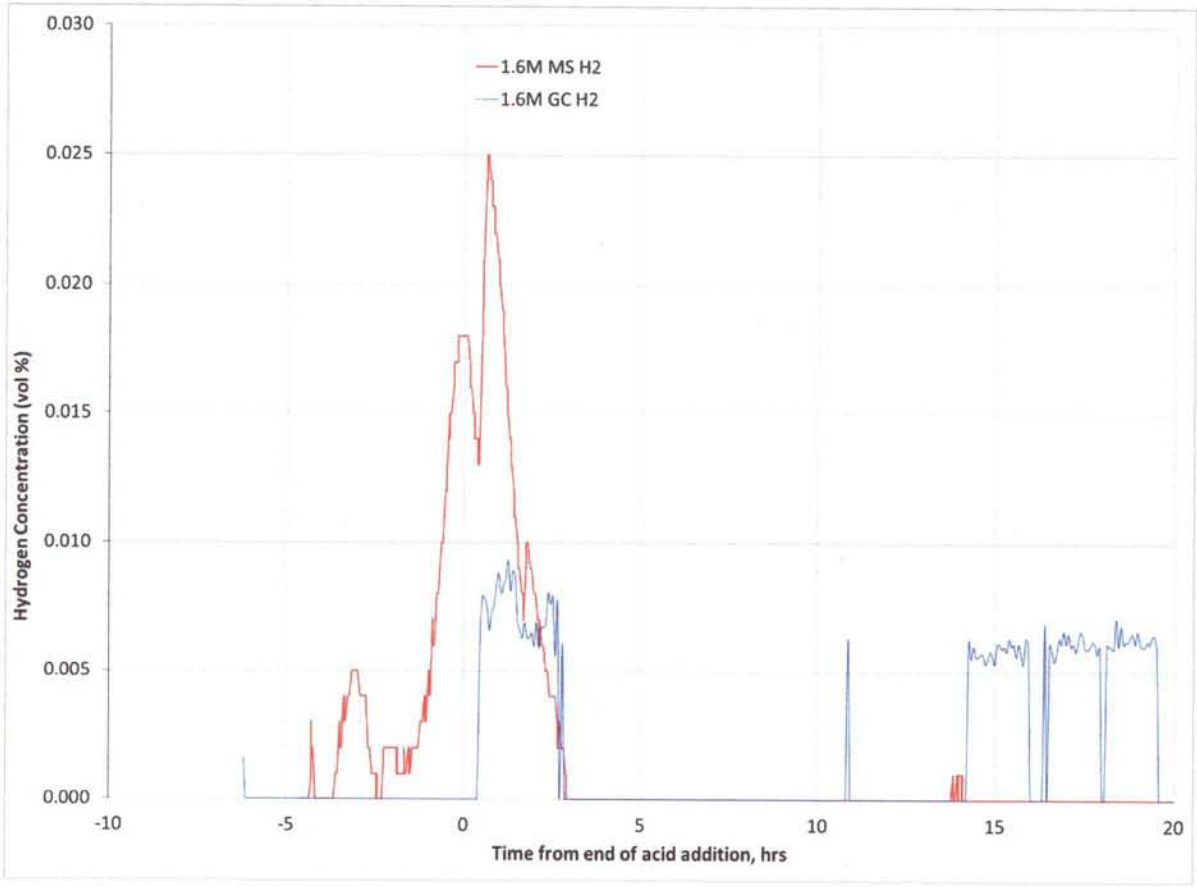

Figure 3-7. MS and GC Hydrogen Concentration

3.2.1.2 Other Off-gas Components

In addition to generation of hydrogen, other gases including carbon dioxide, carbon monoxide, and a number of oxides of nitrogen are produced. Only carbon dioxide and nitrous oxide (N_2O) can be quantified using the gas chromatographs and calibration gas standards.

Carbon dioxide is the major off-gas generated, produced by the decomposition of carbonate species during acid addition. Table 3-4 and Figure 3-8 summarizes the carbon dioxide generation in the SRAT cycle. Table 3-5 and Figure 3-9 summarizes the carbon dioxide generation in the SME cycle. The CO_2 generation post acid addition is mainly due to glycolate decomposition. The total CO2 produced with the glycolic-nitric flowsheet is approximately one-third compared to the baseline flowsheet. The small generation of CO_2 in the SME cycle is triggered by decomposition of the formic acid that was added with the frit in the frit-slurry. This could be eliminated by not adding formic acid with frit in the SME cycle.

Table 3-4. Comparison of SRAT Carbon Dioxide Generation Data

Run	CO_2 from Carbonate, g	CO_2 in off-gas, g
GF34	29.2	38.0
GF34b	29.2	32.4
GF34c	29.2	33.0
GF35	12.5	26.1
GF36	26.5	34.9
GF36b	26.5	29.0
GF36c	26.5	30.5
GF37	25.5	36.5
GF37b	25.5	32.8
GF38	25.5	19.5
GF39a (Hg)	12.9	17.2
GF39b (Hg + NM)	12.9	22.0
GF39c (Hg+NM-Ru)	12.9	18.6
GF39d (Hg + NM)	12.9	16.2
GF40	20.5	45.8
GF41	19.3	50.8

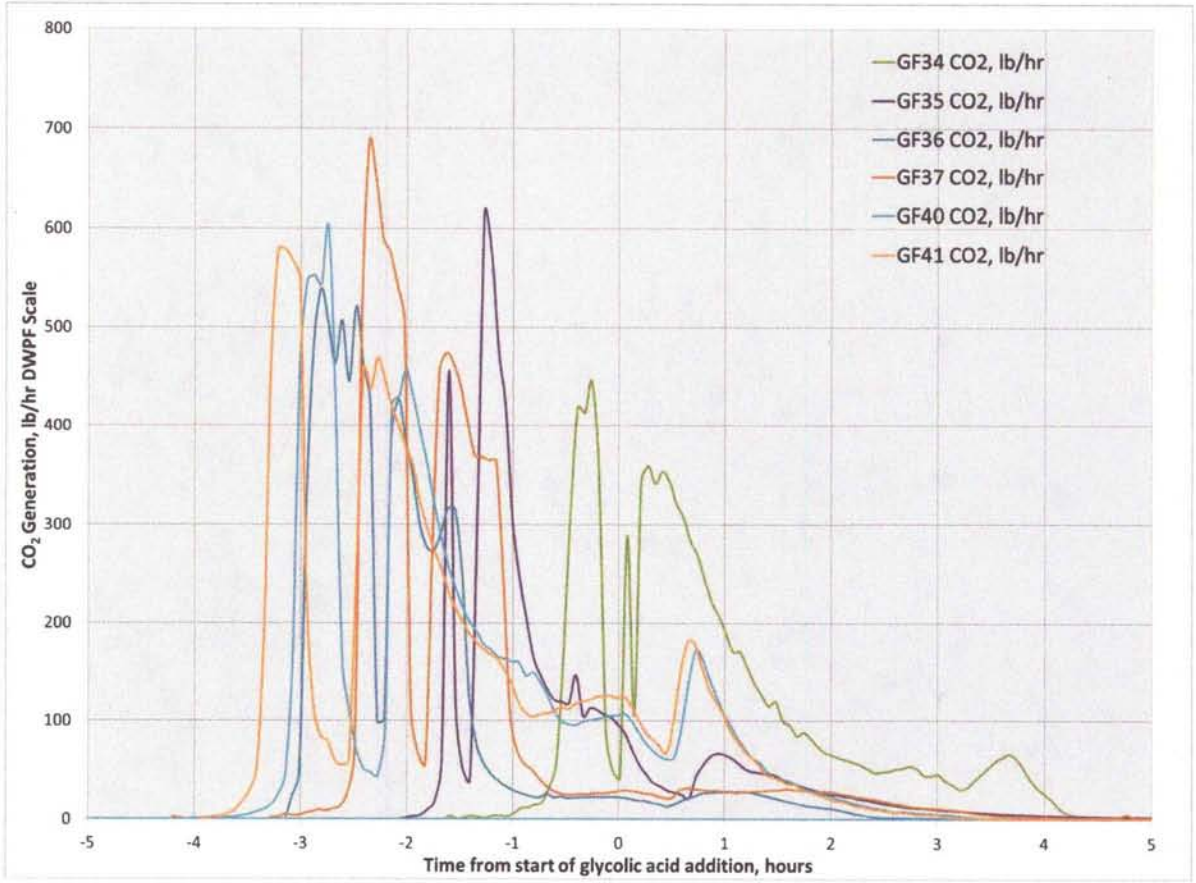

Figure 3-8. Carbon Dioxide Generation in SRAT cycles, lb/hr DWPF Scale

Table 3-5. Comparison of SME Carbon Dioxide Generation Data

Run	Potential CO_2 from Added Formate, g	Measured CO_2 in off-gas, g	Remaining Potential CO_2 as formate, g
GF34	10.2	5.1	5.9
GF35	7.3	1.4	7.1
GF36	9.6	7.1	7.0
GF37	9.1	6.8	6.6
GF40	0	0.40	0[%]
GF41	0	0.56	0

[%] no equivalent CO_2 remaining as formate, since no formic acid was added or detected

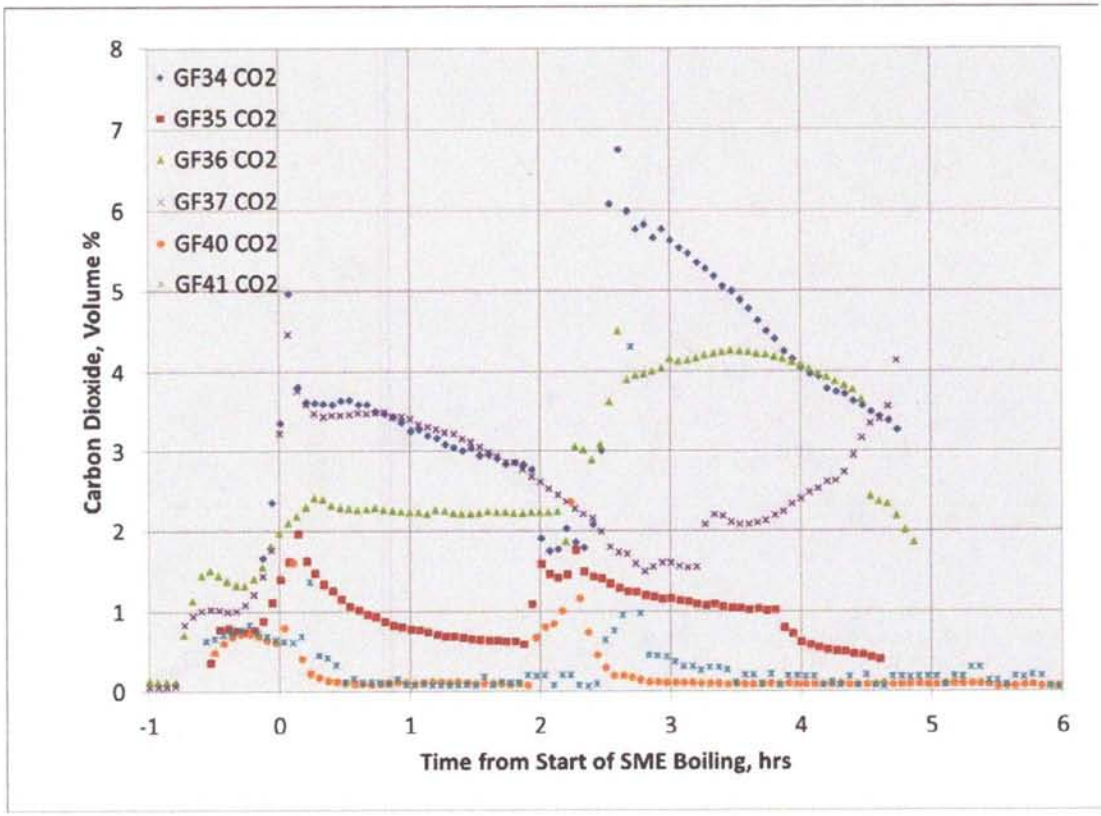

Figure 3-9. Carbon Dioxide Generation in SME cycles, lb/hr DWPF Scale

Most of the nitrite in the feed is converted to NO or NO_2 during the SRAT cycle. However, these cannot be quantified with the gas chromatographs, although the yellow off-gas is indicative of significant NO_2 in the off-gas. The production of N_2O is minor; 1.6% - 4.5% of the nitrite was converted to N_2O. Table 3-6 and Figure 3-10 summarizes the nitrous oxide generation in the SRAT cycle. In runs without added formic acid in the frit slurry, no N_2O was detected in either the GF40 or GF41 SME cycle.

Table 3-6. Comparison of SRAT Nitrous Oxide Generation Data

Run	NO_2^- in feed , g	Potential N_2O from feed, g	Measured N_2O in off-gas, g
GF34	51.9	24.8	0.69
GF34b	51.9	24.8	0.33
GF34c	51.9	24.8	0.31
GF35	27.9	13.3	0.59
GF36	51.6	24.7	0.38
GF36b	51.6	24.7	0.35
GF36c	51.6	24.7	0.34
GF37	52.5	25.1	0.67
GF37b	52.5	25.1	0.45
GF38	52.5	25.1	0.21
GF40	40.9	19.5	0.55
GF41	47.9	22.9	0.77

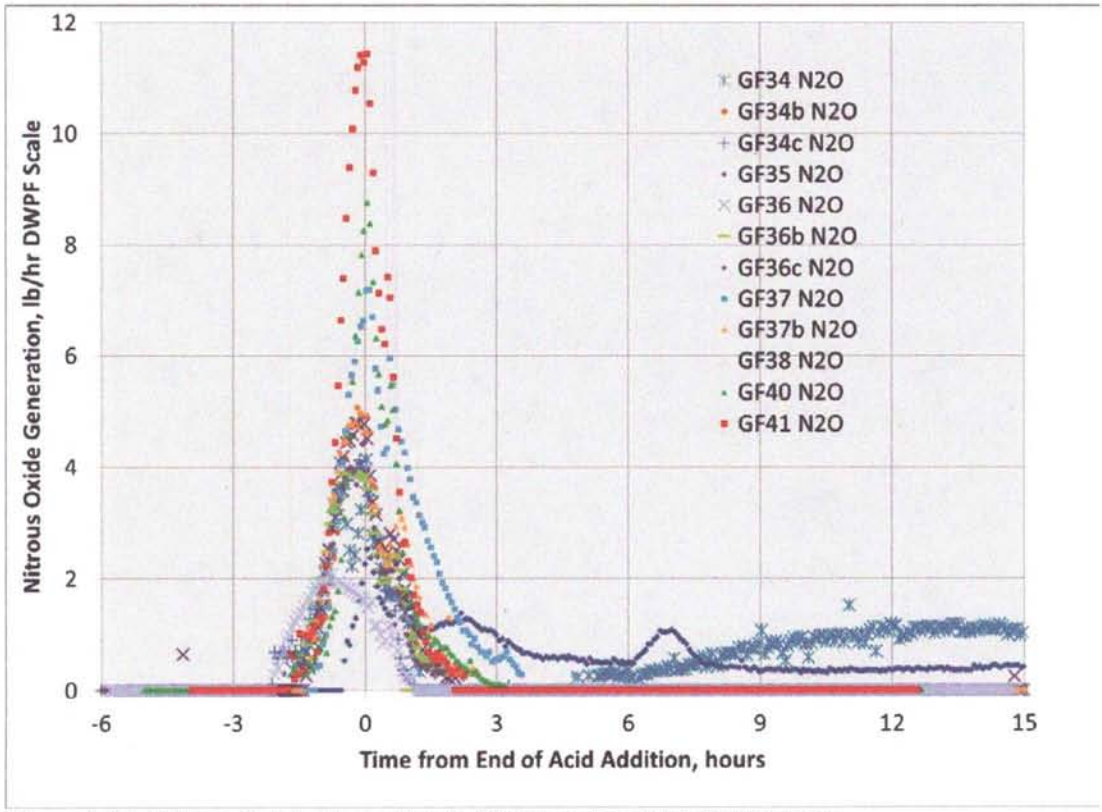

Figure 3-10. Nitrous Oxide Generation in SRAT cycles, lb/hr DWPF Scale

There was excellent agreement between the GC and MS for the major components in the offgas (N_2, O_2, and CO_2). In addition, the MS is able to measure NO_x in the offgas. The data for GF40 is summarized in Figure 3-11.

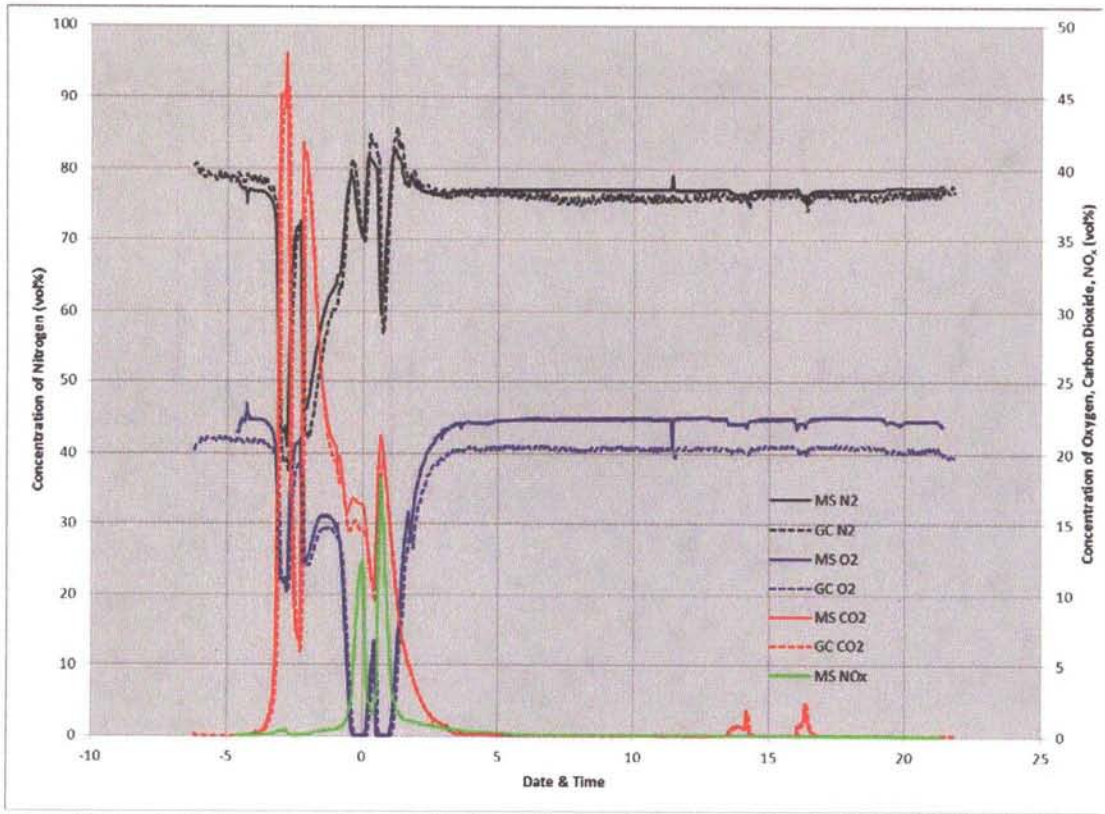

Figure 3-11. Nitrogen, Oxygen, Carbon Dioxide, NO_x Generation in GF40 SRAT Cycle

The FTIR was able to measure CO_2, NO, NO_2, N_2O and HMDSO. HMDSO is an expected degradation product of the current DWPF antifoam. The highest concentration detected for the HMDSO were at SRAT boiling and as boiling was initiated in the SME after each acid addition. The data are summarized in Figure 3-12.

A molar balance was used to compare the measured HMDSO to the potential HMDSO if all the antifoam decomposed to HMDSO. The HMDSO in the offgas was integrated to estimate the total HDMSO produced (1.14 mmol). Based on the antifoam added throughout the run, 0.96 mmol of HDMSO could be produced. Based on this calculation, 119% of the possible HMDSO was found in the offgas. This indicates that the the antifoam is completely hydrolyzing to HDMSO during SRAT and SME processing. The HDMSO is not being removed by the ammonia scrubber or the condensers.

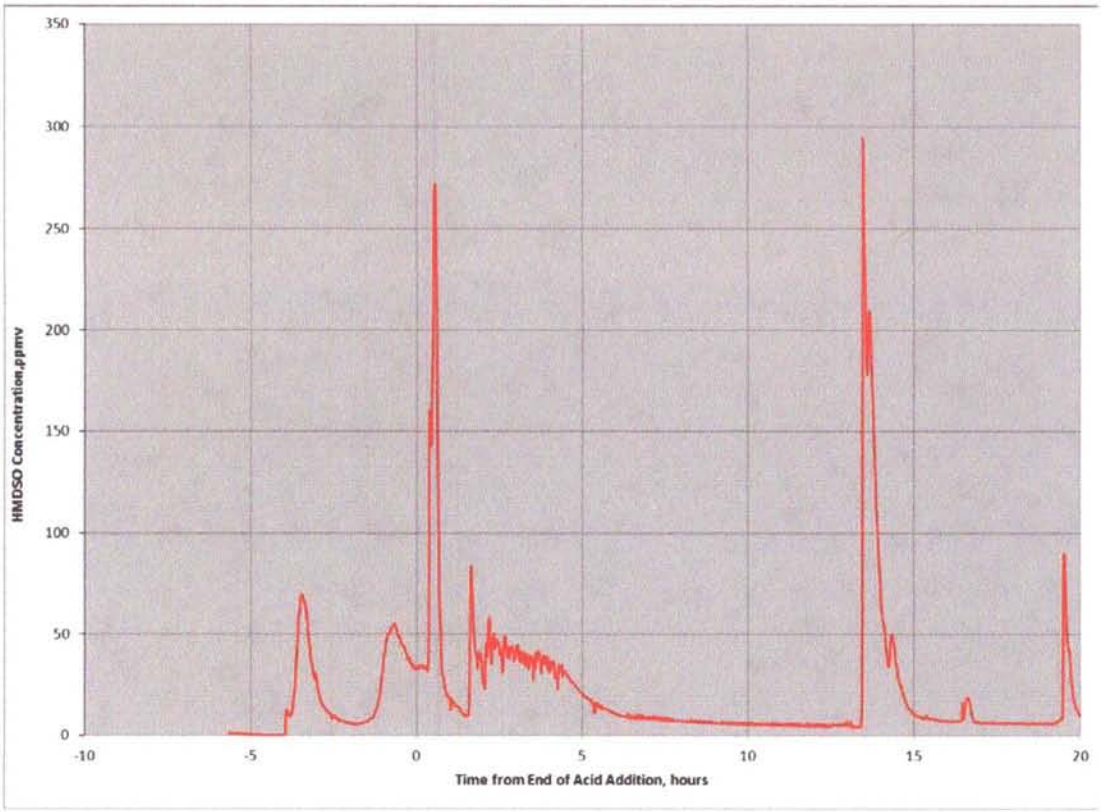

Figure 3-12. GF41 FTIR HMDSO Concentration, ppm_v

A comparison of data from the MS, GC and FTIR showed excellent agreement for CO_2. The data is summarized in Figure 3-13.

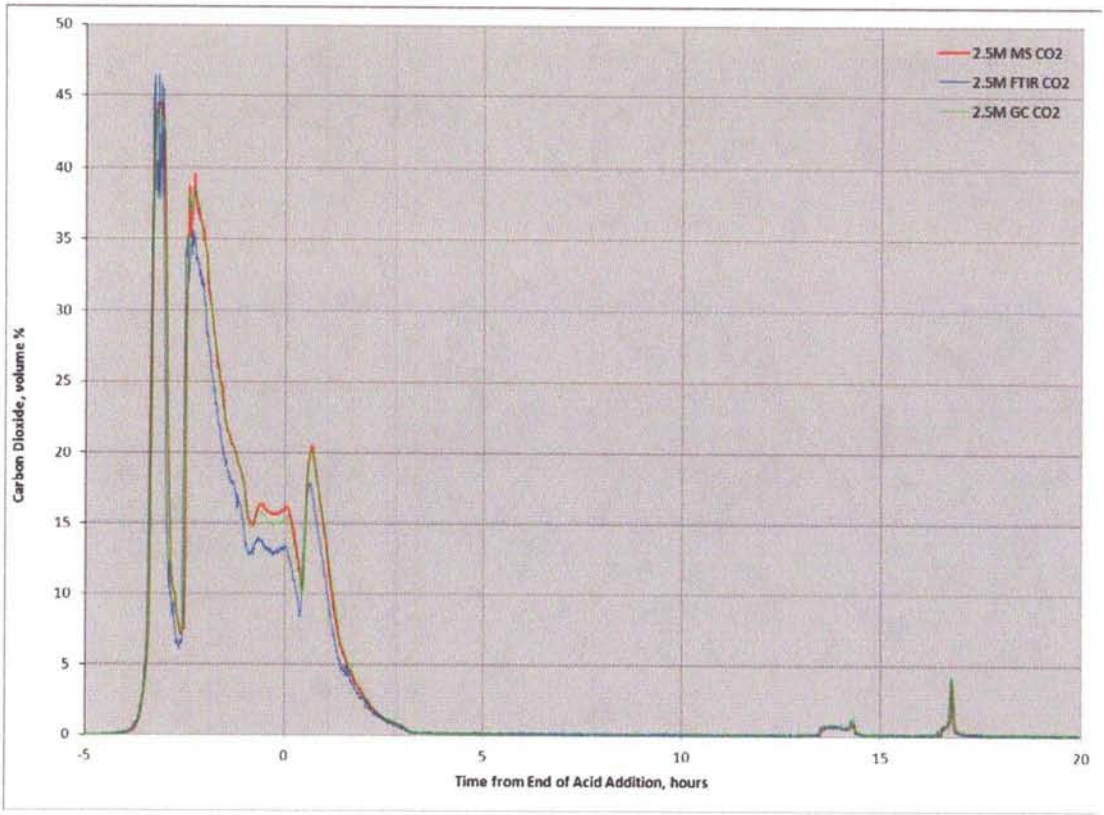

Figure 3-13. GF41 Carbon Dioxide Comparison between GF, MS and FTIR, volume %

Nitrite generally decomposes to nitrate, NO_2, NO, and N_2O. The GC measured only the N_2O concentration. With the addition of the MS and FTIR, all of these components can now be measured. It should be noted that the offgas samples are analyzed after the offgas has been through the SRAT condenser, MWWT, ammonia scrubber, and FAVC. The SRAT condenser and MWWT are both effective at scrubbing NO_2 from the offgas so although NO_2 is the major offgas species in the nitrite decomposition, little NO_2 was measured by the FTIR and MS. In addition, the MS measured concentrations were about two times higher than the FTIR. The concentrations of NO_2, NO, and N_2O are summarized in Figure 3-14.

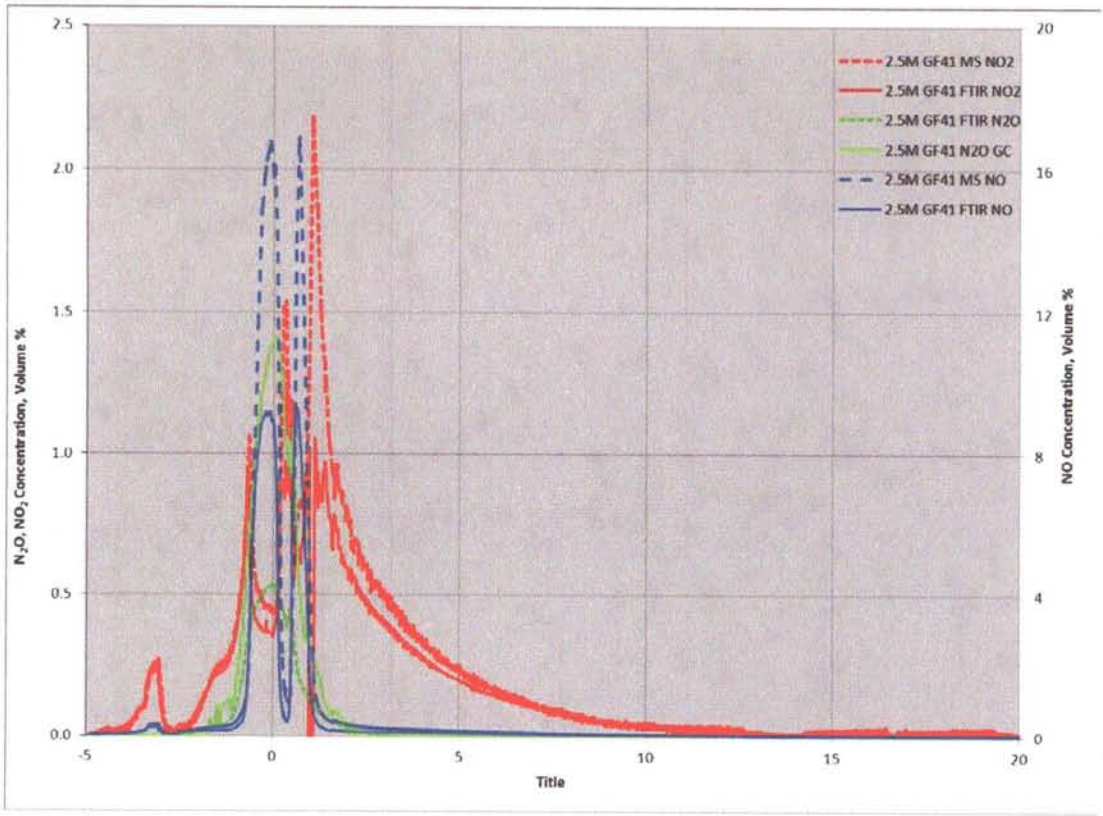

Figure 3-14. GF41 NO_2, NO, or N_2O GC, MS and FTIR, volume %

3.2.2 *SRAT Mercury Reduction and Stripping*

One of the most important questions to resolve concerning the glycolic-nitric acid flowsheet is whether mercury could be effectively reduced and steam stripped in the SRAT cycle without formic acid. In the Baseline flowsheet, mercury is reduced to elemental mercury during formic acid addition and then removed from the slurry by steam stripping during the concentration and reflux periods in SRAT processing.

The starting sludge was trimmed to 1.5 wt% Hg in the total solids. This required a theoretical boiling time of 12 hours to remove mercury to less than 0.80 wt% in the SRAT product total solids using lab-scaled DWPF design basis boil-up rates and a stripping efficiency of 750 g steam/g Hg.

A mass balance was completed for each of the runs to attempt to determine where the mercury had accumulated. The mercury mass balance is summarized in Table 3-7. In three of the first four runs, GF34, 35, 36 and 37, the mercury recovery was poor in the MWWT. As a result, Runs 34, 36 and 37 were repeated (Runs GF34b, GF34c, GF36b, GF36c, GF37b and GF38). The mercury recovery in the second set of runs was typical for lab-scale SRAT cycles[19]. No cause for the differences in duplicate runs has been identified, but it is possible that there was technician error in collecting the mercury. Run GF35 (SB7A sludge) was not repeated, since the sludge was consumed in Run GF35. Run GF38 was performed at 125% acid stoichiometry to determine if acid stoichiometry impacted mercury recovery. Note that about 50% less mercury was recovered in the MWWT in run GF38 (125% acid stoichiometry) than was recovered in run GF37b (100% acid stoichiometry). This phenomenon is also seen in Baseline flowsheet runs.

Two SRAT and SME cycles (GF40 and GF41) were performed with two underwashed SB8 simulants to demonstrate that mercury can be reduced without formic acid in glycolic flowsheet runs with typical (not matrix) sludge simulant. These runs were completed in parallel with two Baseline flowsheet runs. The Glycolic-Nitric Flowsheet runs both had higher mercury recovery in the MWWT (same Koopman acid stoichiometry, same noble metals and mercury, essentially duplicate runs). In all Glycolic-Nitric acid flowsheet testing, the mercury stripping and recovery in the MWWT has either met or exceeded the recovery in the Baseline flowsheet runs.

Table 3-7. Mercury Balance in SRAT and SME Cycle, g

Run	% Acid Koopman	Added	MWWT	Slurry	Conden sate	Total	% Recovery
GF34	104.0	10.56	2.27	12.12	2.27	16.66	160%
GF34b	104.0	10.56	5.89	6.36	NM	12.3	116%
GF34c	104.0	10.56	1.94	7.10	NM	9.04	86%
GF35	100.0	8.25	0.02	0.19	0.17	0.38	4.6%
GF36	106.1	10.17	0.14	5.85	0.53	6.52	64%
GF36b	106.1	10.17	2.27	6.59	NM	8.85	87%
GF36c	106.1	10.17	2.35	7.17	NM	9.53	94%
GF37	100.0	10.28	0.01	7.13	0.48	7.62	74.%
GF37b	100.0	10.28	4.10	4.75	NM	8.56	86%
GF38	125	10.28	1.99	7.40	NM	9.15	91%
GF40	130	11.15	3.79	5.21	0.44	9.44	85%
GF41	130	11.15	3.24	5.34	0.46	9.03	81%

Samples were taken periodically throughout the runs for mercury analysis. The chart below (Figure 3-15) shows the concentration of mercury in the slurry as a function of time for the eight runs. It is expected that the mercury concentration will decrease linearly during SRAT steam stripping and collect in the MWWT. A linear decrease of Hg concentration in the slurry assumes a constant boil-up rate and a constant approach to thermodynamic vapor-liquid equilibrium between the slurry and off-gas phases. The general trend of the mercury profile curves is a linear decrease as expected. It was expected that the SRAT product would have a mercury concentration of 0.8 wt% or 2160 mg/kg. The SRAT product Hg concentration ranged from 0.01-0.92 wt % total solids basis. Results are summarized Table 3-9.

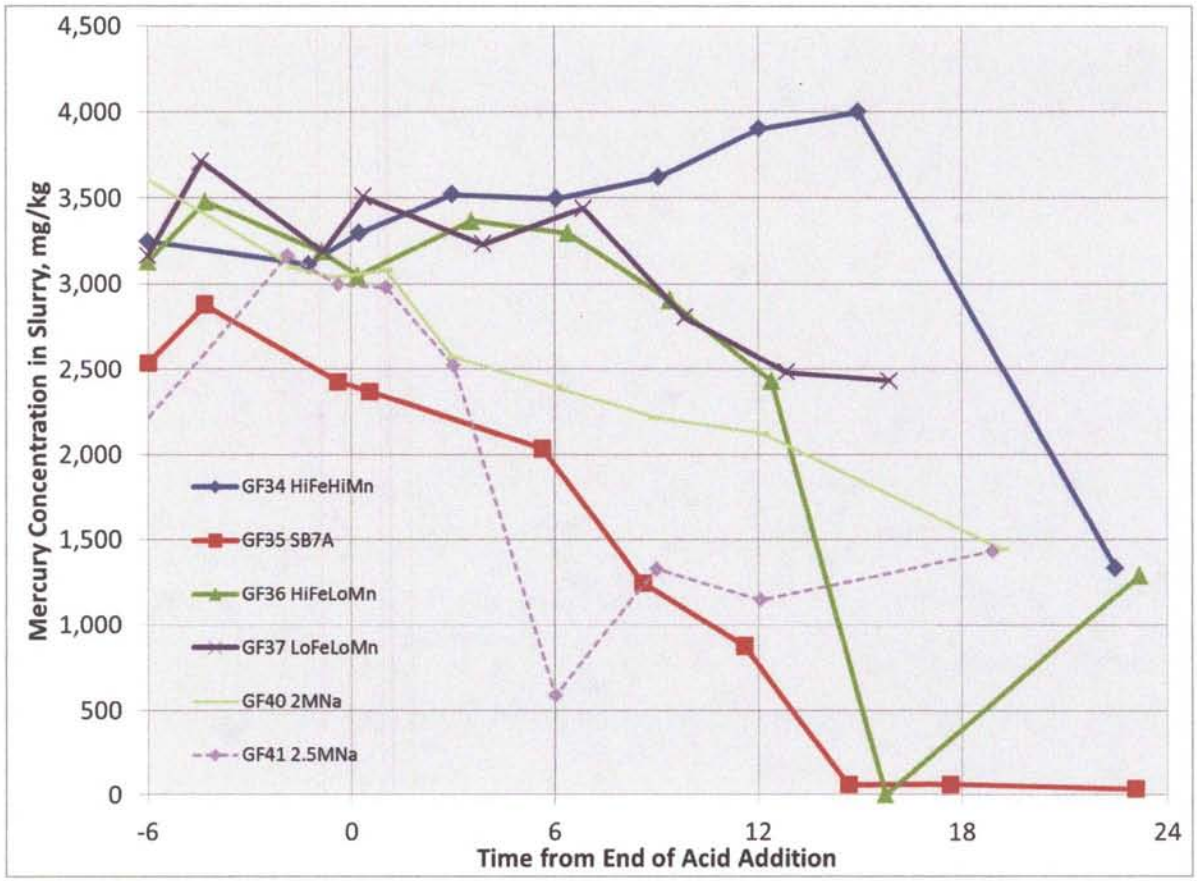

Figure 3-15. Mercury concentration versus time in Selected SRAT and SME cycles

Mercury is added to the sludge as HgO. In these runs the HgO was slurried with water and homogenized using the vortex mixer to break up any clumps and allow an even dispersal of the mercury. During SRAT processing the mercury is first dissolved and may later be reduced to elemental mercury. Once it is reduced, it is insoluble and can be steam stripped. In Runs GF37b and GF38, extra samples were pulled during the acid addition and dewater phase to understand when these reactions occur. In both runs, approximately 90% of the mercury was dissolved prior to the completion of nitric addition and the Hg was completely dissolved by midway through the glycolic acid addition. The mercury then is reduced during the first two hours of dewatering (faster during GF38, the 125% acid stoichiometry run, than during GF37b, the 100% acid stoichiometry run). The dissolution and reduction of mercury was very similar to that seen for Pd. The concentration of Hg and Pd are summarized in Figure 3-16.

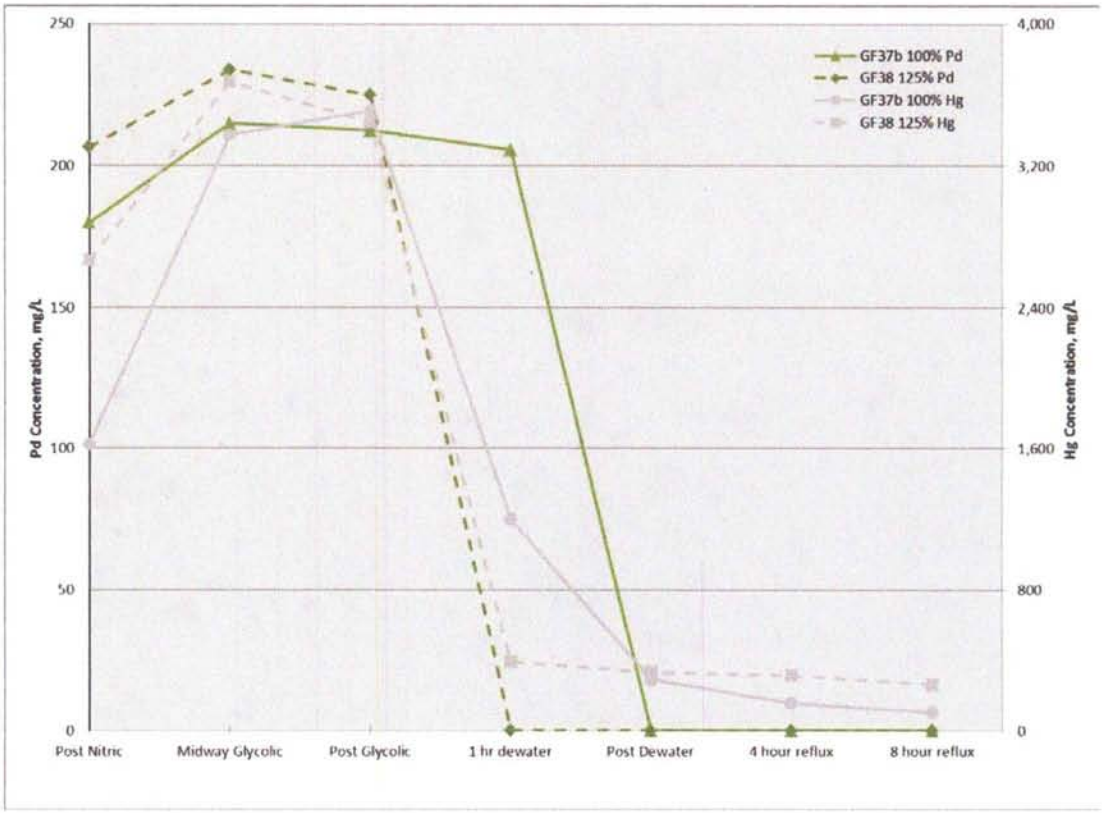

Figure 3-16. Mercury and Palladium Concentration for GF37b and GF38 SRAT Cycles

Mercury recovered in the MWWT was submitted to AD for crystal identification for the non-metallic mercury recovered (the majority of the mercury is elemental mercury). The samples were analyzed by both X-ray Diffraction (XRD) and X-ray Fluorescence (XRF). Note that calomel formed in all four Glycolic Flowsheet runs and chloromagnesite formed in all runs with the underwashed sludges (the Mg concentration was nearly identical in all three sludges). Mosesite was only detected in the Baseline flowsheet runs. The main source of chloride in these runs is added chloride in $RuCl_3$. The results are summarized in Table 3-8.

Table 3-8. XRD and XRF Identification of MWWT Crystals

Run	Calomel (Hg_2Cl_2)	Mosesite ($Hg_2NCl{\cdot}H_2O$)	Chloromagnesite ($MgCl_2$)
GF34b	Yes	No	No
GF34c	Yes	No	No
Baseline 1.6 M Na	No	Yes	Yes
Baseline 1.9 M Na	No	Yes	Yes
GF40 (1.6 M Na)	Yes	No	Yes
GF41 (1.9 M Na)	Yes	No	Yes

Mercury is being reduced by glycolic acid and approximately 30% of the mercury is removed from the SRAT by steam stripping and is collected in the MWWT. Approximately 40% of the mercury remains in the SME product. Another 4% was found in the condensate. There are two likely paths for condensate namely it can be removed by steam stripping (but not collect in the MWWT). This

can happen in the SRAT cycle and SME cycle. In addition, the mercury can be dissolved by the strong acid in the condenser/MWWT condensate and overflow to the SMECT. In these tests little mercury was collected in the ammonia scrubber samples.

3.2.3 *SRAT Data*

SRAT cycle data is discussed in this section.

3.2.3.1 SRAT Elemental Data

General SRAT product slurry data for the twelve runs are tabulated below. Analyses were completed of both the slurry and supernate from all SRAT and SME products. The slurry results are summarized in Table 3-9. Conversion of the elemental data to the expected oxide form allows summing the oxides as a measure of both complete sample dissolution and accurate analysis of the major elements in the sludge product. The sum of oxides range from 98.2-100.5 over this data set (95-105 is considered acceptable). The slurry samples were filtered and the supernate results of these analyses are summarized in Table 3-10. The solubility of the cations is summarized in Table 3-11

Table 3-9. SRAT Product Slurry PSAL Elemental Data, wt % calcined solids basis

Run	GF34	GF34b	GF34c	GF35	GF36	GF36b	GF36c	GF37	GF37b	GF38	GF40	GF41
Al	9.01	8.77	8.69	15.2	9.1	9.2	9.1	23.7	23.5	23.9	14.7	11.7
B	<0.100	NM	NM	<0.100	<0.100	<0.100	<0.100	<0.100	<0.100	<0.100	<0.100	<0.100
Ba	0.080	0.077	0.081	0.108	0.095	0.094	0.092	0.063	0.064	0.063	0.090	0.051
Ca	3.58	3.74	3.77	0.80	2.12	1.95	1.94	1.68	1.66	1.69	0.601	0.431
Cd	<0.010	NM	NM	<0.010	<0.010	<0.010	<0.010	<0.010	<0.010	<0.010	NM	NM
Cr	0.017	0.016	0.016	0.067	0.273	0.269	0.269	0.223	0.224	0.220	0.025	0.023
Cu	0.070	0.051	0.054	0.052	0.054	0.043	0.040	0.051	0.040	0.041	0.030	0.026
Fe	32.3	31.1	31.3	20.5	32.0	32.9	32.9	12.6	12.3	12.3	14.2	12.7
Hg@	1.27	0.82	0.89	0.02	0.65	0.81	0.87	0.83	0.59	0.92	0.52	0.52
K	0.080	0.087	0.118	0.075	0.061	0.077	0.083	0.071	0.079	0.086	0.412	0.442
Li	<0.100	NM	NM	<0.100	<0.100	NM	NM	<0.100	<0.100	<0.100	<0.100	<0.100
Mg	0.410	0.389	0.401	0.382	2.57	2.77	2.76	2.36	2.40	2.43	0.398	0.258
Mn	4.01	3.80	3.77	5.02	0.706	0.640	0.631	0.666	0.600	0.596	4.51	4.15
Na	14.2	13.8	13.9	15.5	13.5	13.4	13.2	15.3	14.1	14.4	23.0	26.1
Ni	0.212	0.182	0.189	3.42	2.69	2.73	2.73	2.37	2.35	2.37	1.95	1.55
P	<0.100	<0.100	<0.100	<0.100	<0.100	<0.100	<0.100	<0.100	<0.100	<0.100	<0.100	<0.100
Pb	0.080	0.069	0.071	0.023	0.056	0.049	0.041	0.058	0.050	0.039	<0.010	<0.010
Pd	<0.100	0.03	0.03	<0.100	<0.100	<0.010	<0.010	<0.100	<0.010	<0.010	<0.100	<0.100
Rh	0.031	<0.100	<0.100	0.032	0.033	<0.100	<0.100	0.047	<0.100	<0.100	<0.100	<0.100
Ru	0.032	<0.100	<0.100	0.031	0.032	<0.100	<0.100	0.030	<0.100	<0.100	<0.100	<0.100
S	0.276	0.282	0.281	0.347	0.276	0.264	0.269	0.294	0.283	0.260	0.292	0.341
Si	1.48	1.57	1.50	1.70	1.95	1.82	1.76	1.30	1.42	1.39	1.41	0.86
Sn	<0.010	NM	NM	0.029	0.107	0.102	0.102	0.089	0.094	0.093	NM	NM
Ti	0.010	<0.010	<0.010	0.025	0.010	<0.010	<0.010	0.010	<0.010	<0.010	0.022	0.012
Zn	0.062	0.063	0.065	0.064	0.072	0.071	0.070	0.061	0.062	0.062	0.046	0.039
Zr	0.055	0.051	0.054	0.236	0.117	0.110	0.110	0.045	0.040	0.044	0.201	0.178

@ Hg reported on a total solids basis

Table 3-10. SRAT Product Supernate PSAL Elemental Data, mg/L supernate basis

Run	GF34	GF34b	GF34c	GF35	GF36	GF36b	GF36c	GF37	GF37b	GF38	GF40	GF41
Al	292	1,060	1,230	217	411	2,280	2,250	554	2,210	4,040	1,720	1,970
B	1.22	NM	NM	1.28	1.23	<10.0	<10.0	1.49	<10.0	<10.0	<10.0	<10.0
Ba	2.18	4.33	4.44	0.99	1.65	3.28	3.32	1.26	2.69	3.37	9.37	11.0
Ca	2,390	4,150	4,200	109	2,390	3,350	3,490	2,150	3,040	2,870	368	403
Cd	<0.010	NM	NM	<0.010	<0.010	<0.100	<0.100	<0.010	<0.100	<0.100	NM	NM
Cr	2.58	4.34	4.85	3.52	32.0	54.8	53.7	86.0	103	198	27.4	29.8
Cu	11.6	20.8	23.0	1.33	11.9	25.9	24.6	15.1	24.7	38.5	19.4	21.9
Fe	1,670	4,470	5,220	141	1,040	2,810	3,290	328	1,490	3,560	5,510	4,950
K	392	303	422	321	272	16.4	5.23	290	265	247	918	985
La	27.8	NM	NM	2.84	18.6	239	269	39.2	NM	NM	<10.0	<10.0
Li	<10.0	NM	NM	<10.0	<10.0	<1.00	<1.00	<10.0	<1.00	<1.00	<10.0	<10.0
Mg	309	256	268	203	4,830	4,460	4,040	4,410	4,090	4,180	280	316
Mn	8,850	7,060	7,370	2,670	1,330	1,280	1,150	1,300	1,280	922	5,130	4,190
Na	30,100	24,900	15,400	33,700	26,500	28,200	25,900	30,400	29,800	28,500	44,300	47,800
Nd	7.13	NM	NM	0.61	4.58	10.77	9.84	10.71	NM	NM	NM	NM
Ni	121	117	123	100	2,940	3,160	2,850	3,160	3,180	3,960	732	659
P	0.86	<1.00	<1.00	1.04	1.13	1.54	1.86	1.56	<10.0	<10.0	14	20.6
Pb	4.10	4.73	5.14	0.17	0.61	2.29	2.01	2.31	4.15	18.9	6.73	9.91
Pd	0.16	0.123	0.122	0.21	0.16	0.18	0.13	0.18	<0.100	<0.100	<1.00	<1.00
Rh	2.97	15.9	10.4	9.21	10.7	18.4	15.0	12.0	36.0	78.3	30.5	31.4
Ru	106	174	125	25.6	181	229	206	289	330	453	54.1	65.9
S	645	439	446	880	572	453	482	672	599	513	583	622.7
Si	23.5	52.3	55.8	38.3	17.4	132	68.8	67.4	121	103	44.4	77.8
Sr	4.17	NM	NM	2.32	3.06	NM	NM	2.99	41.6	77.3	NM	NM
Ti	<0.010	<0.100	<0.100	<0.010	<0.010	<0.100	<0.100	<0.010	<0.100	<0.100	0.700	0.867
Zn	25.7	30.3	33.7	0.400	28.6	34.1	34.0	39.6	42.8	64.6	22.0	27.1
Zr	6.29	20.9	23.8	22.6	14.5	60.9	62.0	17.7	38.3	50.7	195	208

Table 3-11. Major Components: SRAT Product % of Element Dissolved

Run	Al	Fe	Na	Mg	Mn
GF34 HiFeHiMn	1.3	2.1	87.5	31.0	90.8
GF34b HiFeHiMn	0.0011	7.3	90.8	33.3	93.8
GF34c HiFeHiMn	0.0010	8.5	92.7	34.1	99.9
GF35SB7A	0.6	0.3	92.9	22.7	22.7
GF36 HiFeLoMn	2.0	1.5	88.2	84.0	84.6
GF36b HiFeLoMn	12.9	4.4	88.2	84.0	84.6
GF36c HiFeLoMn	12.7	5.1	108.6	83.2	103.4
GF37 LoFeLoMn	1.1	1.2	94.9	89.0	93.1
GF37b LoFeLoMn	4.8	6.3	108.8	88.1	110.2
GF38 LoFeLoMn	9.4	16.2	109.6	95.8	86.0
GF40	6.0	20.1	99.7	48.7	58.8
GF41	9.3	21.7	102	68.2	56.1

3.2.3.2 SRAT Anion Data

Ion Chromatography using weighted dilutions of samples (not the AD acid strike oxalate method) was performed on both the slurry and supernate from all SRAT and SME products. The slurry results are summarized in Table 3-12. The slurry samples were filtered and the supernate results of these analyses are summarized in Table 3-13. SRAT Product Filtrate PSAL Anion Data, mg/L Supernate Basis

Anion balance data for nitrite, nitrate, formate and glycolate are presented in the table below for all runs (Table 3-14).

The SRAT and SME product oxalate results are of particular interest. The starting sludge contained about 800 mg/kg oxalate, which could be partially destroyed catalytically during the SRAT cycle. In the glycolic/formic flowsheet runs, however, oxalate was being created. The glycolic acid is likely oxidized to glyoxylic acid ($HCOCO_2H$) by nitrite, which is further oxidized to oxalic acid by the reduction of mercury. However, more experiments are needed to pinpoint the reaction pathways.

Table 3-12. SRAT Product Slurry PSAL Anion Data, mg/kg Slurry Basis

Run	Formate	Chloride	Nitrite	Nitrate	Sulfate	Oxalate	Glycolate
GF34	<100	650	<100	57,150	1,250	1,990	44,850
GF34b	<100	649	<100	54,450	1,910	4,970	46,450
GF34c	<100	717	<100	53,900	2,720	5,860	50,000
GF35	<100	572	<100	43,450	1,910	4,370	39,850
GF36	<100	622	<100	57,500	1,210	3,955	37,250
GF36b	<100	591	<100	56,650	1,280	3,190	51,250
GF36c	<100	602	<100	56,350	1,240	3,210	53,100
GF37	<100	821	<100	56,550	1,500	2,755	42,200
GF37b	<100	590	<100	52,500	1,445	2,420	55,450
GF38	<100	583	<100	56,900	1,420	2,655	77,850
GF40	<100	<500	<100	48,200	1,780	17,000	49,200
GF41	<100	<500	<100	41,700	1,220	13,300	48,600

Table 3-13. SRAT Product Filtrate PSAL Anion Data, mg/L Supernate Basis

Run	Formate	Chloride	Nitrite	Nitrate	Sulfate	Oxalate	Glycolate
GF34	<100	894	<100	80,500	2,250	1,570	56,300
GF34b	<100	806	<100	71,000	2,280	6,310	58,400
GF34c	<100	931	<100	70,900	3,520	7,730	66,500
GF35	<100	823	<100	63,700	2,790	3,800	48,600
GF36	<100	858	<100	86,300	2,170	3,250	46,700
GF36b	<100	736	<100	74,000	1,530	4,060	64,500
GF36c	<100	783	<100	74,300	1,610	4,240	70,700
GF37	<100	913	<100	82,100	2,740	3,860	61,300
GF37b	<100	772	<100	70,900	1,850	3,030	72,500
GF38	<100	746	<100	77,300	1,790	3,605	98,100
GF40	<500	<500	<500	60,400	1,910	11,100	50,300
GF41	<500	<500	<500	76,100	2,340	14,700	57,500

Table 3-14. SRAT Cycle Anion Balance Data, %

Run	Nitrite Destruction	Glycolate Destruction	Nitrite to Nitrate Conversion	SRAT Oxalate Generation
GF34	100	32.8	54.7	623
GF34b	100	29	40	1700
GF34c	100	25.9	37.2	2010
GF35	100	26	14.7	-49.4
GF36	100	42.6	27.1	1,420
GF36b	100	20.1	32.9	1,140
GF36c	100	16.7	31.9	1,150
GF37	100	27.4	49.5	867
GF37b	100	9.8	19.9	-18
GF38	100	-12.4	18.3	-11.1
GF40	100	-5.7	65.9	22.5
GF41	100	0.81	41.5	17.1

As a result of uncertainty of the anion analyses, four samples were submitted to AD for both TOC and anion analysis. The data below (Table 3-16) shows the results from both PSAL and AD for comparison. The agreement is fairly good, with the exception of the glycolate and oxalate. In addition, the carbon species (formate, oxalate, glycolate) were converted to carbon concentrations and summed to estimate the Total Organic Carbon (TOC) result for each sample. These results were compared to the AD measured TOC result. It is obvious that the TOC predicted from the PSAL results agreed well with the TOC measurement.

Table 3-15. % Anion Dissolved in SRAT Products

Run	Chloride	Glycolate	Nitrate	Oxalate	Sulfate	Sulfate (S)*
GF34	101.7	92.9	104.1	58.2	133.1	96.1
GF34b	99.6	59.3	98.7	41.6	114.8	78.5
GF34c	99.9	60.0	106.2	51.4	88.4	80.6
GF35	94.9	91.7	110.4	65.4	110.1	108.0
GF36	108.2	93.8	112.4	61.5	134.2	92.8
GF36b	98.5	97.9	101.6	99.0	92.9	88.9
GF36c	103.2	103.8	102.7	102.9	101.1	92.2
GF37	96.8	111.4	111.3	107.3	139.9	109.1
GF37b	101.3	101.8	105.2	97.7	99.4	109.6
GF38	104.8	98.3	105.9	105.8	98.5	109.6
GF40	85.2	60.1	94.1	61.1	103.6	103.4
GF41	101.9	65.5	94.4	93.8	157.2	101.7

* Sulfate (S) is a calculation of SO_4 from measured ICP-AES Sulfur analysis

Table 3-16. SRAT Product AD and PSAL Anion with Comparison to AD TOC, mg/kg

Analyte	GF36b	GF36c	GF37b	GF38
PSAL glycolate	50,200	55,100	55,500	77,900
AD Glycolate	33,900	34,400	35,900	54,500
PSAL Oxalate	3,160	3,300	1,340	2,390
AD Formate	<500	<500	<500	<500
PSAL Formate	<100	<100	<100	<100
PSAL Calculated TOC	20,900	24,100	24,100	32,400
AD Calculated TOC	11,500	11,500	11,900	18,100
AD Measured TOC	19,700	28,600	24,500	26,200

3.2.3.3 SRAT Condensate

Samples collected during SRAT dewater, and the liquid remaining post SRAT in the MWWT and FAVC were analyzed. The results are summarized in Table 3-17 for the SRAT dewater, Table 3-18 for the MWWT and Table 3-19 for the FAVC. Note that no samples were analyzed for duplicate runs.

Table 3-17. SRAT Dewater Composition, mg/L

Analyte	GF34	GF35	GF36	GF37	GF40	GF41
Ca	1.78	0.456	0.603	0.641	<10.0	<10.0
Cd	<0.100	<0.100	<0.100	<0.100	NM	NM
Hg	NM	NM	NM	NM	556	553
K	<10.0	<10.0	<10.0	<10.0	15.85	16.45
Na	NM	NM	NM	NM	30.0	105
Si	99.0	8.68	25.9	220	1,100	1,660
NO_3^-	8,150	7,940	4,670	4,600	32,000	50,200
SO_4^{2-}	143	123	<100	<100	277	<100
$C_2O_4^{2-}$	<100	<100	<100	<100	278	<100
$C_2H_3O_3^-$	<100	<100	<100	<100	<100	118
HCO_2^-	<100	<100	<100	<100	<100	179
Density, g/mL	NM	NM	NM	NM	1.0160	1.0101
pH (unitless)	NM	NM	NM	NM	0.51	0.35

Note: The following were less than detection limits: Al, B, Ba, Cd, Cr, Cu, Fe, Mg, Mn, Ni, P, Pb, Pd, Rh, Ru, S, Ti, Zn, Zr, F^-, Cl^-, NO2-, HCO_2^-. NM is not measured.

Table 3-18. Post SRAT MWWT Composition

Analyte	GF40	GF41
Ca	3.89	4.95
Hg	36.6	61.8
K	14.9	31.8
Na	8.85	6.44
Si	606	957
NO_3^-	22,000	21,400
Density	1.0058	1.0059
pH	0.74	0.75

Note: The following were less than detection limits: Al, Cr, Cu, Fe, Mg, Mn, Ni, P, S, Ti, Zn, Zr, NO_2^-, SO_4^{2-}, $C_2O_4^{2-}$, HCO_2^-

Table 3-19. Post SRAT FAVC Composition

Analysis	GF40	GF41
NO_2^-	<100	<100
NO_3^-	213,000	192,000
SO_4^{2-}	<100	144
HCO_2^-	<100	<100
$C_2O_4^{2-}$	234	171
$C_2H_3O_3^-$	<100	<100

Note: The following were less than detection limits: F^-, Cl^-

3.2.3.4 Nitrogen Balance

A nitrogen balance was completed for GF41. In this balance, it is assumed that the nitrogen in air does not participate in any reactions. As a result, the nitrogen in the slurry as nitrate and nitrite, the nitrate in the ammonia scrubber solution, the added nitrate from the nitric acid, the nitrate present in the SRAT product, ammonia scrubber solution and condensate (dewater, MWWT, and FAVC), and the nitrogen from the measured NO, NO_2, and N_2O. The total balance has 0.363 moles N_2 more than was added to the original sludge (1.6% more nitrate post run). The balance is summarized below in Table 3-20. Note that the nitrite is completely destroyed producing nitrate in the SRAT product (42% of nitrite), condensate (26% of nitrite), and ammonia scrubber solution (24% of nitrite). A smaller contribution comes from the NO, NO_2, and N_2O in the offgas (15% of nitrite).

Table 3-20. GF41 Nitrogen Balance

	Moles N			
	Feed	Added	Product	Delta
Slurry Nitrite	1.040	0.000	0.000	-1.040
Slurry Nitrate	0.492	2.677	3.601	0.432
Nitrate in Condensate	0.000	0.000	0.272	0.272
Nitrate in Scrubber	0.011	0.000	0.261	0.250
N_2O in offgas	0.000	0.000	0.035	0.035
NO in offgas	0.000	0.000	0.091	0.091
NO_2 in offgas	0.000	0.000	0.032	0.032
NH3 in Scrubber	0.000	0.000	0.007	0.007
Total	1.544	2.677	4.292	0.071

3.2.3.5 Other SRAT Data

Other SRAT product data are summarized in Table 3-21.

Table 3-21. Other SRAT Product Data

Run	Total Solids, wt%	Insoluble Solids, wt%	Calcined Solids, wt%	Soluble Solids, wt%	pH	Slurry Density, g/mL	Supernate Density, g/mL	NH_4^+, mg/L
GF34	31.5	17.7	18	13.8	4.35	1.25	1.11	30
GF34b	27.3	14.2	15.4	15.2	3.58	1.20	1.10	NM
GF34c	27.3	13.7	15.3	15.7	3.38	1.19	1.11	NM
GF35	29.6	17.7	17.6	12.0	6.85	1.23	1.10	9
GF36	30.3	17	16.7	13. 3	4.22	1.21	1.11	18
GF36b	27.6	13.7	15.0	13.9	4.05	1.20	1.11	NM
GF36c	27.7	13.3	15.1	14.4	4.23	1.21	1.11	NM
GF37	29.7	14.9	16.1	14. 8	4.32	1.21	1.11	20
GF37b	28.1	13.4	15.1	14.8	4.28	1.20	1.11	NM
GF38	27.9	12.4	14.0	15.5	3.47	1.20	1.12	NM
GF40	27.6	10.2	14.4	17.4	4.84	1.21	1.13	<10
GF41	27.6	7.53	13.7	20.1	5.01	1.22	1.15	<10

Ammonia was below detection limit of 5 mg/L in ammonia scrubber samples. SRAT products were slightly above the detection limit (Table 3-21) as were some SME products, though the concentrations were smaller.

3.2.4 *SME Data*

SME data is discussed in this section.

3.2.4.1 SME Elemental Data

General SME product sample data for the four runs (GF34, GF35, GF36 and GF37 had SME cycles) are tabulated below. The waste loading for these runs was targeted at 36% using frit 418. Elemental analyses were completed of both the slurry and supernate from all SME products. The slurry results are summarized in Table 3-22. Conversion of the elemental data to the expected oxide form allows summing the oxides as a measure of both complete sample dissolution and accurate analysis of the major elements in the sludge product. The sum of oxides range for 98.6-100.5 over this data set (95-105 is considered acceptable). The slurry samples were filtered and the supernate results of these analyses are summarized in Table 3-23.

Table 3-22. SME Product Slurry Elemental Data, wt % calcined solids basis

Run	GF34	GF35	GF36	GF37	GF40	GF41
Al	3.35	5.47	3.4	9.00	5.06	5.03
B	1.32	1.40	1.30	1.30	1.50	1.59
Ba	0.031	0.041	0.036	0.026	0.027	0.023
Ca	1.28	0.25	0.680	0.651	0.304	0.300
Cd	<0.010	<0.010	<0.010	<0.010	NM	NM
Cr	0.016	0.037	0.119	0.103	0.017	0.016
Cu	0.035	0.037	0.035	0.029	0.013	0.015
Fe	11.8	7.4	11.9	4.85	4.08	3.45
K	0.063	0.048	0.041	0.049	0.174	0.173
Li	2.20	2.31	2.27	2.18	NM	NM
Mg	0.152	0.145	0.924	0.858	0.115	0.102
Mn	1.44	1.79	0.231	0.220	1.35	1.13
Na	8.60	9.23	8.60	9.06	11.2	10.8
Ni	0.073	1.21	1.00	0.92	0.58	0.49
P	<0.100	<0.100	<0.100	<0.100	<0.100	<0.100
Pb	0.038	0.014	0.036	0.035	<0.100	<0.100
Pd	<0.100	<0.100	<0.100	<0.100	<0.100	<0.100
Rh	0.017	0.018	0.027	0.025	<0.100	<0.100
Ru	0.015	0.024	0.034	0.023	<0.100	<0.100
S	0.099	0.116	0.102	0.114	0.075	0.082
Si	23.35	24.3	23.45	22.9	25.0	26.2
Sn	<0.010	0.013	0.044	0.038	NM	NM
Ti	0.007	0.013	0.012	0.008	0.064	0.066
Zn	0.026	0.027	0.028	0.026	0.017	0.016
Zr	0.026	0.103	0.051	0.024	0.182	0.173

Table 3-23. SME Product Supernate Elemental Data, mg/L supernate basis

Run	GF34	GF35	GF36	GF37	GF40	GF41
Al	178	343	320	922	2,240	2,680
B	54. 0	55.0	48.0	47.2	<10.0	<10.0
Ba	2.22	1.06	1.68	1.35	14.3	16.5
Ca	2,090	169	2,110	1,960	399	419
Cd	<0.010	<0.010	<0.010	<0.010	NM	NM
Cr	1.93	7.03	34.6	69.4	35.3	37.7
Cu	5.82	3.16	12.8	16.7	27.0	28.8
Fe	1,280	326	1,200	973	10,100	12,250
K	396	311	252	212	991	1,095
La	18.2	10.2	17.6	36.6	NM	NM
Li	2670	216	234	183	352	376
Mg	315	223	4,660	3,460	5,230	4,680
Mn	8,610	3,620	1,280	998	46,300	52,800
Na	29,500	37,000	24,750	25,500	46,300	52,800
Ni	114	226	2,800	2,490	1,070	868
P	0.77	2.49	1.02	1.87	10.2	10.8
Pb	4.01	0.30	0.81	2.01	15.7	19.1
Pd	0.18	0.24	0.14	0.13	<1.00	<1.00
Rh	2.83	12.2	12.6	7.95	36.7	37.9
Ru	86.8	35.3	166	205	85	97
S	679	874	575	516	715	755
Si	30.6	102	27.6	71.5	62.3	86.7
Sr	4.22	2.67	3.05	2.77	NM	NM
Ti	<0.010	<0.010	<0.010	<0.010	0.938	1.194
Zn	20.6	2.40	28.4	17.0	41.9	44.2
Zr	5.25	38.0	32.1	22.2	261	258

3.2.4.2 SME Anion Data

Ion Chromatography was completed for both the slurry and supernate from all SME products. The slurry results are summarized in Table 3-24. The slurry samples were filtered and the supernate results of these analyses are summarized in Table 3-25. Anion balance data for nitrite, nitrate, formate and glycolate are presented in the table below for all runs (Table 3-26).

The anion data is inconsistent. For example, in Run GF37, the data indicates there was high nitrite to nitrate conversion in the SRAT and high nitrate loss in the SME. Also, it indicates that glycolate was destroyed in the SRAT and generated in the SME. It is more likely that there was a lower nitrite to nitrate conversion and lower glycolate loss in the SRAT with minimal nitrate and glycolate loss in the SME. The inconsistent results is likely due to fouling of the IC columns by metals and oxalate that are soluble at pH 4 but insoluble at pH 10 (approximately sample of eluent). It is recommended that removal of metals with an appropriate guard column be considered. An anion round robin has been initiated to resolve the issues with the analytical technique.

Table 3-24. SME Product Slurry Anion Data, mg/kg Slurry Basis

Run	GF34	GF35	GF36	GF37	GF40	GF41
Chloride	525	445	494	821	500	500
Nitrite	<100	<100	<100	<100	<100	<100
Nitrate	43,650	34,750	43,650	56,550	48,200	41,700
Sulfate	1,060	1,470	1,000	1,500	1,780	1,220
Oxalate	1,670	3,290	4,150	2,755	17,000	13,300
Glycolate	37,250	30,750	28,200	42,200	49,150	48,600
Formate	1,405	2,330	1,720	<100	<100	<100
Phosphate	<100	<100	<100	<100	<100	<100

Table 3-25. SME Product Filtrate Anion Data, mg/L Supernate Basis

Run	GF34	GF35	GF36	GF37	GF40	GF41
Formate	<100	<100	<100	<100	<500	<500
Chloride	892	770	884	726	<500	<500
Nitrite	<100	<100	<100	<100	<500	<500
Nitrate	79,100	58,200	84,750	60,100	94,000	84,000
Sulfate	2,345	2,825	2,710	2,570	2,330	2,540
Oxalate	1,620	4,845	3,960	3,395	10,400	13,500
Glycolate	59,400	42,150	45,550	45,600	60,400	58,500
Formate	1,715	3,785	2,251	1,940	<500	<500
Phosphate	<100	<100	<100	<100	<500	<500

Table 3-26. SME Anion Balance Data, %

	GF34	GF35	GF36	GF37	GF40	GF41
SME Nitrate Destruction	9.9	-2.5	10.1	21.8	6.5	15.6
SME Glycolate Destruction	5.3	15.1	4.9	35.8	22.2	14.3
SME Formate Destruction	41.5	61.8	42.6	62.2	0.0	0.0

3.2.4.3 SME Condensate

The SME condensate was not analyzed for GF34-38. However, GF40 and GF41 SME condensate samples were collected. Each sample was analyzed for elementals via ICP-AES, and anions via IC. The condensate was very low in anions and cations. The largest component is the silicon, likely an antifoam degradation product, not frit, as the same concentration was seen in the SRAT condensate. Note also that the pH of the SME condensate is considerably higher than the SRAT condensate. The SME dewater results are summarized in Table 3-27.

Table 3-27. SME Condensate, mg/L

Analyte	GF40	GF41
Hg	24.6	15.4
K	14.6	14.5
Na	15.3	8.62
Si	1,455	553
Ti	<1.00	<1.00
NO_3^-	329	125
Density	0.9976	0.9970
pH	3.28	3.39

Note: The following were less than detection limits: Al, Ca, Cr, Cu, Fe, Mg, Mn, Ni, P, S, Ti, Zn, Zr, NO_2^-, SO_4^{2-}, $C_2O_4^{2-}$, $C_2H_3O_3^-$, HCO_2^-

3.2.4.4 Other SME Data

Other SME product data are summarized in the Table 3-28. Of particular note is that the GF37 SME was not completed prior to kettle breakage. As a result, the total solid result of the recovered product is significantly lower than had been targeted. Also, no analyses were completed on the SME condensate from Runs GF34-GF37.

Table 3-28. Other SME Product Data

Run	GF34	GF35	GF36	GF37	GF40	GF41
Total Solids, wt%	48.8	46.3	45.8	39.3	49.8	54.0
Insoluble Solids, wt%	37.9	37.6	35.3	29.7	36.9	41.0
Calcined Solids, wt%	38.5	37.3	35.8	29. 7	38.0	42.9
Soluble Solids, wt%	10.9	8.71	10.5	9.53	12.9	13.0
pH	4.66	6.18	4.39	4.31	4.76	4.81
Slurry Density, g/mL	1.42	1.34	1.38	1.29	1.137	1.150
Supernate Density, g/mL	1.11	1.10	1.10	1.09	1.243	1.234
Ammonium, mg/L	14	<5	<5	7	<10	<10

Note: GF40 and GF41 SME products were too thin and the frit settled quickly. It was difficult to maintain a uniform mixture. Higher total solid targets are recommended in future processing of underwashed sludges as significantly less insoluble solids are present in the SME product, as the sodium is included in the waste loading calculation.

3.2.5 *Supernate Chemistry -- Dissolution of Metals and Solubility of Anions*

One of the major unknowns revolving around the glycolic flowsheet is what is happening to the anions and cations during and after processing. The addition of glycolic acid and the ability to keep the pH low throughout SRAT and SME processing combine to dissolve insoluble metal species leading to higher concentrations of metals in solution. However in these runs, we have also seen crystalline solids form during storage, after the SRAT and SME cycles were complete. A photo below (Figure 3-17) shows the solids formation in some of the SRAT products.

Figure 3-17. Photo of SRAT Product Samples 11/30/2011 (4 days after SME cycle)

It should be noted that the solids formed primarily on the surface of the sample bottle and were easily reincorporated into the slurry by gentle mixing. The samples from GF34, GF35, GF36 and GF37 SRAT and SME products were submitted to SRNL/AD and identified as Gibbsite (γ-$Al(OH)_3$), Quartz (SiO_2), Bayerite (α-$Al(OH)_3$), Boehmite (γ-AlO(OH)), and Goethite (α-FeOOH). Note that there were no crystals noted in the GF35 (SB7A) simulant, only in some of the matrix simulants. The X-ray Diffraction (XRD) results are summarized in Appendix C.

3.2.5.1 SRAT Supernate Chemistry

The composition of the SRAT product slurry and supernate anions is summarized in Table 3-12, Table 3-13. SRAT Product Filtrate PSAL Anion Data, mg/L Supernate Basis
and Table 3-14. Figure 3-18 and Figure 3-19 show the amount of each element found in the SRAT product supernate expressed as a percentage of the total element present. These data are calculated by dividing the supernate concentration (converted to mg/kg on a slurry basis) by the total slurry fraction of each element (converted to mg/kg). Numbers greater than 100% are not physically possible and are a result of error in one of the analytical measurements used in the calculation.

The % solubility of each anion is approximately 100% (80-120% based on method uncertainty), except for oxalate, which had a solubility of approximately 60% in the GF34 and GF35 runs. The solubility of Al and Fe was low in all runs. The solubility of Na, Mg, and Mn are all high in the glycolic flowsheet runs. For most of the metals, which are present primarily as hydroxides and oxides in the sludge, the concentration in the supernate increases throughout the SRAT cycle, but appear to be constant by the end of the SRAT cycle. Samples were pulled at the completion of nitric acid addition, midway through glycolic acid addition, after completing glycolic acid addition, one-hour into dewater, post dewater, 4 hours into reflux and 8 hours into reflux. These samples were centrifuged soon after being pulled to make sure no further reactions occurred due to insoluble solids. One interesting observation is that the centrifuged GF37b samples (100% acid stoichiometry) had almost no supernate after centrifuging at the completion of dewater (0.3 g of supernate typical in these samples). Prior to dewater and throughout run GF38 approximately 6-7 g of supernate was easily removed after centrifuging.

Based on this data, the order of dissolution for the "major components" is: Hg>Ca>Mn>Ni>Mg>Al>Fe. The data is summarized for major metals (>1,000 g/L) in Figure 3-18 and minor metals in Figure 3-19. The graphs show the approach to maximum solubility, defined as 100% for each element on these graphs. This does not indicate that 100% of these individual elements went into solution during processing.

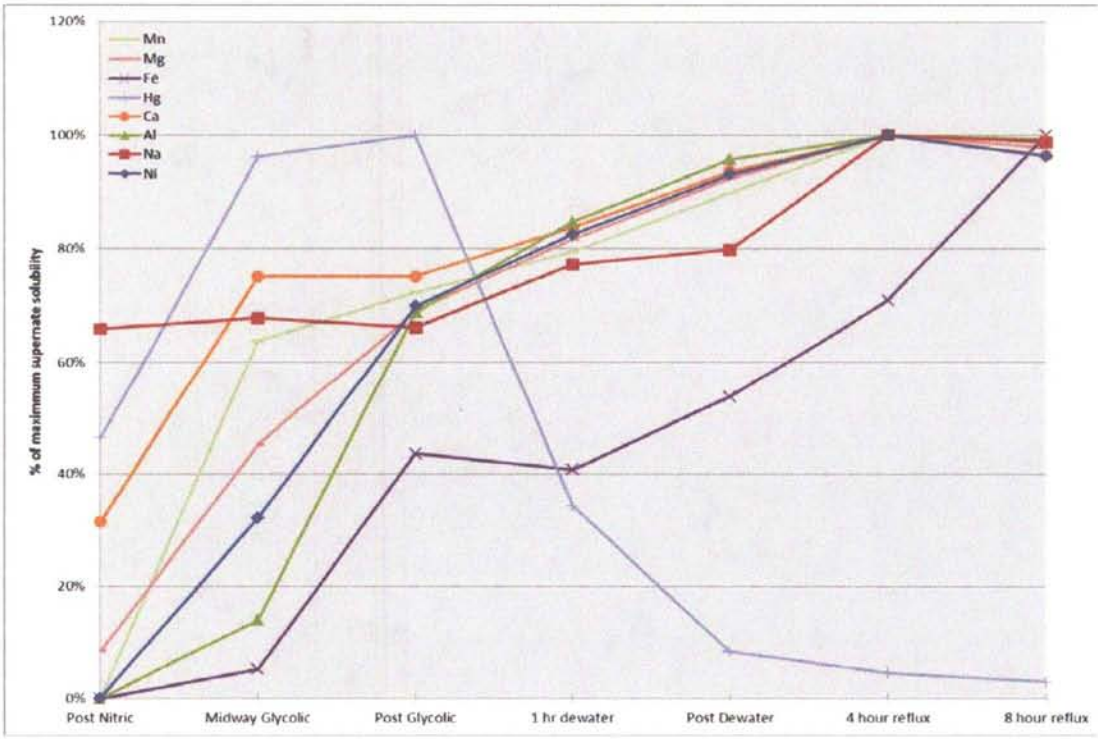

Figure 3-18. Order of Dissolution of "Major Metals" During SRAT Processing

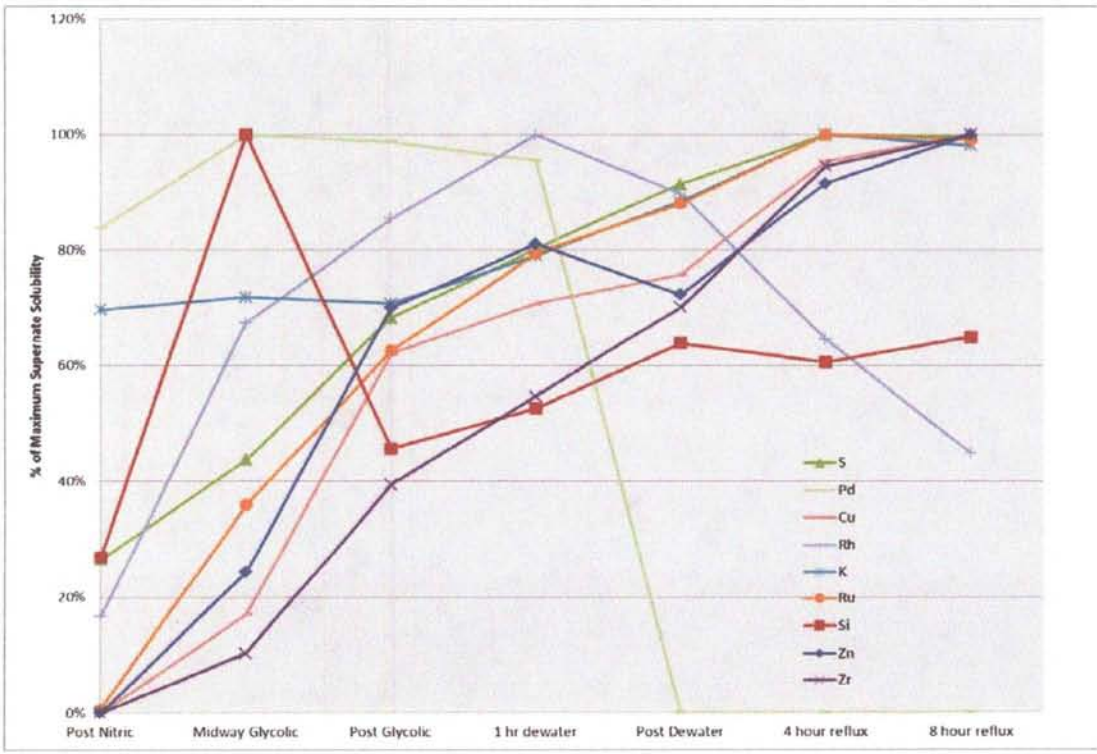

Figure 3-19. Order of Dissolution of "Minor Metals" During SRAT Processing

Several metals are of particular interest during SRAT processing. Note that mercury is discussed in Section 3.2.2. The reduction of Mn is important especially in the melter and cold cap in order to minimizing foaming in the melter. As can be seen in Figure 3-18, the Mn is dissolved (and likely reduced) early in the SRAT cycle and is >90% of the maximum solubility by the end of dewater. There are several metals that are essentially totally soluble such as Na, K, and Ca. The concentration of each metal changes as the metal is first diluted during acid addition, then concentrated during the dewater phase. In addition, the concentration of soluble metals should remain constant throughout the post dewater stage of the SRAT cycle. In GF37b, the concentration of both Na and Ca increased during this time, likely due to the extended centrifuge time necessary to squeeze out the 0.3 g of supernate from a 15 mL centrifuge tube. Note that for the lower acid run, GF37b, the calcium was not completely soluble until midway through glycolic acid. This may indicate that it may take more than 100% acid stoichiometry to produce a SRAT product that is easily concentrated in the SME.

In order to understand the dissolution of metals and the timing of their dissolution, additional samples were pulled during runs GF37b and GF38 (LoFeLoMn sludge). The dissolution of Hg is discussed in the mercury section.

3.2.5.2 SME Supernate Chemistry

The main change in supernate chemistry during the SME cycle is that formic acid is added to the frit slurry to prevent caking. Formic acid is very reactive in DWPF SRAT and SME processing, ultimately leading to the noble metal catalyzed decomposition to hydrogen and CO_2. No formic acid was added or detected during the SRAT cycle. The solubility of the anions during the SME cycle is summarized in Table 3-29.

Table 3-29. Major Components: SME Product % of Anion Soluble

Run	GF34	GF35	GF36	GF37	GF40	GF41
Formate	68.1	92.5	76.7	67.4	NA	NA
Glycolate	89.0	78.1	94.6	95.8	62.4	57.6
Nitrate	101	95.4	114	101	99.0	96.5
Oxalate	54.1	83.9	55.9	77.4	31.1	48.6
Sulfate	123	109	159	136	66.4	99.7
Sulfate (S)	98.9	115.0	91.9	98.4	128	103

* Sulfate (S) is a calculation of SO_4 from measured ICP-AES Sulfur analysis

Frit 418, nominally containing 8% B_2O_3, 8% Li_2O, 8% Na_2O, and 76% SiO_2, is added in the SME cycle. The added frit components are very insoluble, with the concentration of B, Li and Si <1% in the six SME cycles. In addition, the Na solubility drops from near 100% in the SRAT cycle to 50-60% by the time the SME cycle is complete due to the insoluble sodium in the frit. The solubility of the elements is summarized in Table 3-30. Note that the solubility of aluminum and iron are much higher and the solubility of magnesium and manganese are lower in the underwashed sludges (GF40 and GF41) compared to the matrix sludges (GF34-GF37).

Table 3-30. Major Components: SME Product % of Element Dissolved

Run	Al	Fe	Na	Mg	Mn
GF34 HiFeHiMn	0.8	1.6	49.5	30.0	86.7
GF35SB7A	1.0	0.7	61.1	23.4	30.8
GF36 HiFeLoMn	1.5	1.7	47.3	82.6	90.8
GF37 LoFeLoMn	2.2	4.4	61.2	87.5	98.5
GF40	5.9	33.1	55.3	41.0	51.6
GF41	6.0	39.7	54.6	41.2	46.3

3.2.5.3 Post Processing Supernate Chemistry

The formation of crystals in some of the SRAT and SME products could have been caused by continuing reactions after completion of CPC simulations or by changes in solubility caused by the lower temperature during storage. The addition of nitric and glycolic acid may have dissolved some species (i.e. Al and Fe) to solubility at 102°C, then the species became supersaturated upon cooling (15-20°C). Crystal growth can be slow or fast. If crystal growth is fast, the crystals found have likely peaked, whereas with flow crystal growth the crystals can continue increasing.

3.2.5.4 Improved Understanding of Supernate Chemistry

OLI software has become the industry standard for simulation of electrolyte systems. However, the OLI database lacks many of the components needed to simulate the electrolyte systems in a SRAT or SME product. As a result, DWPF[20] has requested that OLI "Update OLI database to include glycolate species and validate updated database against the latest SRNL test data".

The solubilities of all components are needed to evaluate the capability of OLI to predict solubility. The change in solubility over time will also be useful because the trend versus time will give an indication of kinetic effects (OLI ignores kinetics and assumes equilibrium in its calculations). However, if a component remains soluble for a short time (compared to the equilibrium assumption), it may remain soluble until fed to the melter.

A much more rigorous data collection program will be needed to compare the OLI predictions to sample results. It is useful to know the solubility of metals as a function of temperature to validate the OLI models. Supernate samples taken at temperature by the centrifuge method should be analyzed for total metals and dissolved metals. In addition, the temperature of the supernate when removed from the centrifuge tube should be recorded to determine the solubility at that temperature. The time between taking samples and analyzing them should be recorded and noting whether there are changes in the solubility versus time. Other data needed includes concentrations of dissolved anions including carbonate, concentrations of undissolved anions (including oxalate, sulfate, and phosphate), concentrations of metal cations, pH and the temperature pH was taken.

In addition, it is necessary to understand whether changes are occurring during storage. Crystals were noted in several early runs that had been over-concentrated. Periodic analysis of SRAT and SME products is needed to understand the kinetics of any crystal growth during storage.

3.2.6 *SRAT and SME Rheology*

Flow curves for the four initial SRAT and SME slurry products were obtained by using a Haake RS600 rheometer and the current DWPF simulant rheology protocol.[21] The up and down curves were fit to a Bingham plastic model to determine yield stress and consistency. Down flow curve

data are the generally preferred choice for comparisons between systems. The data for all runs are tabulated below for the SRAT (Table 3-31) and SME (Table 3-32).

Table 3-31. SRAT Product Rheology Summary

SRAT Product Sludge Type	Wt % Insoluble Solids	Up Yield Stress, Pa	Down Yield Stress, Pa	Up Consistency, cP	Down Consistency, cP
DWPF Ranges	10-15	1.5 to 5	1.5 to 5	5 to 12	5 to 12
GF34 Hi Fe-Hi Mn	17.7	1.9	1.9	11.7	11.7
GF35 Lo Fe-Hi Mn	17.7	0.3	0.3	5.7	5.8
GF36 Hi Fe-Lo Mn	17.0	3.7	3.6	16.2	16.8
GF37 Lo Fe-Lo Mn	14.9	10.8	11.0	13.4	13.0
GF40 1.6 M Na	10.2	0.15	0.10	3.05	3.09
GF41 1.9 M Na	7.53	0.08	0.03	3.00	3.04

Table 3-32. SME Product Rheology Summary

Sludge Type	Wt % Insoluble Solids	Up Yield Stress, Pa	Down Yield Stress, Pa	Up Consistency, cP	Down Consistency, cP
DWPF Ranges	20-35	2.5 to 15	2.5 to 15	10 to 40	10 to 40
GF34 Hi Fe-Hi Mn	37.9	9.1	12.2	33.1	26.4
GF35 Lo Fe-Hi Mn	37.6	-0.1	1.5	20.2	11.7
GF36 Hi Fe-Lo Mn	35.3	12.3	15.9	34.8	24.7
GF37 Lo Fe-Lo Mn*	29.7	8.9	11.1	24.6	18.0
GF40	36.9	0.15	0.12	14.2	5.02
GF41	41.0	0.34	1.53	47.1	18.0

The SME products from runs GF35-36 were further concentrated by evaporation to determine the extent of concentration that could be achieved with each SME product (for example GF35-48% means the total solids target was 48%, Insoluble solids was 39.7%). Insufficient material was remaining from run GF37, so no concentration of this sample was completed. The data is summarized in Table 3-33.

Table 3-33. Post Concentration SME Product solids content, wt % total solids basis

Sample #	Insoluble Solids	Sample #	Insoluble Solids
GF35-48%	39.7%	**GF36-48%**	37.4%
GF35-51%	43.1%	**GF36-51%**	39.0%
GF35-54%	46.6%	**GF36-54%**	43.2%
GF35-57%	49.4%	**GF36-57%**	41.6%
GF35-60%	50.6%		

The rheology of these concentrated SME products was analyzed to determine the rheology and the data is summarized in Figure 3-20.

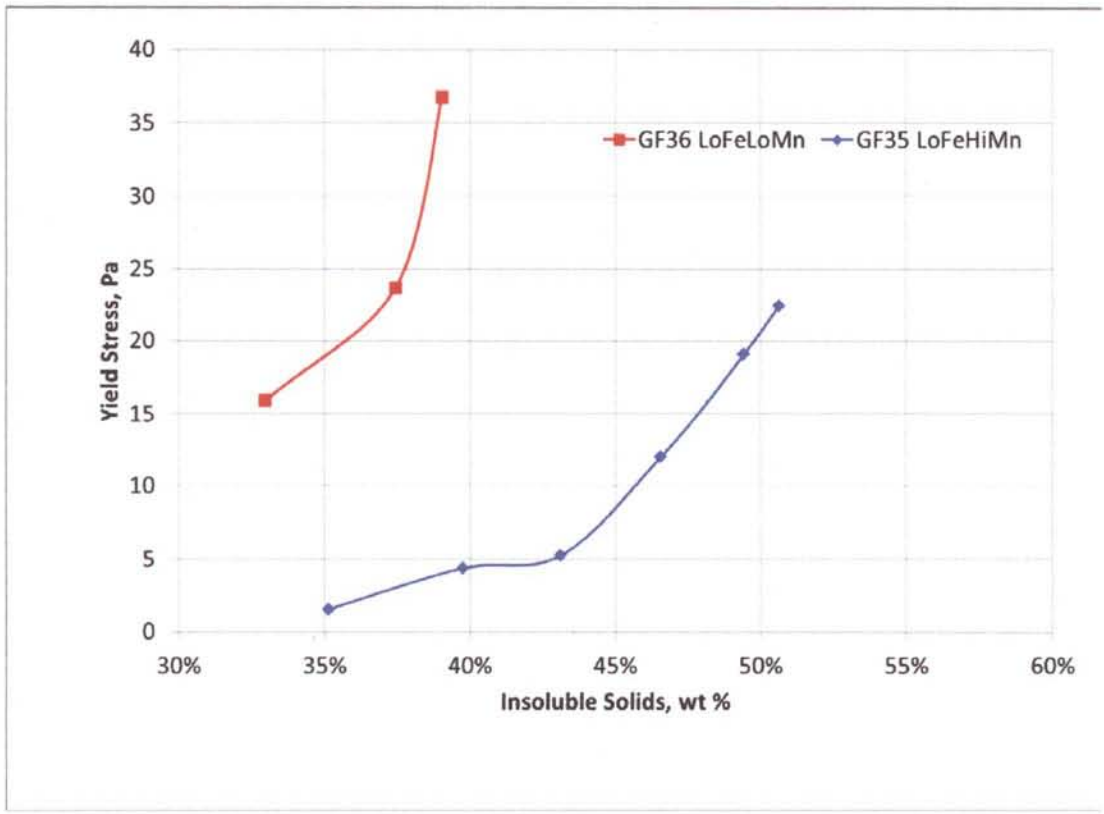

Figure 3-20.SME Product Rheology of Concentrated Subsamples

Lab-scale concentration of the two SME products to high wt% solids was problematic. Several laboratory rig kettles broke during concentration. It was important to mix well and to not have solids buildup during evaporation. The solids buildup led to localized overheating where the solids built up and to subsequent glass breakage. The high agitation speeds needed to mitigate solids buildup also led to breakage of the glassware, especially when the total solids exceeded 60 wt%. However, in most sludge tanks it is expected that the maximum concentration of SRAT and SME product will be significantly higher with the Glycolic-Nitric Flowsheet than with the Baseline Flowsheet.

3.2.7 *SRAT/SME REDOX*

SME products from GF34, GF35, GF36 and GF37 (SME products) were added to an alumina crucible, dried to peanut butter consistency, and vitrified in nepheline sealed crucibles. SRAT product samples from runs GF36b, GF36c, GF37b and GF38 were prepared for the redox measurement by taking the SRAT product and adding frit 418 to produce a waste loading of 36%. The resulting slurry was placed in a crucible, dried to peanut butter consistency and vitrified like the SME product samples from runs GF34, GF35, GF36 and GF37.

The REDOX prediction equation used in this study with an added term for glycolate is:

$Fe^{2+}/\Sigma Fe = 0.2358 + 0.1999 * (2[F] + 4[C] + 6[G] + 4[O] - 5[N] - 5[Mn])*45/T$

Where
[F] = formate (mol/kg feed)
[C] = coal (carbon) (mol/kg feed)
[O] = oxalate (soluble and insoluble) (mol/kg feed)
[G] = glycolate (mol/kg feed)
[N] = nitrate + nitrite (mol/kg feed)
[Mn] = manganese (mol/kg feed)

Values less than zero or greater than one can be calculated with the REDOX equation, because it is a linear regression equation fit to experimental data. Values outside the range of zero to one, however, are physically impossible. A number less than zero can be interpreted as fully oxidized and likewise a number greater than one as fully reduced.

Table 3-34 below shows the appropriate SME product data with the corresponding predicted REDOX values as well as the REDOX as measured. Note that the REDOX equation generally underpredicts the measured REDOX.

Table 3-34. SME product data for REDOX calculations, $Fe^{2+}/\Sigma Fe$

Run	Sludge	Predicted Redox*	Measured Redox
GF34	HiFeHiMn	0.064	0.319
GF34b	HiFeHiMn	0.082	0.400
GF34c	HiFeHiMn	0.145	0.507
GF35	SB7A	0.419	0.506
GF36	HiFeLoMn	0.031	0.280
GF36b	HiFeLoMn	0.178	0.286
GF36c	HiFeLoMn	0.207	0.226
GF37	LoFeLoMn	0.123	0.463
GF37b	LoFeLoMn	0.256	0.559
GF38	LoFeLoMn	0.524	0.665
GF40	2.0M Na	0.298	0.329
GF41	2.5M Na	0.355	0.510

* Predicted REDOX was calculated using measured sample results.

Both LoFe (HiAl) runs had significantly higher measured REDOX than the HiFe runs. The melter feed iron concentration may impact the percentage of iron that is reduced to Fe^{2+}. This may not be as evident in sludge batch processing, as the iron concentration doesn't change as much as the matrix sludges. This may be an important clue in developing a REDOX equation for the glycolic-nitric acid flowsheet.

It is possible that the anion analyses used to predict REDOX were inaccurate. As a result, the GF34, GF35, GF36, and GF37 SME products were reanalyzed and the original results (GF3x#1) and reanalysis (GF3x#2) are summarized in Table 3-35.

Table 3-35. Repeat Analysis of SME anion data for REDOX calculations, $Fe^{2+}/\Sigma Fe$

Result	Nitrate, mg/kg	Formate, mg/kg	Glycolate, mg/kg	Oxalate, mg/kg	SME Predicted Redox
GF34#1	43,650	1,405	37,250	1,670	0.064
GF34#2	44,000	1,420	38,200	5,220	0.106
GF35#1	34,750	2,330	30,750	4,370	0.119
GF35#2	33,300	2,710	29,850	4,525	0.133
GF36#1	43,650	1,720	28,200	4,150	0.031
GF36#2	46,150	1,785	31,450	5,700	0.057
GF37#1	38,450	1,855	30,700	2,830	0.147
GF37#2	39,850	1,680	29,850	4,540	0.125

The reanalysis of the anions did not appreciably change the concentrations or the REDOX predications. A comparison of the original and reanalyzed results is summarized in Table 3-36. Note that oxalate concentrations of three of the four samples changed significantly.

Table 3-36. Change in Anion Concentration due to Reanalysis of SME Product Samples

Anion	GF34	GF35	GF36	GF37
Nitrate	0.8%	-4.2%	5.7%	3.6%
Formate	1.1%	16.3%	3.8%	-9.4%
Glycolate	2.6%	-2.9%	11.5%	-2.8%
Oxalate	212.6%	3.5%	37.3%	60.4%

A 10 ppm spike of nitrate, formate, glycolate, and oxalate was added to each diluted SME product subsample and analyzed by PSAL using the glycolate IC method[16]. The spiked samples were analyzed and the added spike was calculated (Table 3-37). Note that the calculated spike concentration of oxalate increased from 8.17 to 10.85 during this testing. It is likely that recovery of the oxalate from the IC column was not equal to the oxalate added, possibly because the column is "dirty".

Table 3-37. Spiked Recovery of SME Product Samples, mg/kg slurry

Anion	GF34	GF35	GF36	GF37
Nitrate	9.81	9.89	9.82	10.0
Formate	10.35	10.11	10.55	10.7
Glycolate	10.05	10.05	10.2	10.25
Oxalate	8.17	9.34	9.64	10.85

The SME products were also analyzed for TOC. This was compared to calculated TOC concentration based on the analyzed glycolate, formate, and oxalate concentrations, converted to TOC. The data are summarized in Table 3-38. The good agreement between the measured and predicted TOC suggests that the analyses of the oxalate, formate, and glycolate concentrations are accurate enough to predict REDOX. No term was added to the TOC for the antifoam contribution

since it was not measured. Based on the 800 ppm antifoam addition and the fact that the antifoam is about half carbon, the predicted TOC could be as much as 400 ppm higher if an antifoam term was added.

Table 3-38. TOC Analysis and Calculation of SME Product Samples, mg/kg slurry

Anion	GF36b	GF36c	GF37b	GF38
Measured TOC	19,700	28,600	24,500	26,200*
Predicted TOC	21,300	23,900	24,100	26,000

* The analytical result was corrected for added frit in preparing melter feed for REDOX testing.

Based on the anion results and using these to predict REDOX, it is evident that either the anion results are inaccurate or that the REDOX prediction equation is inadequate for the glycolic-nitric flowsheet REDOX prediction. In runs using the two HiFe slurries (GF34 and GF36), the predicted REDOX, although still lower than the measured REDOX, better agreed with the measured REDOX. One question it raises is whether additional terms are needed in this equation to adequately predict REDOX. It is also evident that additional work is needed to improve the current IC method, especially concerning oxalate and glycolate analyses. For instance, the measured glycolate was approximately twice that predicted (and much higher than is possible from the known addition of glycolic acid).

3.2.8 *SRAT pH profile*

Time dependent SRAT/SME pH data were collected for all runs. The graph below, Figure 3-21, shows the pH trends of all runs. The pH stays very stable throughout the SRAT and SME cycles, unlike the Baseline flowsheet where the SME product pH may be as high as 10 or 11. In addition, the pH of the duplicate GF36 runs is included in Figure 3-22 to demonstrate the same pH profile was achieved in all three runs.

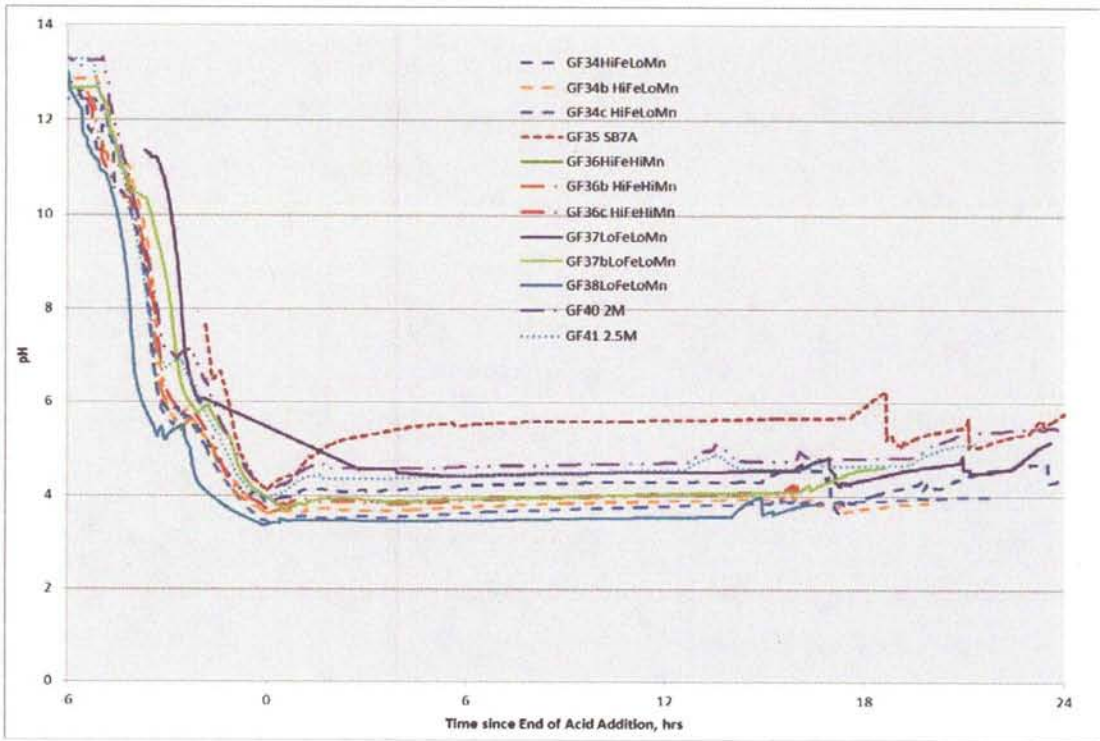

Figure 3-21. pH trends for SRAT and SME Cycles

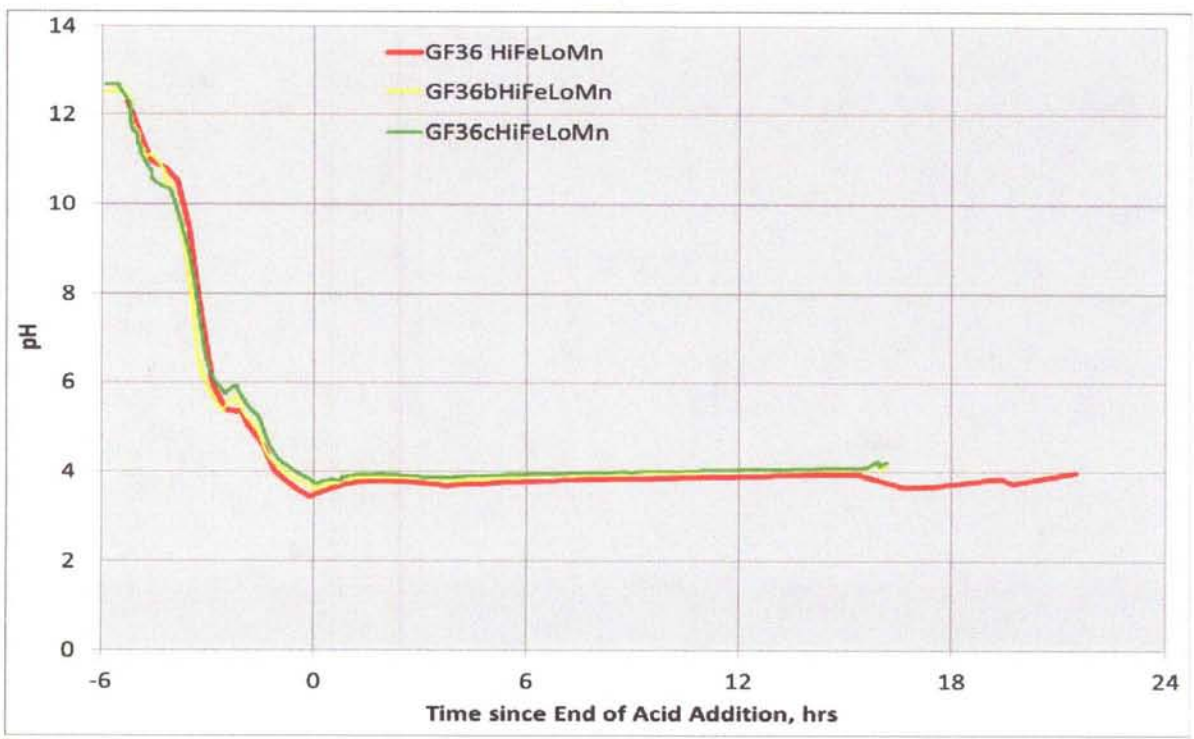

Figure 3-22. pH trends for Duplicate GF36 SRAT Cycles

3.2.9 *Foaming*

Foaminess was not a concern in these runs. The antifoam strategy, 200 ppm before acid addition, 100 ppm after nitric acid addition, 500 ppm at the completion of acid addition and 100 ppm before the start of the SME cycle was more than enough antifoam to control foaming throughout the matrix testing. This is particularly significant since six different simulants containing very different insoluble solids compositions were used in the testing.

Subsequent testing has used a revised antifoam strategy. Since the antifoam is most stable at pH 7, and has good stability from pH 4 to 10, antifoam was not added until the pH dropped below 10 during acid addition. In these tests this was approximately the completion of nitric acid addition. Since DWPF does not have a pH probe in the SRAT, the GC offgas analysis may be useful in determining this point as no foaming is expected until significant offgas generation ensues with the evolution of CO_2 and N_2O. However, the lag time between generation and GC analysis and the lack of CO_2 and N_2O my make this impractical. In these later runs, 100 mg/kg at pH 10, 100 mg/kg prior to SRAT boiling and 100 mg/kg every 12 hours during SRAT processing was sufficient to control foam, even in the underwashed 1.6M and 1.9M Na sludges.

The FTIR was used to monitor the offgas during the GF40 and GF41 runs. HDMSO was detected throughout the SRAT and SME cycle. The HDMSO is a degradation product of the added antifoam and results in decreasing antifoam performance over time. Integration of the HDMSO over the SRAT and SME cycle was used to estimate the antifoam degradation. The mass of HDMSO in Run GF41 was 110% of that predicted by the known antifoam added. The HDMSO peaks correlate well with the antifoam additions. The HDMSO concentration profile is included in Figure 3-23.

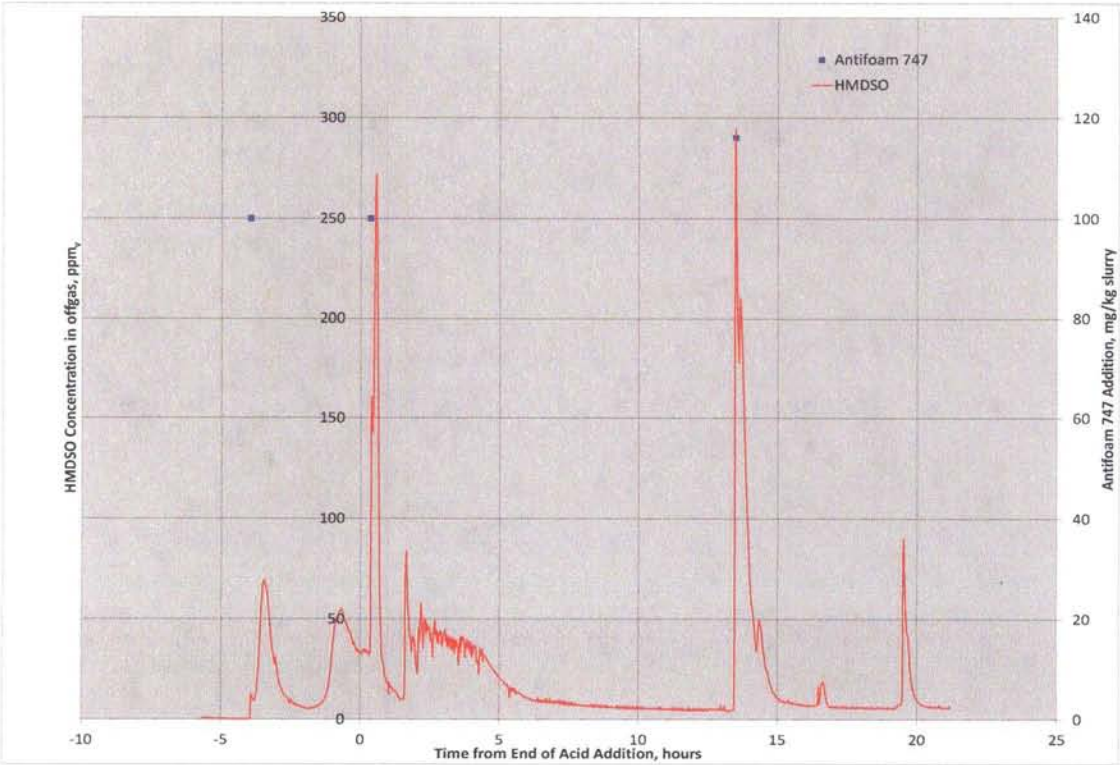

Figure 3-23. HDMSO Concentration during GF41 SRAT and SME cycle

Although this antifoam strategy was successful in processing simulants, the offgas and boiling fluxes are much lower in simulant experiments than DWPF. Plus, the simulants are generally rheologically less viscous than real waste. As a result, the antifoam strategy should be demonstrated in the largest scale testing and with real waste if feasible.

3.2.10 *Heat Transfer Calculations*

The SRAT/SME apparatus used had two immersed heating rods to heat the slurry instead of the mantle that has been used in the past. Each heating rod has a four-inch heated section and has a maximum heat input of 750 watts. The temperature of the rod was limited to approximately 130°C by the temperature controller to prevent overheating the rod in the case of rod fouling. The use of the heating rods has several distinct advantages, including measurement of heating rod temperatures and heat input, allowing calculation of heat transfer coefficients. In addition, the heating rods more closely resemble the steam coils and can "foul" just like a heating coil.

The heat transfer coefficient of the rods was calculated as a function of time throughout the runs. The data are summarized in Figure 3-24. Note that the heat transfer coefficient was very consistent throughout the SRAT cycles. In run GF37 (LoFeLoMn), the heat transfer coefficient dropped from about 0.14 to 0.07. This run was very difficult to concentrate and the SME cycle concentration after the second frit addition was not finished due to breakage of the glassware. Calculation of the heat transfer coefficient is useful in predicting fouling. The power input to the rods is summarized in Figure 3-25.

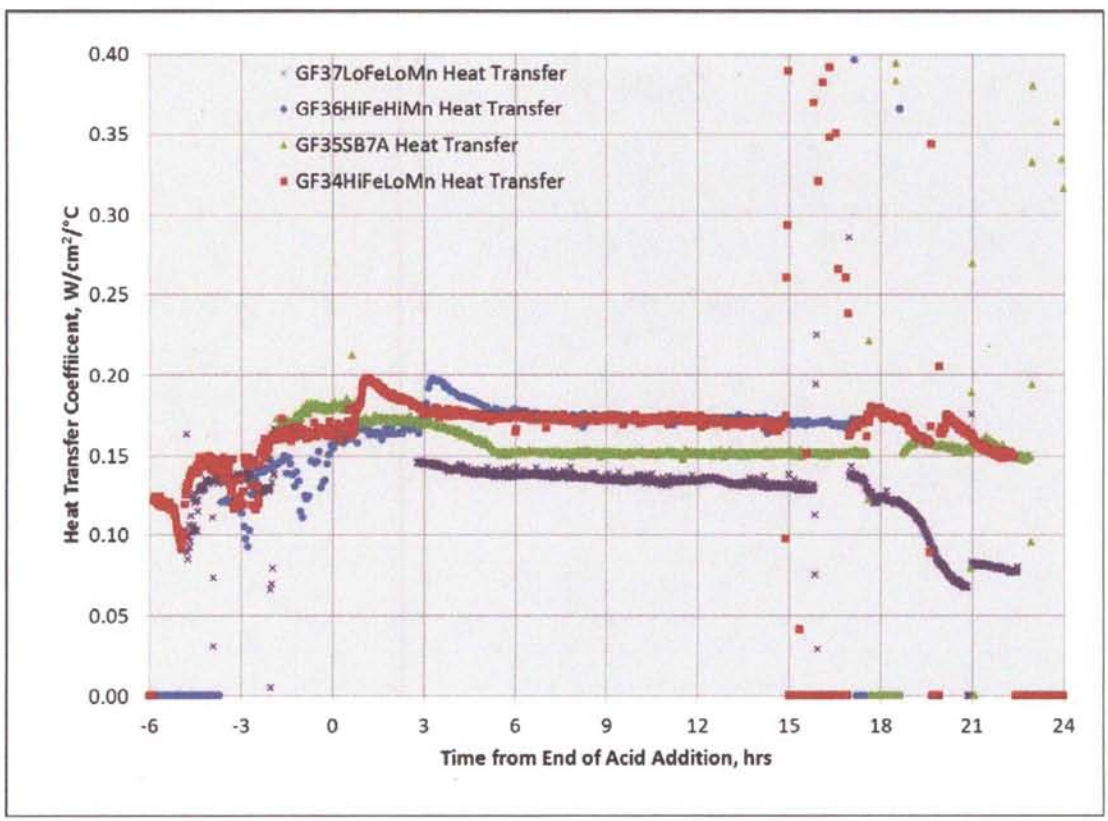

Figure 3-24.Heat Transfer Coefficient, W/cm²/°C

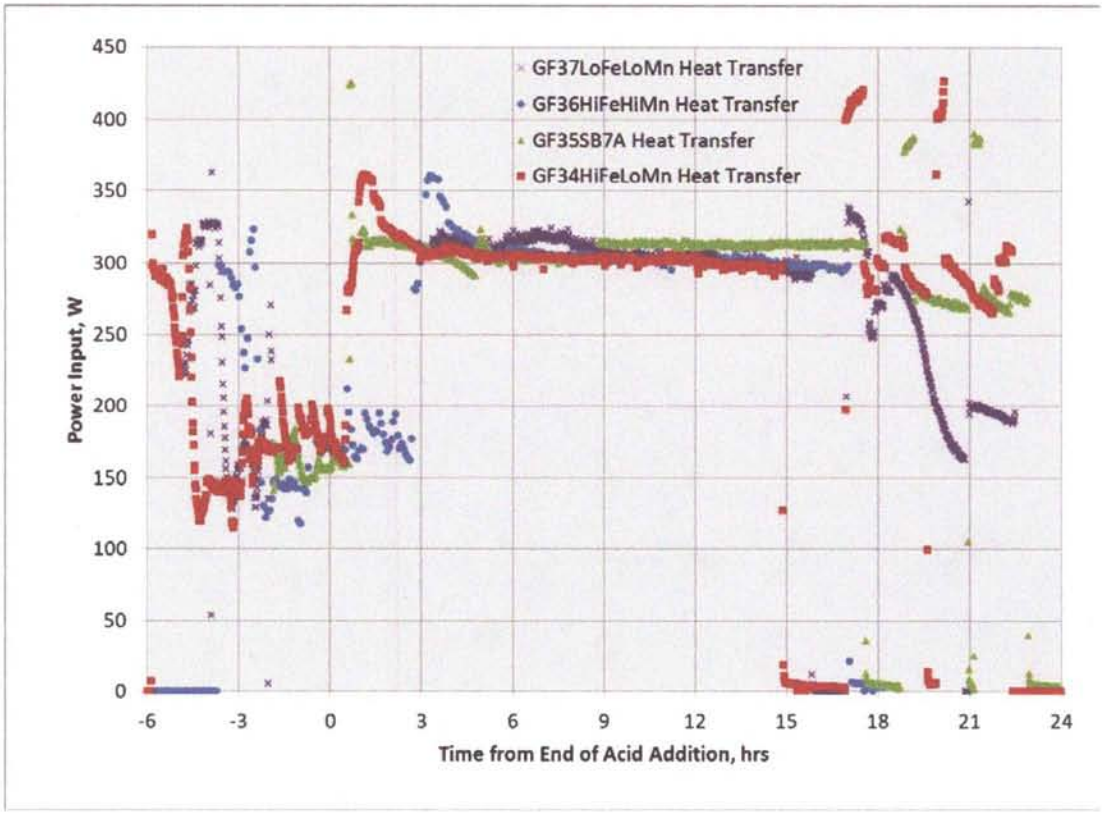

Figure 3-25. Power Input, W

Fouling was experienced in the problematic run GF37 (LoFeLoMn), and the fouled rod was photographed following the SME cycle (Figure 3-26). Note that neither the other rod nor the agitator was fouled.

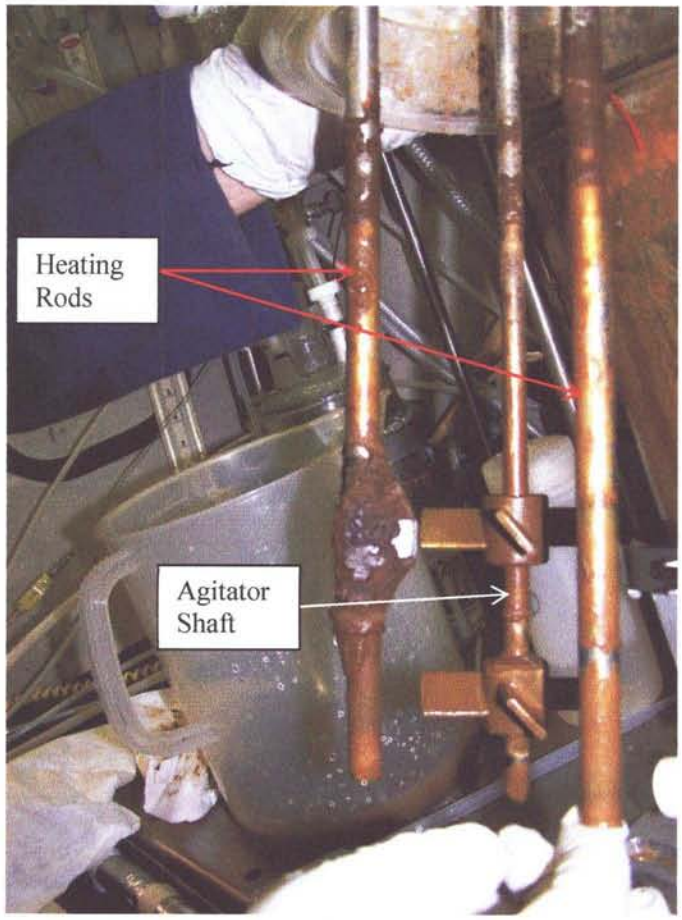

Figure 3-26. Photograph of Fouled Heating Rod after Run GF37 SME

3.2.11 *Comparison of Identical Runs*

After completing the first four runs (GF34-GF37) and recovering relatively little mercury in the MWWT, four additional runs were completed. Run GF36 was duplicated in both the new (GF36b) and older (GF36c) kettle configurations to ensure that the equipment change was not responsible for the poor mercury recovery. In virtually every measure, these two runs were as close to identical as was feasible. The collection of mercury was also very similar in the two duplicate runs. However, the supernate was different in GF36 compared to GF36b and GF36c. For example, the iron and aluminum were higher in the GF36b and 36c and the supernate was also a darker color.

In order to easily compare the identical runs, it is important to put the analytical data on the same basis. Each rig is built separately and can have varying levels of leak tightness. In runs with a tighter seal, less water is lost through the agitator seal, joints and connections. As a result, the solids and ICP-AES supernate results were corrected to the same basis, the target total solid concentration for each run. For Run GF36, the target total solids concentration was 30.3 wt %. Total solids and anion concentrations in GF36b and GF36c were corrected as if these runs had also finished with a SRAT product at 27.9 wt % solids. The corrected results are summarized in Table 3-39.

Table 3-39. GF36 Corrected Solids Concentrations

	Actual			Corrected		
Run	GF36	GF36b	GF36c	GF36	GF36b	GF36c
Total Solids, wt%	30.32	27.58	27.71	27.90	27.90	27.90
Insoluble Solids, wt%	17.03	13.70	13.27	15.68	13.86	13.37
Soluble Solids, wt%	13.28	13.88	14.43	12.22	14.04	14.53
Calcined Solids, wt%	16.68	15.04	15.15	15.35	15.21	15.25
Al, mg/L Supernate	411	2,280	2,250	447	2,250	2,240
Ba, mg/L Supernate	1.65	3.28	3.32	1.79	3.24	3.30
Ca, mg/L Supernate	2,390	3,350	3,490	2,600	3,310	3,460
Cr, mg/L Supernate	32.0	54.9	53.7	34.8	54.2	53.4
Cu, mg/L Supernate	11.9	25.9	24.6	12.9	25.6	24.4
Fe, mg/L Supernate	1,040	2,810	3,290	1,130	2,780	3,270
K, mg/L Supernate	272	16.4	5.23	296	16.2	5.19
Mg, mg/L Supernate	4,830	4,470	4,050	5,240	4,410	4,020
Mn, mg/L Supernate	1,330	1,280	1,150	1,450	1,270	1,150
Na, mg/L Supernate	26,500	28,100	25,900	28,900	27,800	25,700
Ni, mg/L Supernate	2,940	3,160	2,850	3,190	3,120	2,830
Pb, mg/L Supernate	0.610	2.29	2.01	0.663	2.26	1.20
Pd, mg/L Supernate	0.160	0.180	0.130	0.174	0.178	0.129
Rh, mg/L Supernate	10.7	18.4	15.0	11.6	18.2	14.9
Ru, mg/L Supernate	181	229	206	197	226	205
S, mg/L Supernate	572	453	482	622	448	479
Si, mg/L Supernate	17.4	132	68.8	18.9	131	68.3
Zr, mg/L Supernate	14.5	60.9	62.0	15.8	60.2	61.6

Note that the corrected calcined solids analysis is very similar in all three runs. However, the ratio of soluble solids to total solids is much lower for GF36 than for GF36b or GF36c. In addition, both Fe and Al in supernate are much higher in GF36b and GF36c than in GF36. The solids identified in XRD were Al and Fe species. This is consistent with crystal formation post processing in GF36 but not GF36b or GF36c. It also was noted visually that the supernate for GF36 was much clearer than GF36b or GF36c.

Significant differences in these runs are summarized in Table 3-40. Note that the data is reported on slurry basis.

Table 3-40. Analyses of Interest of Duplicate Runs, Anions and Solids Concentrations Corrected

Analyte	GF36	GF36b	GF36c	GF37	GF37b	GF38
Formate, mg/kg slurry	<100	<100	<100	<100	<100	<100
Chloride, mg/kg slurry	622	591	602	821	590	583
Nitrite, mg/kg slurry	<100	<100	<100	<100	<100	<100
Nitrate, mg/kg slurry	57,500	56,700	56,300	56,500	52,500	56,900
Sulfate, mg/kg slurry	1,210	1,280	1,240	1,500	1,445	1,420
Oxalate, mg/kg slurry	3,950	3,190	3,210	2,755	2,420	2,655
Glycolate, mg/kg slurry	37,300	51,300	53,100	42,200	55,500	77,900
Formate, mg/L supernate	<100	<100	<100	<100	<100	<100
Chloride, mg/L supernate	858	736	783	913	772	746
Nitrite, mg/L supernate	<100	<100	<100	<100	<100	<100
Nitrate, mg/L supernate	86,300	74,000	74,300	82,100	70,900	77,300
Sulfate, mg/L supernate	2,170	1,530	1,610	2,740	1,850	1,790
Oxalate, mg/L supernate	3,250	4,060	4,240	3,860	3,030	3,610
Glycolate, mg/L supernate	46,700	64,500	70,700	61,300	72,500	98,100
Al, wt % CS	9.1	9.2	9.1	23.7	23.5	23.9
Ba	0.095	0.094	0.092	0.063	0.064	0.063
Ca	2.120	1.95	1.93	1.67	1.65	1.69
Cr	0.273	0.269	0.269	0.223	0.224	0.220
Cu	0.054	0.043	0.040	0.051	0.040	0.041
Fe	32.0	32.9	32.9	12.5	12.3	12.3
K	0.061	0.077	0.083	0.071	0.079	0.086
Mg	2.57	2.77	2.76	2.36	2.40	2.43
Mn	0.705	0.640	0.631	0.666	0.601	0.595
Na	13.5	13.4	13.2	15.3	14.1	14.5
Ni	2.69	2.73	2.73	2.37	2.35	2.37
Pb	0.056	0.049	0.041	0.058	0.050	0.039
Pd	<0.100	<0.010	<0.010	<0.100	<0.010	<0.010
Rh	0.033	<0.100	<0.100	0.047	<0.100	<0.100
Ru	0.032	<0.100	<0.100	0.030	<0.100	<0.100
S	0.276	0.264	0.269	0.294	0.283	0.260
Si	1.95	1.82	1.76	1.3	1.42	1.39
Sn	0.107	0.102	0.102	0.089	0.094	0.093
Zn	0.072	0.071	0.070	0.061	0.062	0.062
Zr	0.117	0.110	0.110	0.045	0.040	0.044
Al, mg/L	411	2,280	2,250	554	2,200	4,040
Ba	1.65	3.28	3.32	1.26	2.69	3.37
Ca	2,390	3,350	3,490	2,150	3,040	2,87
Cr	32.04	54.85	53.7	86.0	103	198
Cu	11.9	25.9	24.6	15.1	24.7	38.5
Fe	1,040	2,810	3,290	328	1,490	3,560
K	272	16.4	5.23	290	265	247
Mg	4,825	4,470	4,050	4,410	4,090	4,180
Mn	1,330	1,280	1,150	1,300	1,280	922
Na	26,500	28,100	25,900	30,400	29,800	28,500
Ni	2,940	3,160	2,850	3,170	3,180	3,970
Pb	0.61	2.29	2.01	2.31	4.15	18.9
Pd	0.16	0.18	0.13	0.18	<0.100	<0.100
Rh	10.7	18.4	15.0	12.0	36.1	78.3

Analyte	GF36	GF36b	GF36c	GF37	GF37b	GF38
Ru	181	229	206	289	330	453
S	572	453	482	672	599	513
Si	17.4	132	68.8	67.4	121	103
Sr	3.06	NM	NM	2.99	41.6	77.3
Zr	14.5	60.9	62.0	17.7	38.3	50.7

3.2.12 *Reanalysis of Anions*

Since the measured glass REDOX was much more reducing than predicted, the anions were reanalyzed by both Analytical Development (AD) and PSAL (Table 2-1). The accurate measurement of four anions, nitrate, glycolate, oxalate, and formate is necessary to predict redox. It is apparent from the PSAL reanalysis results that nitrate ion concentration is a very robust analysis, but that the oxalate and glycolate concentrations vary during reanalysis. In fact, a number of unreported glycolate results were so high that they greatly exceeded the maximum concentration of glycolate possible based on the glycolic acid added.

Table 3-41. Anion and TOC Analyses for Runs GF36b, 36c, 37b and 38, mg/kg

Sample ID	Lab ID	Cl	NO_3	SO_4	C_2O_4	$C_2H_3O_3$	TOC Calc	Baseline TOC
12-GF36b-6160A	PSAL	736	74,000	1,530	4,060	64,500	21,800	19,700
12-GF36b-6160A	PSAL	717	72,500	1,550	4,130	61,700	20,900	19,700
12-GF36b-6160C	AD	545	57,100	1,030	2,440	33,900	11,500	19,700
12-GF36c-6184A	PSAL	783	74,300	1,610	4,240	70,700	23,800	28,600
12-GF36c-6184A	PSAL	774	74,500	1,650	3,650	72,000	24,100	28,600
12-GF36c-6184C	AD	589	56,000	1,010	1,940	34,400	11,500	28,600
12-GF37b-6217A	PSAL	772	70,900	1,850	3,030	72,500	24,100	24,500
11-GF37b-6217C	AD	559	51,700	1,250	1,340	35,900	11,900	24,500
12-GF38-6249A	PSAL	746	77,300	1,790	3,610	98,100	32,400	26,200
12-GF38-6255C	AD	321	58,100	1,160	2,390	54,500	18,100	26,200

3.2.13 *Less Washed Sludge Processing*

In order to increase waste loading to 40% in future DWPF processing, less washing of sludges may be required[22]. In order to make a feed batch of 2 M Na in Tank 40, a sludge batch as high as 2.5 M Na may need to be prepared in Tank 51. Since the typical qualification of each batch includes a confirmation run in the SRNL Shielded Cells, successful lab-scale cells processing of 2.5 M Na sludge may be required. To support this testing, two sludge simulants were prepared, targeting 1.6 and 1.9 M Na. These sludges, targeting the expected blend concentration in Tank 40 were used in a series of Baseline flowsheet tests to determine whether there was a reasonable CPC processing window (i.e. a suitable range of stoichiometric acid addition factors). In addition, a Glycolic-nitric flowsheet test was completed with each slurry (GF-40 and 41).

The main objective of these runs was to determine if a CPC processing window could be found where the SRAT product nitrite is <1000 mg/kg and hydrogen generation peak is less than 0.65 lb/hr in the SRAT and less than 0.223 lb/hr in the SME. Generally a window of ~30% in the stoichiometric acid factor (such as 100-130%) is the minimum required in the CPC. With the

stoichiometric acid factor (such as 100-130%) is the minimum required in the CPC. With the baseline flowsheet, the width of the processing window is primarily determined by the noble metal concentrations and the stoichiometric acid demand. The higher the noble metals and/or acid demand, the smaller the window. In this testing of the baseline flowsheet, two levels of noble metals were planned, SB7A in round 1 and HM levels of noble metals in round 2. Round 2 was not completed due to high hydrogen generation in round 1.

In order to destroy the nitrite in the SRAT cycle, and have the large hydrogen peak in the SRAT, which has a higher hydrogen limit and a higher purge, a higher acid stoichiometry is needed. Of course the less washed sludges have higher nitrite concentrations and other species that need reduction/destruction requiring more acid to complete the reactions. Processing the less washed sludges with the Glycolic-Nitric flowsheet produces little hydrogen, so the likelihood of a wide window is much greater. A list of these tests is included in Table 3-42.

Table 3-42. Testing with Less Washed Sludge Simulants

Run	Sludge	Acid Stoichiometry	Peak SRAT H_2, lb/hr	Peak SME H_2, lb/hr
Baseline Na2-1	**1.6M Na**	**130**	**2.76E-3**	**1.8E-3**
GF40	**1.6M Na**	**130**	**1.98E-5**	**1.04E-5**
Baseline Na2.5-1	**1.9M Na**	**130**	**5.96E-3**	**2.01E-3**
GF41	**1.9M Na**	**130**	**2.20E-5**	**0.00E0**

Baseline flowsheet testing with 100, 125 and 130% Koopman stoichiometry were not successful in meeting DWPF process requirements. The 100% acid stoichiometry test failed because the nitrite was only partially destroyed. The 125% and 130% runs failed due to high hydrogen generation in the SME cycle. The only successful test was the 110% acid stoichiometry test. If there is a viable window, it is likely between 110% and 120% so it is too small for CPC processing. Approximately 10% additional acid above the stoichiometric prediction was required to destroy nitrite due to the high oxalate concentration. Note that none of the current acid equations include a term for oxalate, though a significant impact was thoroughly documented in preliminary studies for Sludge Batch 3[23].

Both Glycolic-Nitric Flowsheet Tests at 130% Koopman stoichiometry were successful in destroying nitrite and minimizing the hydrogen generation. No lower acid stoichiometry testing was completed as the less washed slurries were consumed in this testing, but it is likely the window would have been from 110% to 200% based on previous testing. Hydrogen was detected in these runs but it was approximately 1% of the peak hydrogen in the Baseline flowsheet runs. As mentioned earlier, it was likely detected only because a lower SRAT air purge was used.

Based on this testing, processing of the less washed sludges with the Glycolic-Nitric Flowsheet is viable. The optimum processing conditions are likely closer to 110% acid stoichiometry since more metals will be dissolved during processing as more acid is used. For example, 30-40% of the iron was soluble by the time the SME cycle was complete in GF40 and GF41 testing. This could lead to a SME product that is not sufficiently viscous to hold the frit in suspension.

3.2.14 *Lower Air Purge in SRAT*

Because of the lower hydrogen generation during Glycolic-Nitric Acid Flowsheet processing, DWPF is considering lowering the purge in the SRAT. At present, to control flammability, DWPF maintains a SRAT air purge of 230 scfm to ensure the purge is at least 190 scfm (230 scfm with

instrument uncertainty) to control flammability. Even with no catalytic hydrogen generation, the SRAT needs an air purge to dilute the Isopar added with the MCU organic species. Calculations by DWPF-E demonstrate that the purge can be reduced to 93.7 scfm[24] with the Glycolic-Nitric Acid Flowsheet. This lower purge was tested in GF34b and GF34c tests and was utilized in the GF40 and 41 testing. Data from these runs will be compared in the following analysis.

The main impact of lowering the purge is that the measured concentrations of the process-generated gases are higher in the Glycolic Flowsheet. However, converting the data to DWPF lb/hr basis allows an easier comparison of the runs. The nitrous oxide profiles are summarized in Figure 3-27. Note that the N_2O profiles look very similar for runs GF34, GF34b and GF34c, so there is no impact on N_2O generation.

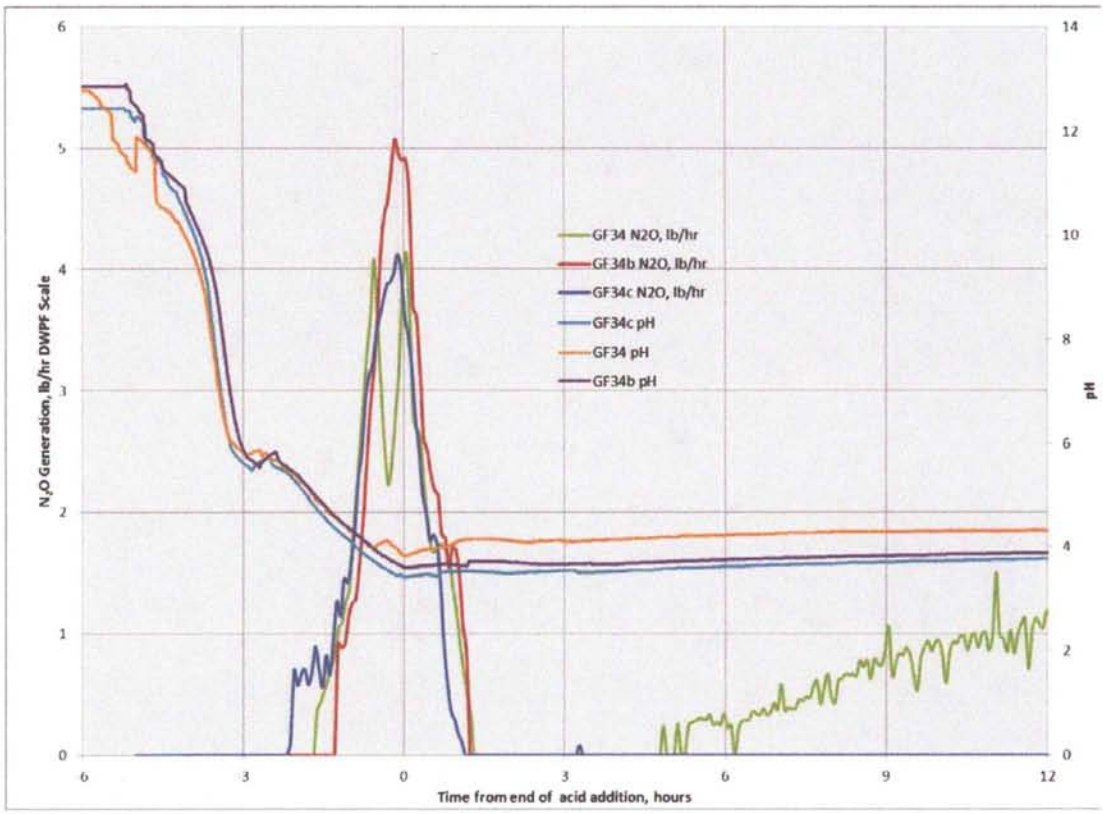

Figure 3-27. Nitrous Oxide Profile, lb/hr

Hydrogen was detected in only one pair of Glycolic-Nitric runs, GF40 and 41, with an apparent quantitation limit of 0.005 volume %. The maximum hydrogen concentration at the lower purge was 0.009 volume %. These concentrations would have been below the quantitation limit using the typical air purge. The peak hydrogen generation rates in runs GF40 and GF41 were 0.00287 and 0.00324 lb/hr respectively. The peak hydrogen generation rates in Baseline flowsheet runs 2M-1 and 2.5M-1 were 0.403 and 0.699 lbs/hr respectively, 140 and 210 times higher respectively than similar Glycolic-Nitric Flowsheet runs. Lowering the purge likely has no impact on hydrogen generation other than to lower the detection limit.

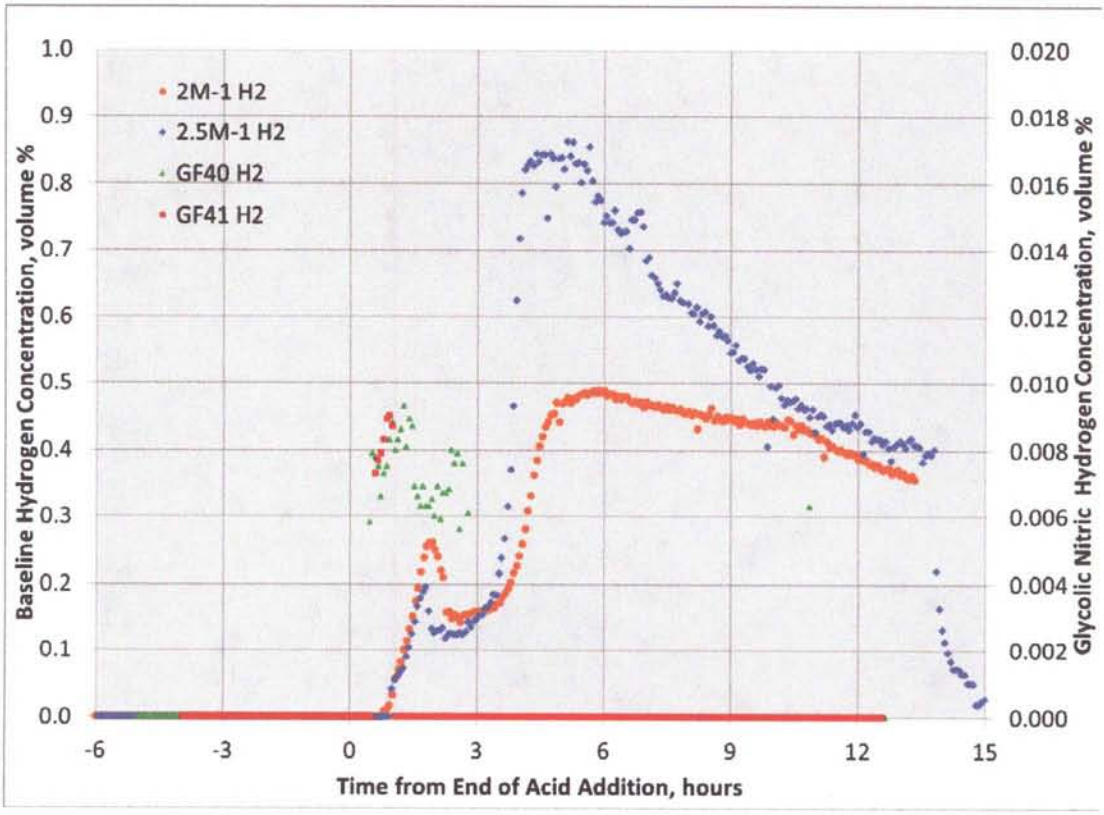

Figure 3-28. Glycolic-Nitric and Baseline Flowsheet SRAT Hydrogen Concentration Profile, volume %

The production of carbon dioxide during Runs GF34, GF34b and GF34c have very similar profiles on a lb/hr scale, From this data, there was no impact on carbon dioxide generation from lowering the air purge. Figure 3-29 is a graph of carbon dioxide during the SRAT cycle. The CO_2 generated in Glycolic-Nitric Flowsheet runs is approximately one-third compared to Baseline Flowsheet runs.

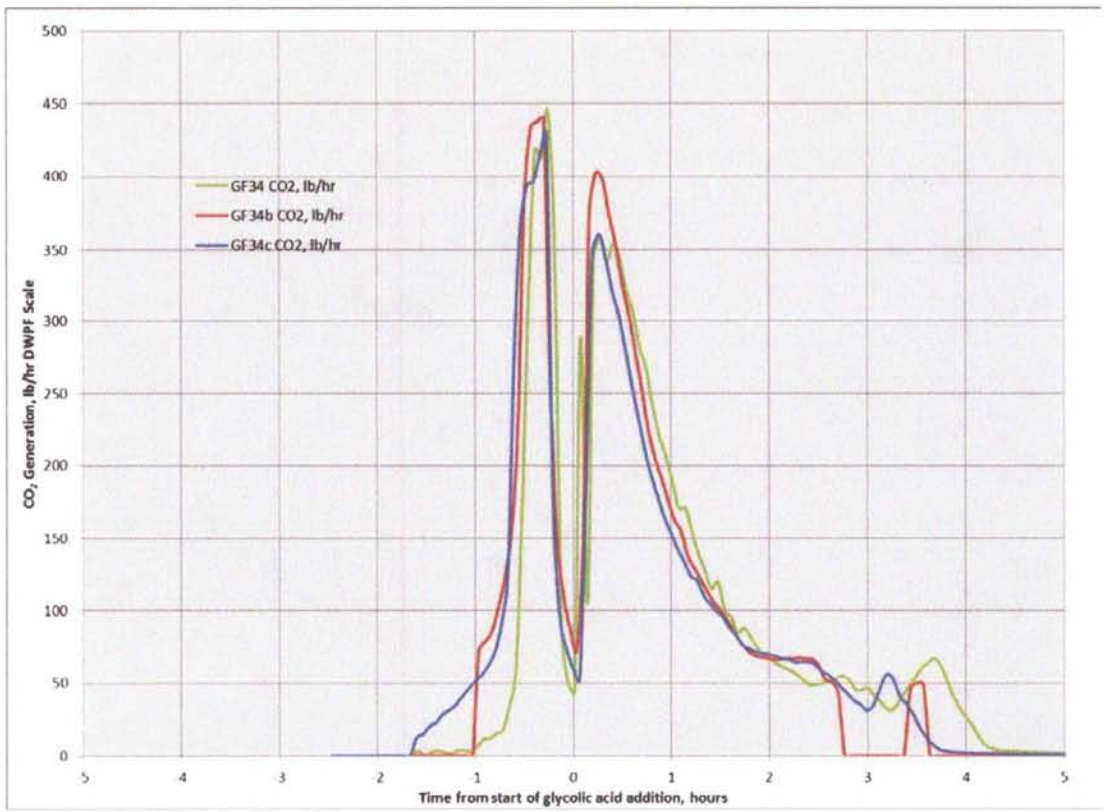

Figure 3-29. Carbon Dioxide Profile, lb/hr

During acid addition and boiling, oxygen is consumed by the oxidation of NO to NO_2. With the lower purge in the Glycolic-Nitric Flowsheet runs, the oxygen is completely depleted during the nitrite destruction phase of the SRAT cycle and remains depleted for several hours. Note that GF34 had a scaled air purge of 230 scfm, GF34b had a scaled air purge of 190 scfm and GF34c had a scaled air purge of 93.7 scfm. Figure 3-30 shows the lower oxygen (completely depleted) in the runs with the lower purge.

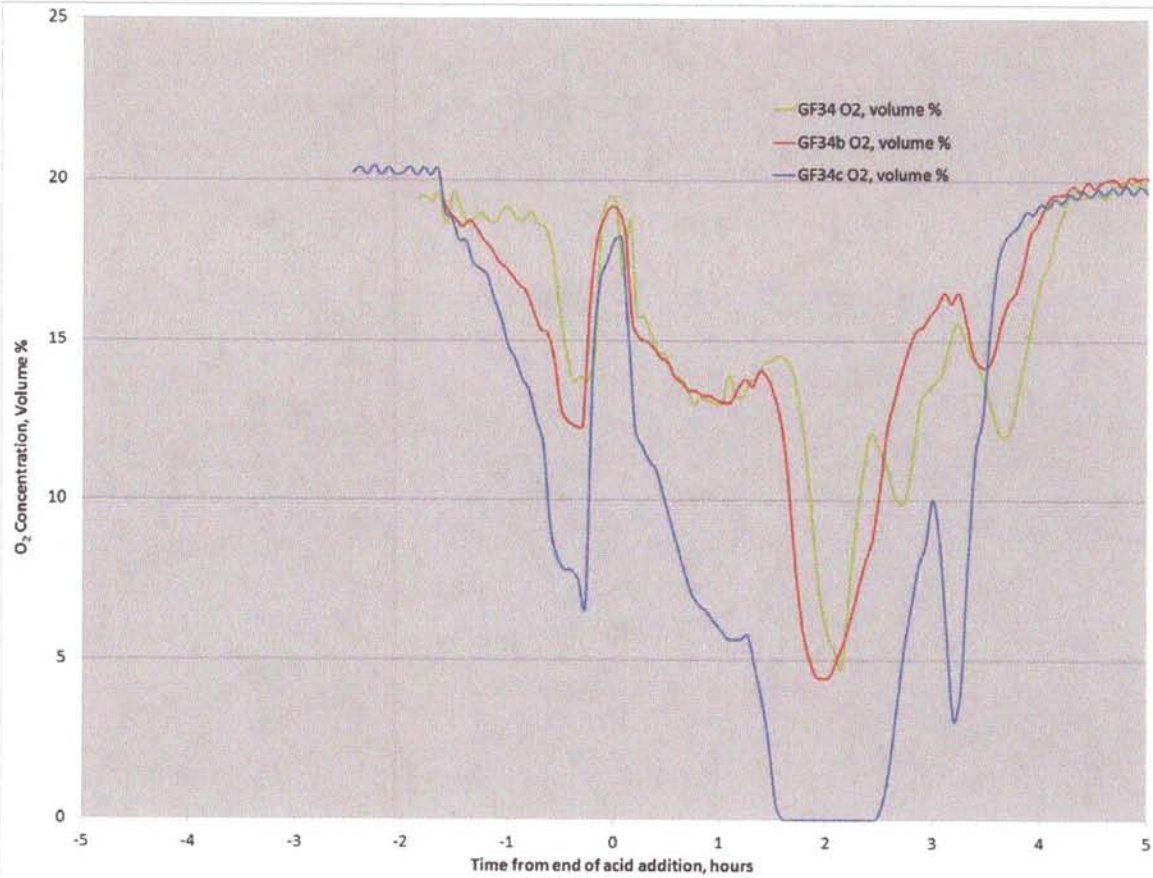

Figure 3-30. Oxygen Profile, Volume %

3.2.15 *Addition of Acid during Heat-up*

One way to decrease the acid addition time during SRAT processing is to add the acid earlier in the SRAT cycle. There are several places this could be accomplished, including during heat-up prior to ARP addition and during heat-up prior to acid addition. In runs GF40 and GF41, nitric acid was added during heat-up to 93°C. No processing issues were noted during this early acid addition. The first part of the acid addition is a neutralization of the soluble base species in the sludge with nitric acid so no impact was anticipated. It is recommended that all future processing utilize this productivity enhancement.

3.2.16 *Closing Reflux Valve during Acid Addition*

One way to decrease the SRAT dewater time is to close the reflux valve throughout acid addition. Condensate is generated during acid addition and a portion of the dewater can be collected during acid addition. The condensate generated during acid addition is very acidic due to generation of NO, oxidation to NO_2 and scrubbing NO_2 in the condenser and scrubber. Runs GF40 and 41 were designed to compare the Glycolic-Nitric Acid flowsheet to the Baseline Flowsheet using underwashed 2.0M and 2.5 M Na sludge simulants. In both glycolic acid runs, the mercury collection was significantly higher than the comparable Baseline flowsheet runs (2MNa-1 and

2.5MNa-1). The results are summarized in Table 3-43. It is recommended that the reflux valve remain closed during future Glycolic-Nitric Acid Flowsheet runs.

Table 3-43. MWWT Mercury Recovery for Runs GF40, 41, 2.0MNa, 2.5M Na

Run	GF40	GF41	2.0M Na-1	2.5M Na-1
Sludge	2.0M Na	2.5 M Na	2.0M Na	2.5 M Na
Hg Recovered, g	3.083	2.697	2.268	1.790

3.2.17 *Processing without Formic Acid in the Frit Slurry*

The addition of formic acid in the frit slurry causes the production of significant hydrogen in the SME cycle. Tests GF40 and GF41 were completed without adding formic acid during SME frit addition. This eliminated the production of hydrogen during the SME cycle. It is recommended that future processing of the Glycolic-Formic Acid Flowsheet eliminate the use of formic acid and use either nitric or glycolic acid if needed as an anticlumping/antigeling agent in the frit slurry.

3.2.18 *Future Processing Improvements*

A number of processing changes should be considered to improve CPC processing in DWPF. These could be tested in future experiments and includes:

- Switch acid addition order for improved mercury recovery. VSL found that adding nitric, then glycolic followed by the rest of the nitric acid led to better mercury removal.
- Adding acids at boiling to improve dewater collection during acid addition and mercury recovery. Determine optimum time for boiling to begin.
- Add acids to SRAT before ARP addition to reduce pH of SRAT and maximize effectiveness of antifoam. This should minimize the antifoam addition volume.
- Determine optimum acid stoichiometry for mercury recovery.
- Determine the optimum total solids and waste loading to hinder settling of frit during dilution by pump priming in Melter Feed Tank.

4.0 Conclusions

Testing was completed to demonstrate the viability of the newly developed glycolic/nitric flowsheet for processing in the Defense Waste Processing Facility's (DWPF) Chemical Process Cell (CPC). The Savannah River National Laboratory (SRNL) initiated a sludge matrix study to evaluate the impact on CPC processing. Four sludge simulants were designed to cover a broad insoluble solid composition range to bracket future sludge batches. The first pair of sludge parameters was high iron/low aluminum versus low iron/high aluminum (referred to as HiFe or LoFe in this report). The second pair of sludge parameters was high calcium-manganese/low nickel, chromium, and magnesium versus low calcium-manganese/high nickel, chromium, and magnesium (referred to as HiMn or LoMn in this report). In addition, a simple supernate simulant was prepared to match the composition of the matrix simulants.

Ten experiments (GF34 to GF37 and GF34b, GF34c, GF36b, GF36c, GF37b and GF38) were completed to demonstrate the glycolic-nitric flowsheet viability using the sludge matrix simulants. In addition, two experiments were performed with less washed simulants (GF40, 2M and GF41, 2.5 M Na endpoints) to demonstrate the viability of processing these sludges. Also, five supernate

experiments (GF39a-GF39eGF39e) were performed to better understand the reaction sequence, particularly the reduction and stripping of mercury.

Composition and physical property measurements were made on the Sludge Receipt and Adjustment Tank (SRAT) and Slurry Mix Evaporator (SME) products. Composition measurements were made on the composited condensates from the Mercury Water Wash Tank (MWWT), and Formic Acid Vent Condenser (FAVC), on the ammonia scrubber solution, and on SRAT samples pulled throughout the SRAT cycle. Updated values for glycolate and formate loss, nitrite-to-nitrate conversion, and oxalate formation were found that can be used in the acid calculations for future process simulations with the glycolic-nitric flowsheet.

Preliminary results of the initial testing indicate:

- Hydrogen generation rate was below detection limits (<11.4E-3 lb/hr DWPF-scale or <0.005 vol%) throughout all SRAT cycles with matrix simulants. Hydrogen generation rate was above detection limits for the less washed simulants (3.2E-3 lb/hr DWPF-scale or 0.009 vol%) due to the higher acid stoichiometry and the lower offgas purge.
- Hydrogen generation rate was below 0.0258 lb/hr DWPF-scale throughout all SME cycles with matrix simulants. Hydrogen was produced in the matrix SME cycles because formic acid was added with the frit slurry. Hydrogen generation rate was above detection limits for the less washed simulant in GF40 (1.8E-3 lb/hr DWPF-scale or 0.007 vol%) but was below detection limit in GF41 due to the higher acid stoichiometry and the lower offgas purge. No formic acid was added in runs GF40 and GF41.
- Mercury was both reduced and stripped without formic acid. The mercury concentration of the SRAT product was below the 0.8 wt % limit in eight of the runs and below 0.92 wt % in the other four runs.
- Nitrite in the SRAT product was <100 mg/kg slurry for all runs.
- Foaminess was not an issue using the nominal antifoam addition strategy or with reduced antifoam in these tests.
- High wt % total solids were achieved while staying within rheological limits which makes the glycolic acid/nitric acid flowsheet an improvement for processing more viscous sludges. However, there may be a tradeoff between excessive dissolution of metals and thinner rheology.
- The pH remained steady throughout processing (i.e. no pH rebound) potentially leading to more consistent processing during the CPC. The SRAT and SME products pH varied from 3.5-5.0 for the 100% and 130% acid stoichiometry runs, significantly lower than is typical of the Baseline nitric acid/formic acid flowsheet.
- The testing apparatus has been significantly modified to improve processing with high viscosity slurries. Testing of the old style and new style rig identified no differences in CPC processing, including steam stripping of Hg.
- The SRAT lower air purge was demonstrated in Run GF34c and used in GF40 and GF41. The SRAT purge can be reduced from 190 scfm to 93.7 scfm without negatively impacting DWPF CPC processing.
- Runs GF40 and 41 demonstrated that processing of less washed sludges is viable with the Glycolic-Nitric flowsheet. However, this flowsheet has not been demonstrated with ARP, MCU or actual waste.

- Several processing improvements were demonstrated in these runs including adding acid during heat-up, adding both acids at higher volumetric flowrates than are currently used in DWPF, and concentrating the SRAT during acid addition. Each of these improvements has the potential to shorten CPC processing time.

5.0 Recommendations Applying to the Glycolic-Nitric Flowsheet

The glycolic-nitric flowsheet is recommended as a viable flowsheet alternative to the Baseline DWPF flowsheet. In the testing that has been performed to date, this flowsheet meets or outperforms the current flowsheet in minimizing off-gas generation, removing mercury, and producing a rheologically thinner product. Previous testing with glycolic/formic acid mixtures demonstrated a wide processing window regarding both the glycolic-formic ratio and acid stoichiometry. The addition of glycolic acid leads to SRAT products that are rheologically less viscous which means that more concentrated products can be produced, leading to potentially higher waste throughput per batch. In addition, the combination of lower pH processing and the complexing power of glycolic acid leads to the dissolution of more metals, which may minimize deposits in the CPC processing vessels and prevent the fouling of steam coils. Follow-up testing is recommended in the following areas:

- Improve glycolate and oxalate analyses. The majority of the glycolate results reported were correct. However, there are issues with anion and cation deposition on the column of the Ion Chromatograph (IC), causing higher than expected glycolate and oxalate in blanks and some samples. Both Process Science and Analytical Laboratory (PSAL) and Analytical Development (AD) have reported results that have varied significantly from expectations. Modification to the sample preparation method is likely needed to improve analytical accuracy and minimize the cleaning and replacement of the IC column. An alternative to the IC measurement of glycolate should also be considered.
- Determine the appropriate REDOX model for the glycolic-nitric flowsheet. The REDOX model may need more terms due to the more extensive reduction of some metals, including Mn and Fe. In addition, accurate measurement of glycolate (and possibly oxalate) and nitrate is needed to accurately predict REDOX. REDOX testing of the matrix sludges should be repeated using acceptable frits that meet Product Composition Control System (PCCS).
- Testing should be completed with alternate forms of ruthenium to determine whether the elimination of the chloride added as ruthenium chloride would improve the reduction and stripping of the mercury. Comparison testing should be completed with the Baseline and glycolic-nitric flowsheets.
- Test the glycolic-nitric flowsheet at acid stoichiometries of less than 100%. Demonstration of this flowsheet at an acid stoichiometry of <100% is recommended and might be useful for mercury stripping.
- Demonstrate the glycolic-nitric flowsheet (previously demonstrated in SRAT cycle with 80:20 glycolic:formic acid blend) with actual waste in SRNL Shielded Cells SRAT and SME processing, to include periodic slurry sampling throughout the SRAT and SME processing along with a glass REDOX measurement.
- Add the nitric and glycolic acid flowrate at the same scaled molar flowrate as formic acid to minimize glycolic-nitric flowsheet batch time.

- The nitric acid can be added during heat-up to decrease the SRAT cycle time. The nitric acid primarily neutralizes soluble the base species in the slurry with little offgas generation.
- Improve understanding of process chemistry, the decomposition of glycolate and the production of oxalate which are important to REDOX.
- Improve understanding of mercury reduction, stripping and accumulation during processing. Determine whether alternative equipment or processing changes are needed to maximize the collection of mercury in the Mercury Water Wash Tank.
- If confirmed by actual waste testing and larger scale testing with simulants, the antifoam addition can be reduced for this flowsheet. The addition of 100 mg/kg prior to glycolic acid addition, 100 mg/kg prior to boiling and 100 mg/kg each 12 hours of processing was adequate during simulant testing.
- More rigorous data collection is needed to validate the OLI aqueous model's solubility predictions with sample results. The methodology is summarized in the discussion.

Recommendations Applying to both Baseline and Glycolic-Nitric Acid Flowsheet

- Testing should be completed with alternate forms of ruthenium to determine whether the elimination of the chloride added as ruthenium chloride would improve the reduction and stripping of the mercury. Testing should be completed with the Baseline and glycolic-nitric flowsheets.

6.0 Acknowledgements

The authors would like to thank a number of SRNL employees who supported this testing.

Thanks to Jon Duvall, Vickie Williams, Phyllis Workman, David Healy, Tony Burckhalter, and Beverly Walls for their excellent support during these around the clock runs.

Thanks to Whitney Riley, Beverly Walls, Phyllis Workman, Russ Eibling and Pat Simmons for their excellent and timely analysis of the hundreds of samples that were submitted as part of this study.

Thanks to Tom White, Amy Ekechukwu, and David Missmer for the AD analysis of samples for IC, TOC and XRD.

Thanks to Frances Williams and John Pareizs for their support of the GC calibration, analysis, and post run processing.

Thanks to Jack Zamecnik for his calibration, operation and post run analysis of the FTIR and MS.

Thanks to Jackie Best for her excellent administrative support.

7.0 Reference

1 Pickenheim, B.R., M.E. Stone, SRAT Alternative Reductant Feasibility Assessment – Phase I, SRNL-STI-2009-00120, Savannah River National Laboratory, Aiken, SC, February 2009.

2 Pickenheim, B.R., M.E. Stone, J.D. Newell, Glycolic-Formic Acid Flowsheet Development, SRNL-STI-2010-00523, Rev 0, Savannah River National Laboratory, Aiken, SC, November 2010.

3 D.P. Lambert, B.R. Pickenheim, M.E. Stone, J.D. Newell, D.R. Best, Glycolic - Formic Acid Flowsheet Final Report for Downselection Decision, SRNL-STI- 2010-00523, Rev 1, Savannah River National Laboratory, Aiken, SC, March 2011.

4 Fellinger, T.L., "*Alternate Reductant Flowsheet Development – Phase I*", HLW-DWPF-TTR-2012-0003, Revision 0, October 2011.

5 Lambert, D.P., Task Technical and Quality Assurance Plan for Glycolic Acid Flowsheet Development, SRNL-RP-2011-01586, Savannah River National Laboratory, Aiken, SC, November 2011.

6 D. C. Koopman, D. P. Lambert, Initial Characterizations and SRAT Simulations of Four Sludge Matrix Study Simulants, SRNL-STI-2009-00606, Revision 0, Savannah River National Laboratory, Aiken, SC, December 2009

7 Lambert, D.P., Acid Calculation Spreadsheet for DWPF Simulations, Revision 1, SRNL-PSE-2006-00176, Savannah River Site, Aiken, SC 29808 (2006).

8 Koopman, D.C., A.I. Fernandez, B.R. Pickenheim, Preliminary Evaluations of Two Proposed Stoichiometric Acid Equations, Revision 0, Savannah River Site, Aiken, SC 29808 (2009).

9 Stone, M. E., Lab-Scale CPC Equipment Set-up, SRNL-ITS-2006-000742011-00127, Savannah River Site, Aiken, SC 29808 (2011).

10 Manual L29, Procedure ITS-0094, Rev. 6, Laboratory Scale Chemical Process Cell Simulations, Savannah River Site, Aiken, SC 29808, November 2011.

11 Glycolic/Nitric Acid Flowsheet Development Notebook, SRNL-NB-2012-00039, Savannah River Site, Aiken, SC 29808 (2012).

12 Jantzen, C. M. and M. E. Stone, Role of Manganese Reduction/Oxidation (REDOX) on Foaming and Melt Rate in High Level Waste Melters, WSRC-STI-2006-00066, Savannah River Site, Aiken, SC, 29808 , March 2007.

13 Jantzen, C.M., J.R. Zamecnik, D.C. Koopman, C.C. Herman, and J.B. Pickett, Electron Equivalents Model for Controlling Reduction-Oxidation (REDOX) Equilibrium during High Level Waste (HLW) Vitrification, WSRC-TR-2003-00126, Savannah River Site, Aiken, SC 29808 (2003).

14 Lambert, D. P., Koopman, D. C., Glycolic-Formic Acid Flowsheet Sludge Matrix Study, SRNL-STI-2011-00275, Savannah River Site, Aiken, SC, 29808 (June 2011).

15 D. C. Koopman, D. P. Lambert, Initial Characterizations and SRAT Simulations of Four Sludge Matrix Study Simulants, SRNL-STI-2009-00606, REVISION 0, Savannah River National Laboratory, Aiken, SC, December 2009.

16 Best, D.R., Anion Analysis by Ion Chromatography for the Alternate Reductant Program for the Defense Waste Processing Facility, SRNL-STI-2010-00389, Savannah River National Laboratory, Aiken, SC, June 2010.

17 Manual L29, Procedure ITS-0052, Rev. 2, Heat Treatment of Waste Slurries for REDOX (Fe2+/$\sum$Fe) and Chemical Composition Measurement.

18 Koopman, D. C., *Noble Metal Chemistry and Hydrogen Generation during Simulated DWPF Melter Feed Preparation*, WSRC-STI-2008-00002, SRNL, Aiken, SC, 29808 (June 2008).

19 Zamecnik, J.R., Behavior of Mercury during DWPF Chemical Process Cell, SRNL-STI-2012-00051, REVISION 0, Savannah River National Laboratory, Aiken, SC, April 2012.

20 (HLW-DWPF-TTR-2012-0013)

21 Koopman, D. C., Rheology Protocols for DWPF Samples, WSRC-RP-2004-00470, Savannah River Site, Aiken, SC, 29808 (October 2004).

22 McIlmoyle, D.W., SB8 Projected Compositions Based on Latest Plans, Interoffice Communication, Savannah River Site, Aiken, SC 29808 (June 28, 2012 with attached spreadsheet, SB8_COMPOSITIONS_6_28_12.xls).

[23] Herman, C.C., D.C. Koopman, D.R. Best, T.K. Snyder, M.F. Williams, Sludge Batch 3 Simulant Flowsheet Studies: Phase II SRAT/SME Results, WSRC-TR-2003-00158, Revision 0, Savannah River Site, Aiken, SC, 29808 (April 2003).

[24] Fellinger, T.L., Purge for Low Purge Experiments, Interoffice Memorandum, Savannah River Site, Aiken, SC, 29808 (April 2012)

Appendix A. Acid Spreadsheet Inputs

Table A-1. Sludge Analyses for Acid Calculations

Run #	GF34 GF34b GF34c	GF35	GF36 GF36b GF36c	GF37 GF37b GF38	GF40	GF41	Units
Mass without trim chemicals	2,900.0	2,900.0	2,900.0	2,900.0	3,038.3	3,038.0	g slurry
Weight % Total Solids	23.70	18.47	22.81	23.07	24.14	25.43	wt%
Weight % Calcined Solids	17.81	13.56	16.95	16.00	17.01	17.85	wt%
Weight % Insoluble Solids	16.70	13.01	16.35	16.05	16.51	16.97	wt%
Density	1.185	1.144	1.180	1.176	1.174	1.215	kg / L slurry
Supernate density	1.057	1.051	1.055	1.057	1.076	1.091	kg / L supernate
Nitrite	17,900	9,605	17,800	18,100	13,450	15,750	mg/kg slurry
Nitrate	13,550	5,880	13,400	13,250	7,895	9,935	mg/kg slurry
Formate	0	0	0	0	0	0	mg/kg slurry
Sulfate	1,770	1,345	1,575	1,585	1,975	2,605	mg/kg slurry
Chloride	116	0	131	127	0	0	mg/kg slurry
Phosphate	0	0	0	0	0	0	mg/kg slurry
Oxalate	300	7,220	275	294.5	18750	20000	mg/kg slurry
Slurry TIC	2,751	1,066	2,492	2,403	1840	1732	mg/kg slurry
Supernate TIC	1,080	664	1,310	1,280	1790	1760	mg/L supernate
Base Equivalents) pH = 7	0.5903	0.580	0.562	0.522	0.838	0.879	MolesBase/L slurry
Coal/Carbon source	0.000	0.000	0.000	0.000	0.000	0.000	wt% dry basis
Manganese	4.040	5.115	0.690	0.662	4.625	4.230	wt % calcined basis
Mercury	0.0000	0.0000	0.0000	0.0000	0.0000	0.0000	wt% dry basis
Magnesium	0.448	0.413	2.970	2.420	0.286	0.264	wt % calcined basis
Sodium	12.500	14.700	12.900	14.200	23.290	23.986	wt % calcined basis
Potassium	0.110	0.120	0.076	0.096	0.345	0.407	wt % calcined basis
Cesium	0.000	0.000	0.000	0.000	0.000	0.000	wt % calcined basis
Calcium	3.840	0.831	2.115	1.970	0.576	0.514	wt % calcined basis
Strontium	0.000	0.000	0.000	0.000	0.000	0.000	wt % calcined basis
Nickel	0.214	3.310	2.600	2.310	1.937	1.756	wt % calcined basis
Supernate Manganese	0	0	0	0	0	0	mg/L supernate

Table A-2. SRAT Processing Assumptions

Run #	GF34 GF34b GF34c	GF35	GF36 GF36b GF36c	GF37 GF37b		GF38	GF40	GF41	Units
Conversion of Nitrite to Nitrate in SRAT Cycle	30.00	30.00	30.00	30.00	30.00	30.00	30.00	30.00	gmol NO_3^-/100 gmol NO_2^-
Destruction of Nitrite in SRAT and SME cycle	100.00	100.00	100.00	100.00	100.00	100.00	100.00	100.00	% of starting nitrite destroyed
Destruction of Formic acid charged in SRAT	0.00	0.00	0.00	0.00	0.00	0.00	0.00	0.00	% formate converted to CO_2 etc.
Destruction of Glycolic acid charged in SRAT	30.00	30.00	30.00	30.00	30.00	30.00	30.00	30.00	% glycolate converted to CO_2 etc.
Conversion of Glycolic acid to Oxalate	3.00	3.00	3.00	3.00	3.00	3.00	3.00	3.00	% glycolate converted to C2O4
Destruction of Oxalate charged	0.00	0.00	0.00	0.00	0.00	0.00	0.00	0.00	% of total oxalate destroyed
Percent Acid in Excess Stoichiometric Ratio	103.97	100.00	106.07	100.00	100.00	125.00	133.92	130.00	%
SRAT Product Target Solids	27.90	27.90	27.90	27.90	27.90	27.90	27.90	27.90	%
Nitric Acid Molarity	10.304	10.304	10.304	10.304	10.304	10.304	10.312	10.312	Molar
Formic Acid Molarity	23.552	23.552	23.552	23.552	23.552	23.552	23.552	23.552	Molar
Glycolic Acid Molarity	11.930	11.930	11.930	11.930	11.847	11.847	11.441	11.441	Molar
DWPF Nitric Acid addition Rate	4.572	4.572	4.572	4.572	4.572	4.572	4.568	4.568	gallons per minute
REDOX Target	0.100	0.100	0.100	0.100	0.100	0.100	0.100	0.100	Fe^{+2} / ΣFe
Ag metal	0.0014	0.0014	0.0014	0.0014	0.0014	0.0014	0.0144	0.0135	total wt% dry basis
wt% Hg dry basis	1.5000	1.5000	1.5000	1.5000	1.5000	1.5000	1.5000	1.4095	total wt% dry basis
Pd metal	0.0790	0.0790	0.0790	0.0790	0.0790	0.0790	0.0033	0.0031	total wt% dry basis
Rh metal	0.0380	0.0380	0.0380	0.0380	0.0380	0.0380	0.0192	0.0180	total wt% dry basis
Ru metal	0.2170	0.2170	0.2170	0.2170	0.2170	0.2170	0.0877	0.0824	total wt% dry basis
Oxalate	0.1235	3.8086	0.1176	0.1246	0.1246	0.1246	7.6001	7.7045	total wt% dry basis
Dilution Water	250.00	250.00	250.00	250.00	250.00	250.00	250.00	250.00	g

Run #	GF34 GF34b GF34c	GF35	GF36 GF36b GF36c	GF37 GF37b		GF38	GF40	GF41	Units
Acid flush water	20.00	20.00	20.00	20.00	20.00	20.00	20.00	20.00	g
Mass of SRAT cycle samples	450.00	450.00	450.00	450.00	450.00	450.00	500.00	500.00	g
Active Agent In Antifoam Solution	10	10	10	10	10	10	10	10	wt%
Basis Antifoam Addition for SRAT	100	100	100	100	100	100	100	100	mg/kg slurry
Number of basis antifoam additions	8	8	8	8	8	8	8	8	
SRAT air purge	230	230	230	230	230	230	93.7	93.7	scfm
SRAT boil-up rate	5000	5000	5000	5000	5000	5000	5000	5000	lbs/hr
SRAT total boil-up (reflux)	60,000	60,000	60,000	60,000	60,000	60,000	60,000	60,000	lbs
SRAT Steam Stripping Factor	750	750	750	750	750	750	750	750	g steam/g mercury

Table A-3. SME Processing Assumptions

Run #	GF34	GF35	GF36	GF37	GF40	GF41	Units
Frit type	418	418	418	418	418	418	
Destruction of Formic acid in SME	0	0	0	0	0	0	% Formate converted to CO_2 etc.
Destruction of Nitrate in SME	5	5	5	5	5	5	% Nitrate destroyed in SME
Destruction of Glycolate in SME	5	5	5	5	5	5	% glycolate converted to CO_2 etc.
Assumed SME density	1.40	1.40	1.40	1.40	1.440	1.440	kg / L
Basis Antifoam Addition for SME cycle	100	100	100	100	100	100	mg/kg slurry
Number of basis antifoam additions added	3	3	3	3	3	3	
Sludge Oxide Contribution (Waste Loading)	36	36	36	36	36	36	%
Frit Slurry Formic Acid Ratio	1.50	1.50	1.50	1.50	1.50	1.50	g 90 wt% FA/100 g Frit
Target SME Solids total Wt%	45	45	45	45	45	45	wt%
Number of frit additions in SME Cycle	2	2	2	2	2	2	
# DWPF Canister decons simulated	0.0	0.0	0.0	0.0	0	0	
Volume of water per deconed can	1,000	1,000	1,000	1,000	1,000	1,000	gal at DWPF scale
Water flush volume after frit slurry addition	0.0	0.0	0.0	0.0	0.0	0.0	gal
SME air purge	74	74	74	74	74	74	scfm

Appendix B. Offgas Results

Raw off-gas data from the GCs are presented in this Appendix for the twelve SRAT cycles and six SME cycles from the process simulations with slurry simulants.

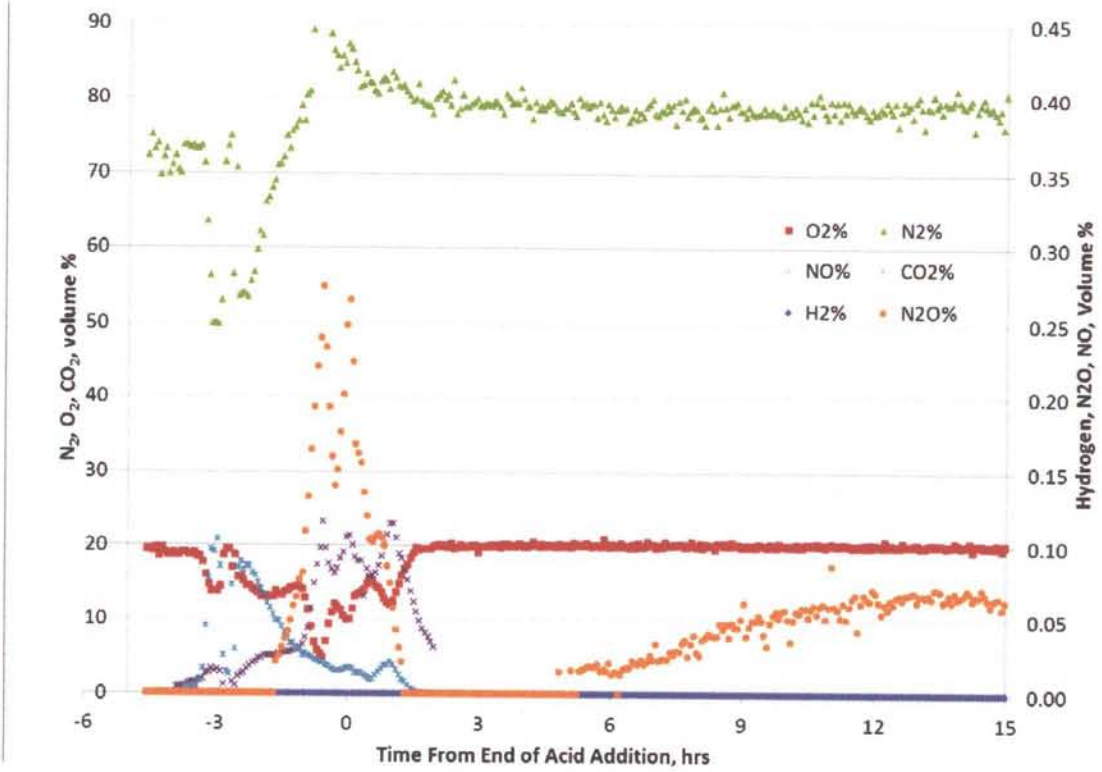

Figure B-1.GF34 SRAT Off-gas Data

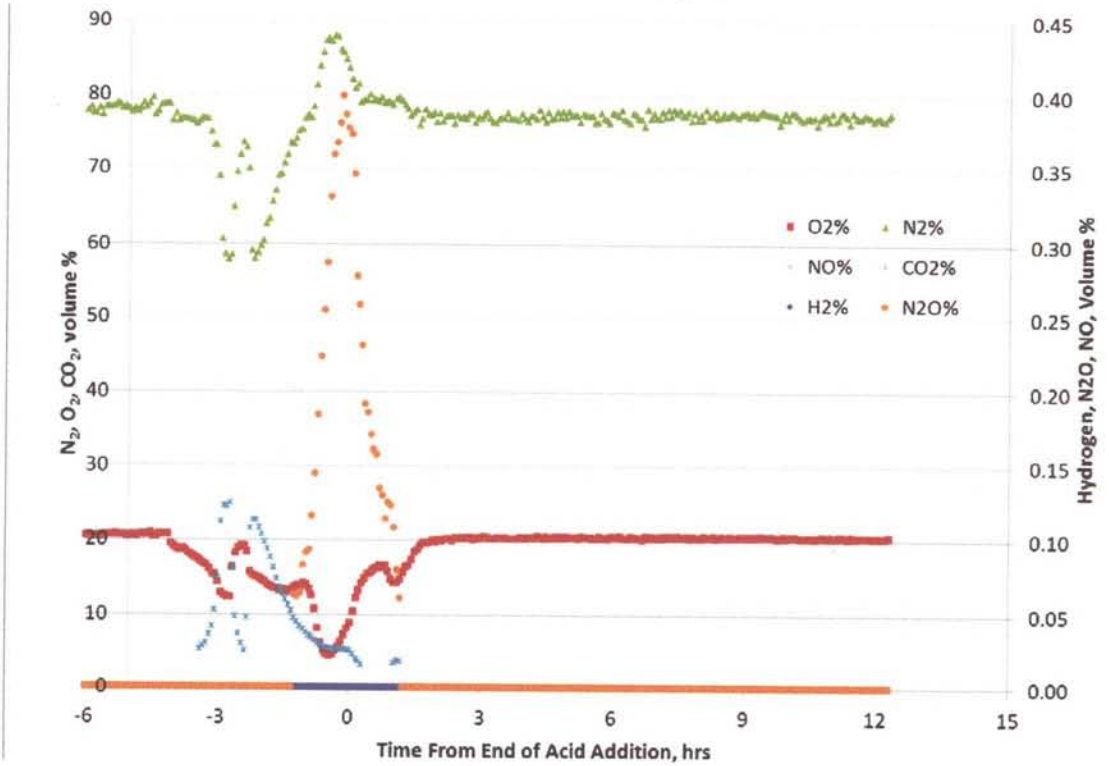

Figure B-2. GF34b SRAT Off-gas Data

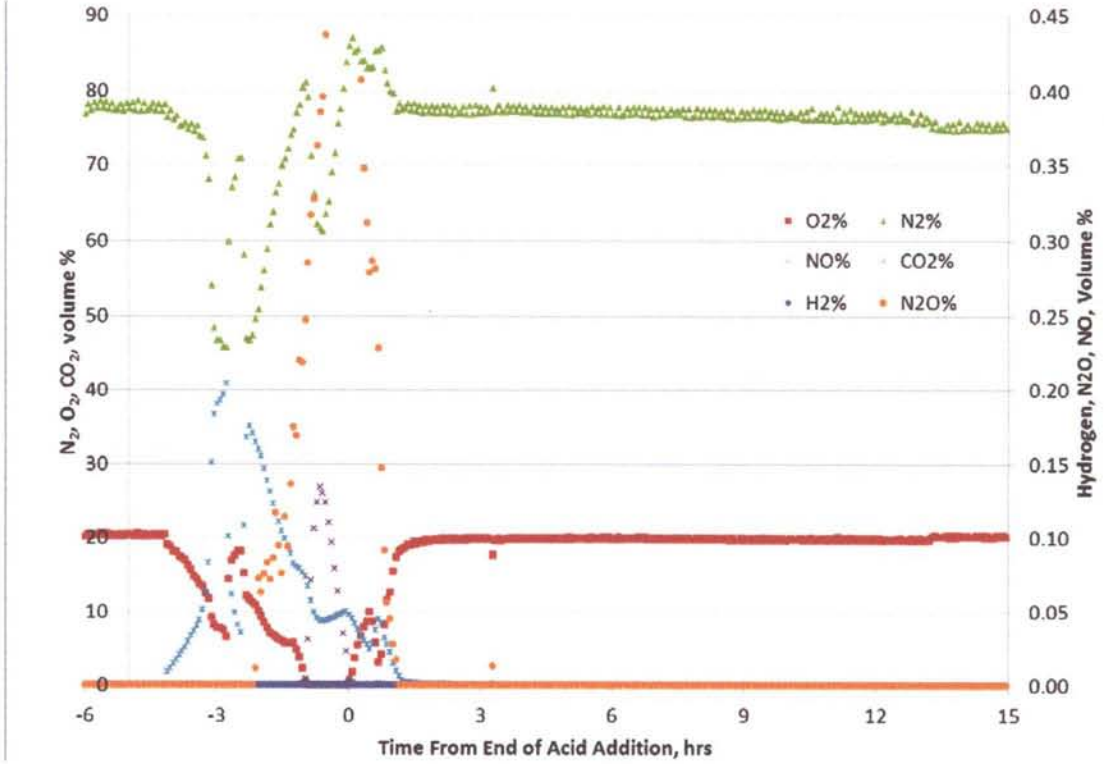

Figure B-3. GF34c SRAT Off-gas Data

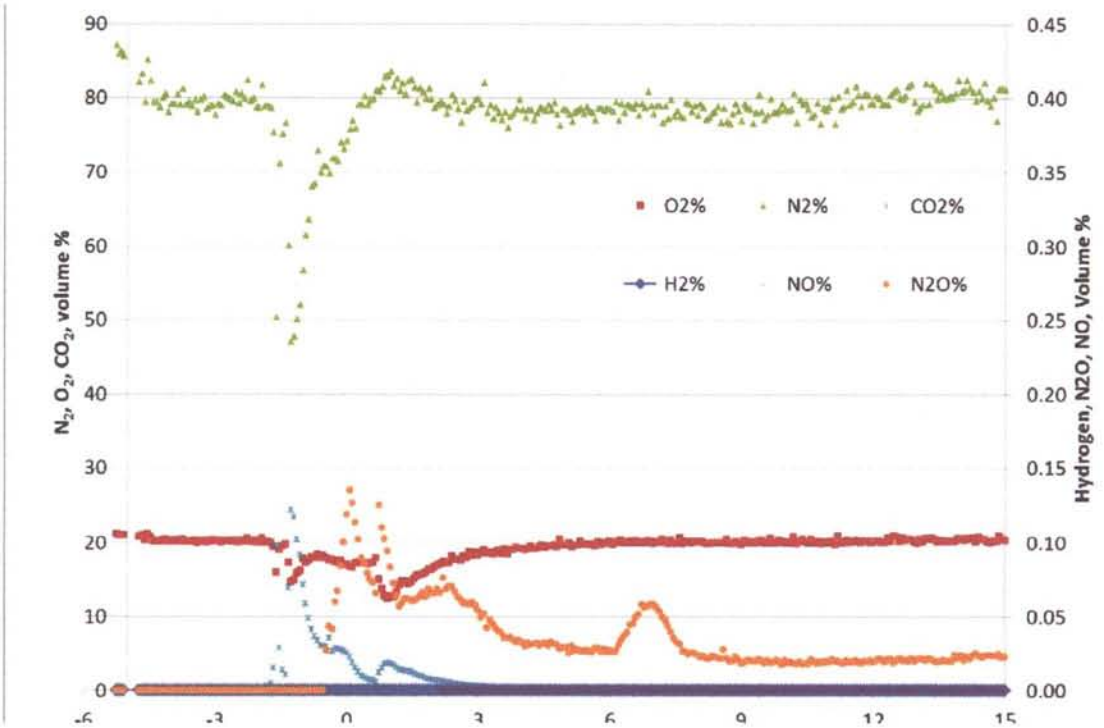

Figure B-4. GF35 SRAT Off-gas Data

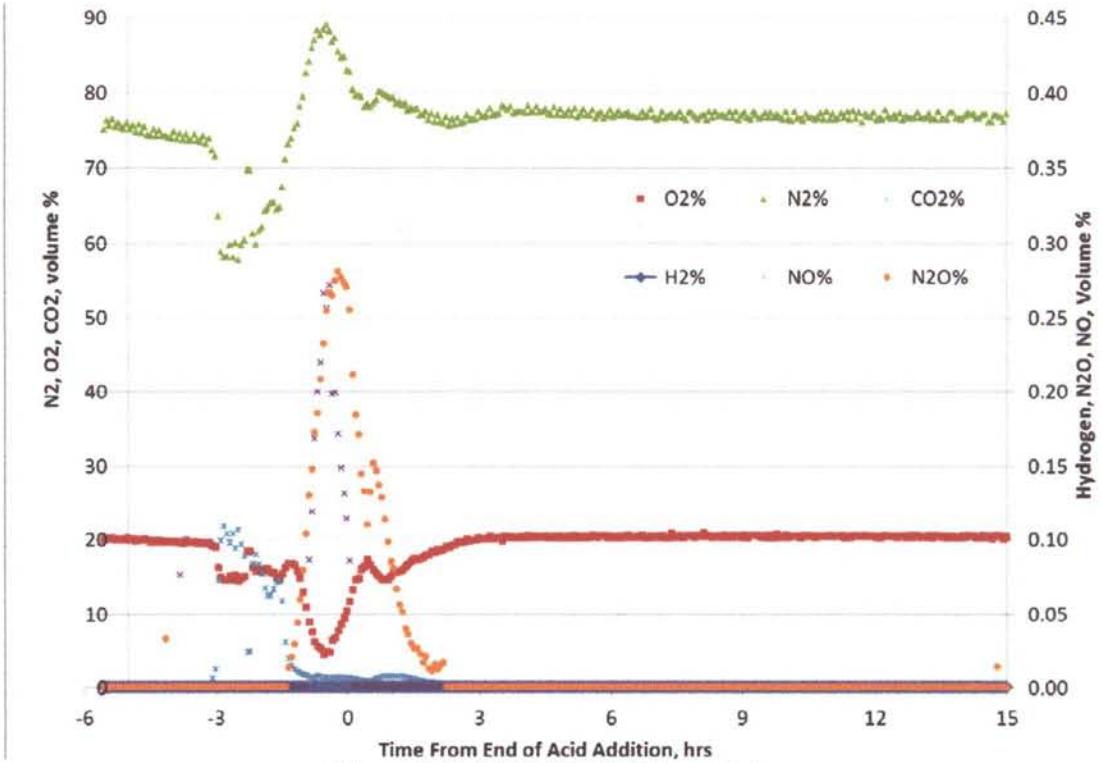

Figure B-5. GF36 SRAT Off-gas Data

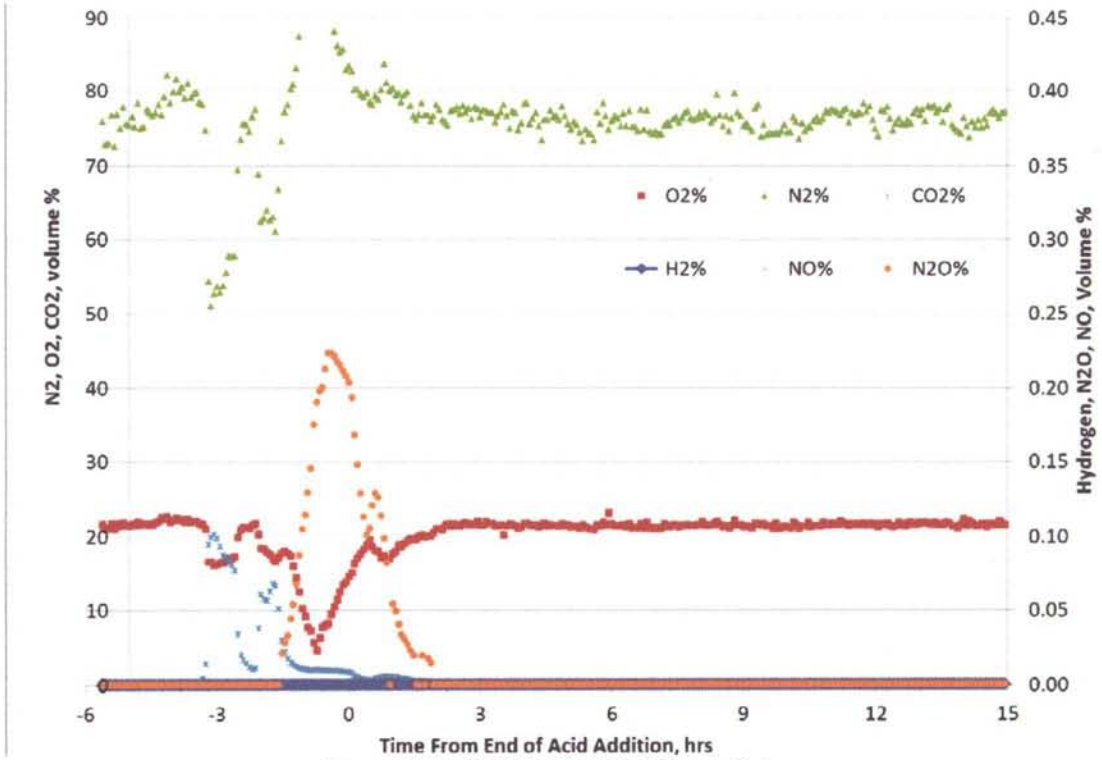

Figure B-6. GF36b SRAT Off-gas Data

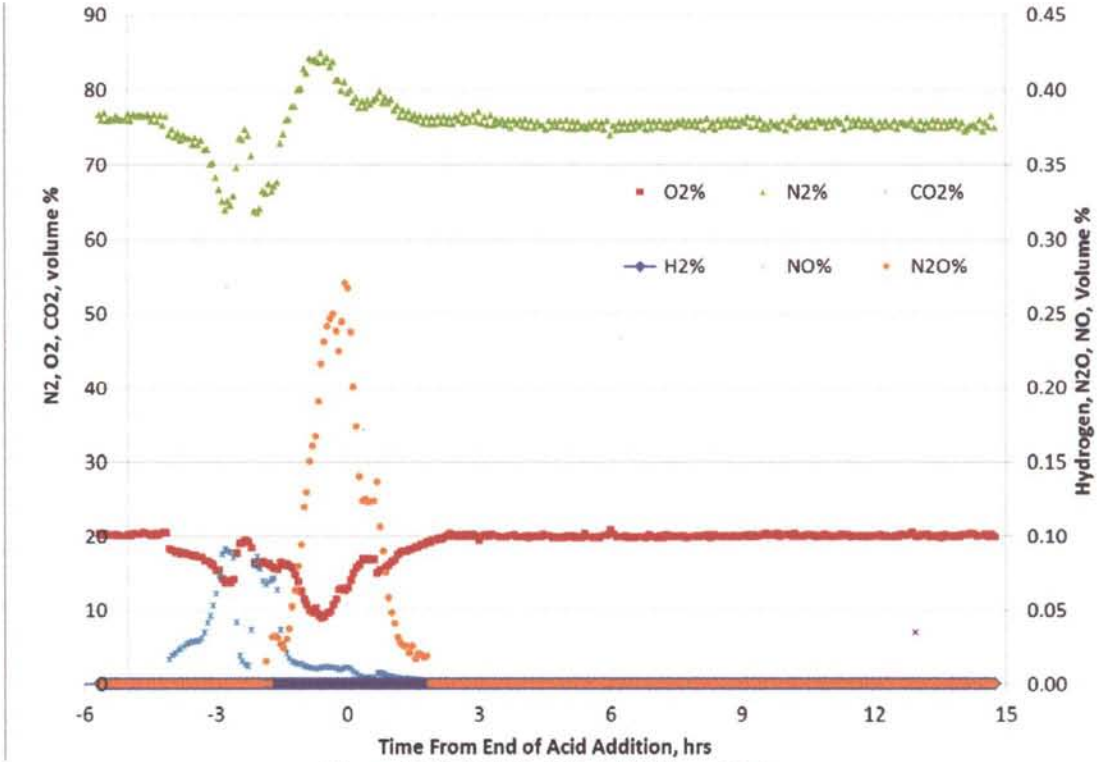

Figure B-7. GF36c SRAT Off-gas Data

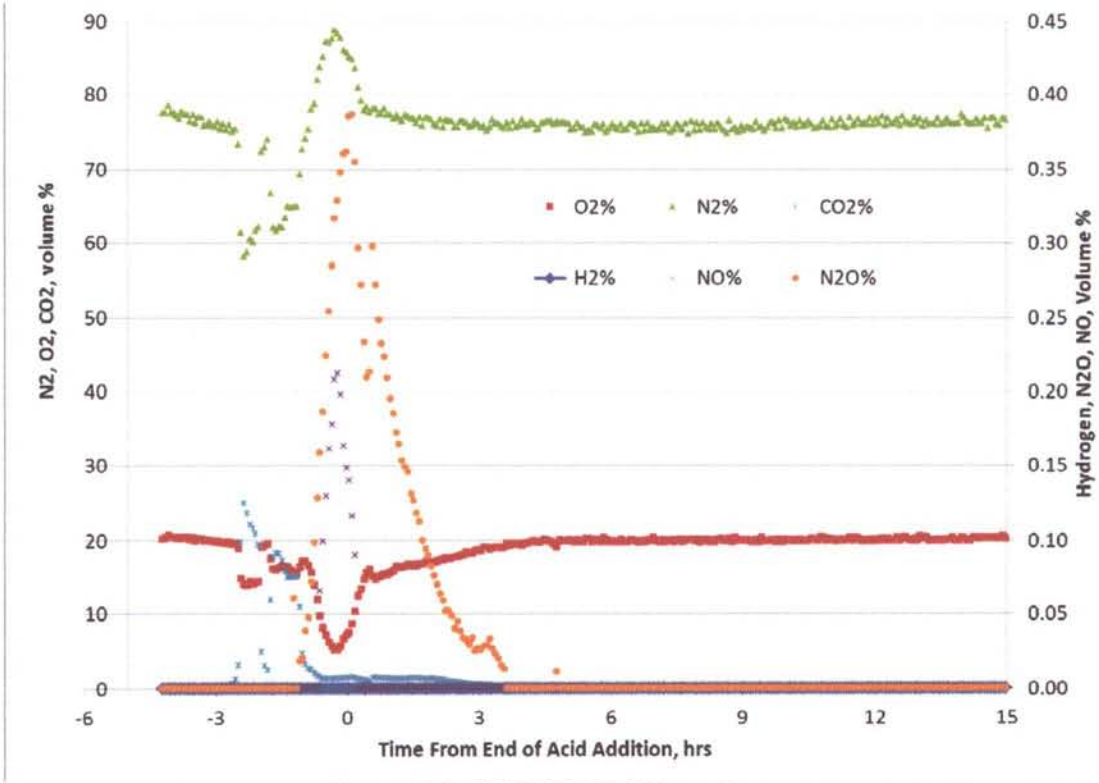

Figure B-8. GF37 SRAT Off-gas Data

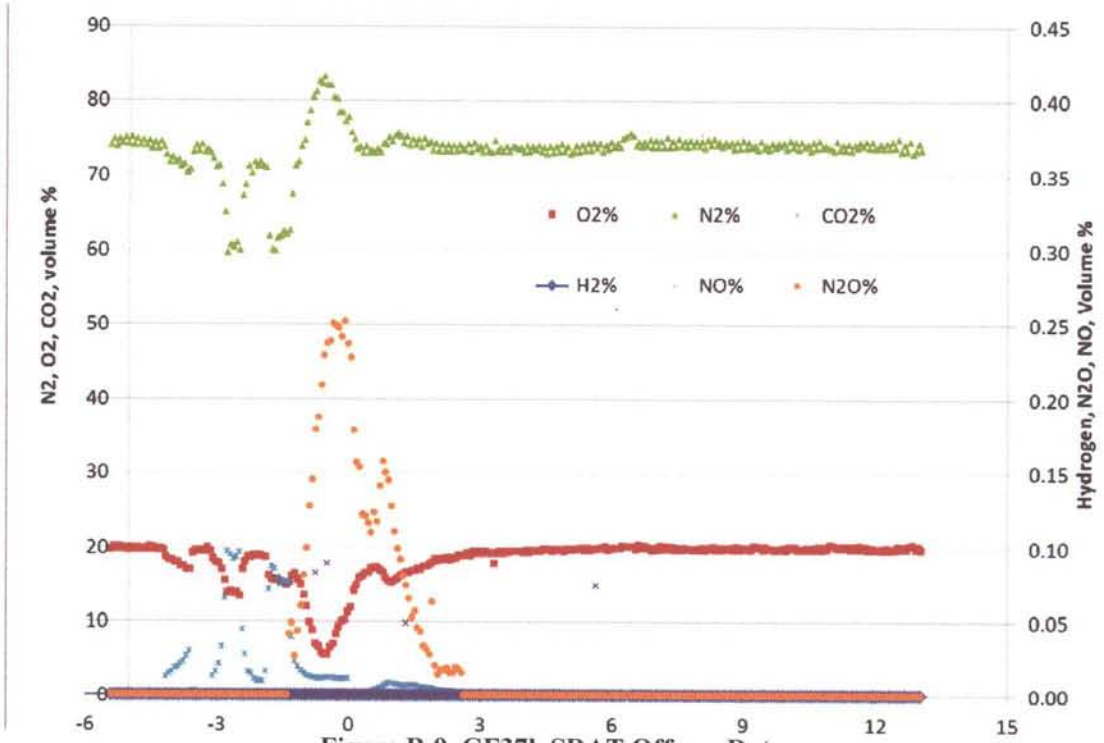

Figure B-9. GF37b SRAT Off-gas Data

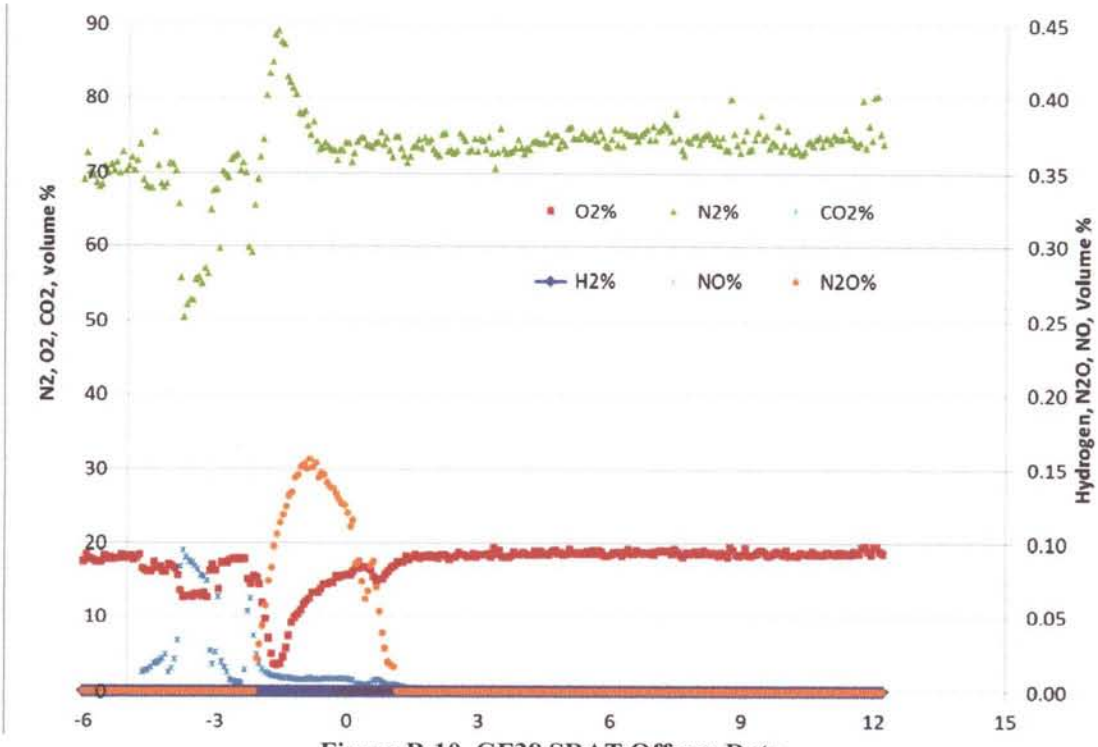

Figure B-10. GF38 SRAT Off-gas Data

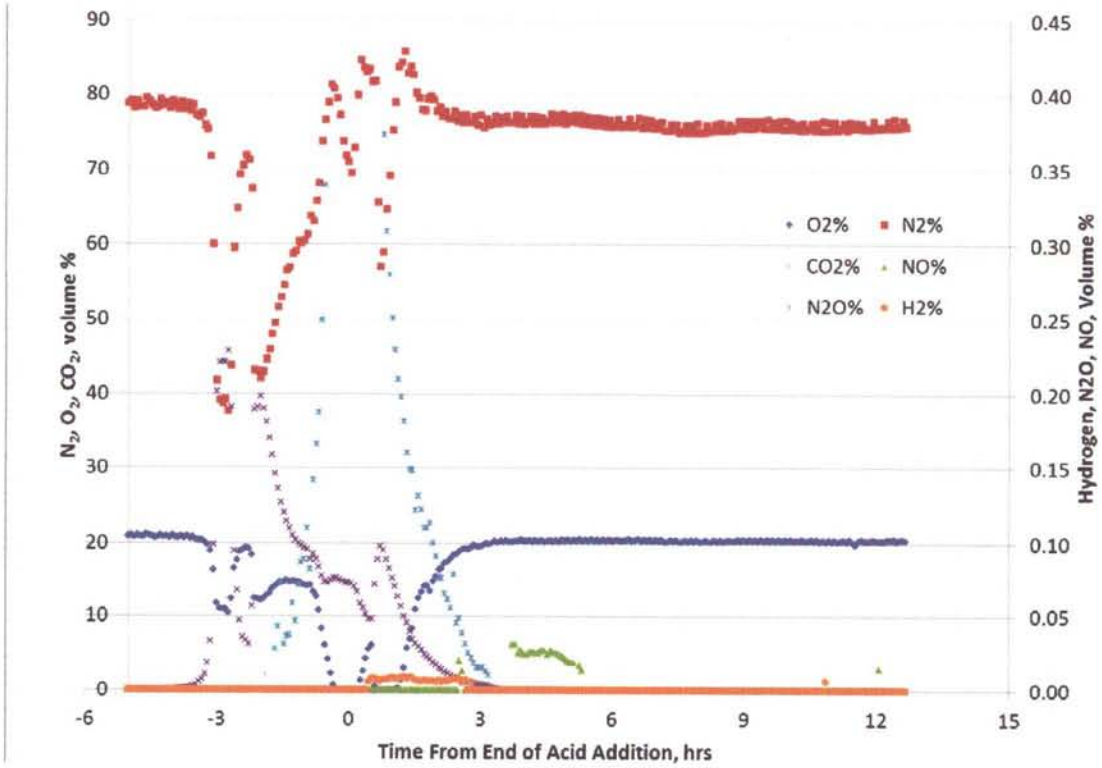

Figure B-11. GF40 SRAT Off-gas Data

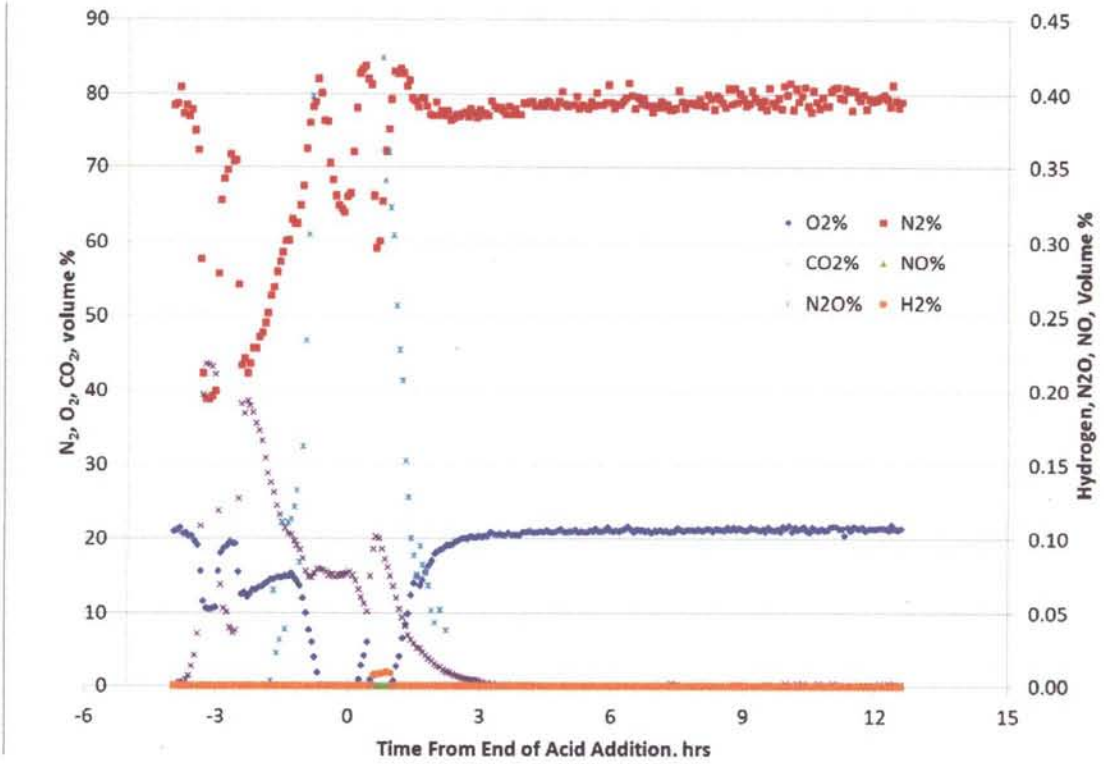

Figure B-12. GF41 SRAT Off-gas Data

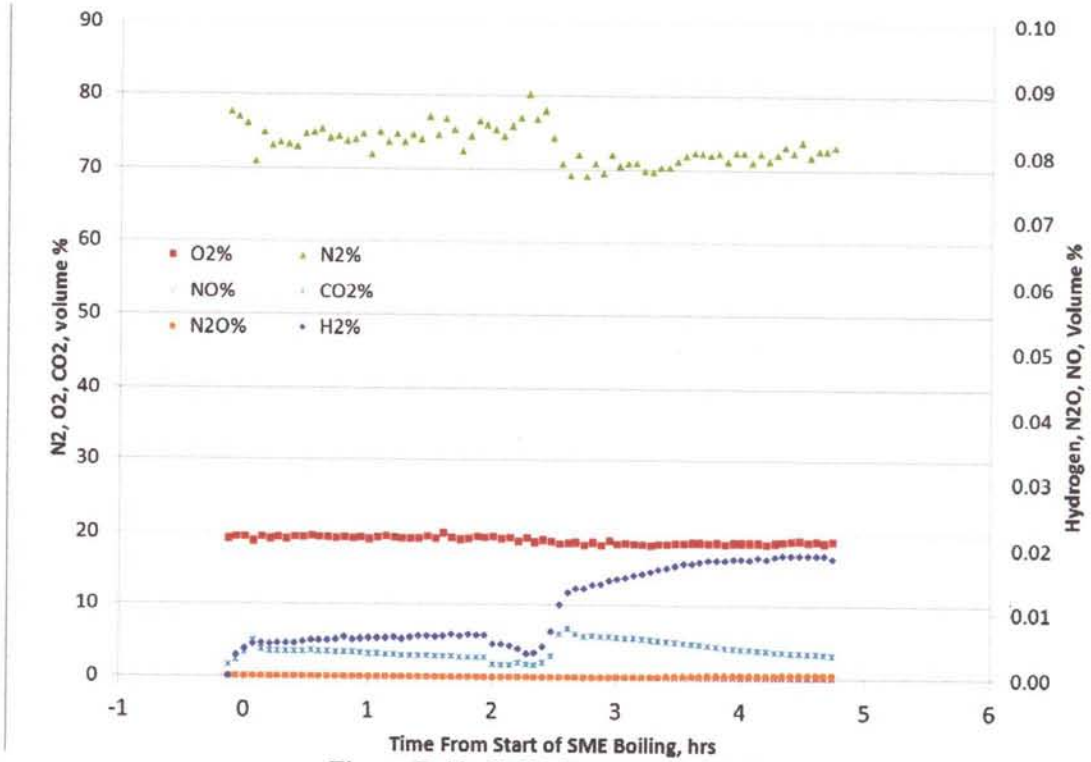

Figure B-13. GF34 SME Off-gas Data

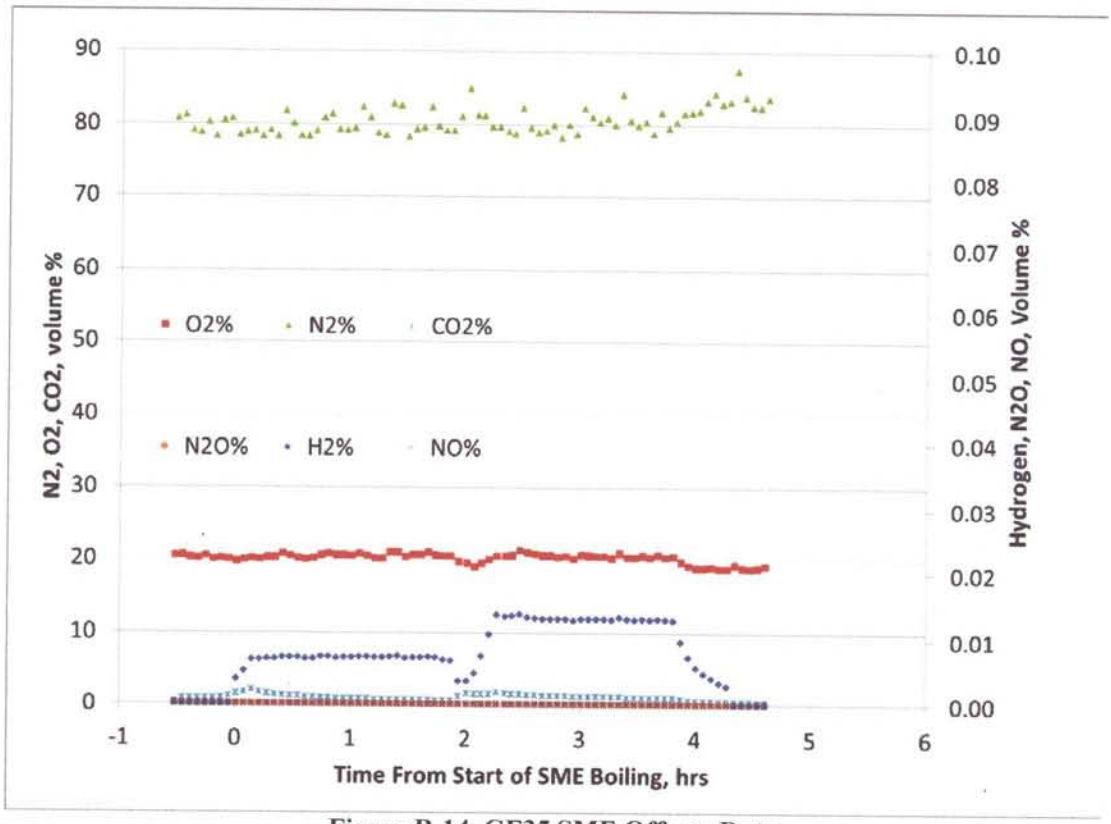

Figure B-14. GF35 SME Off-gas Data

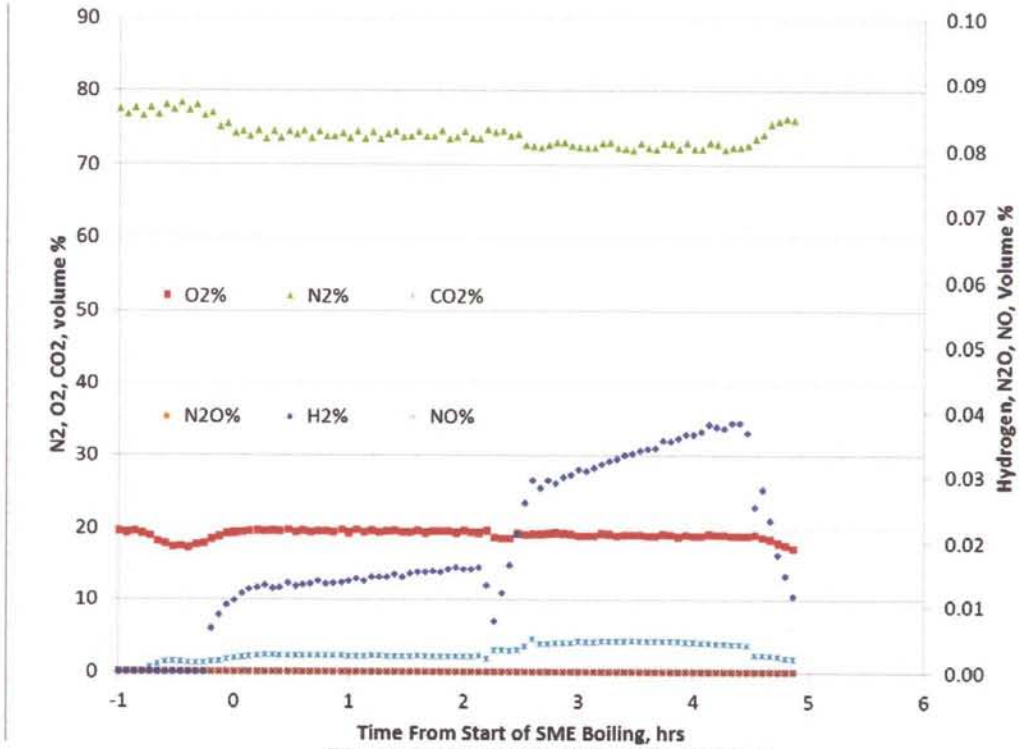

Figure B-15. GF36 SME Off-gas Data

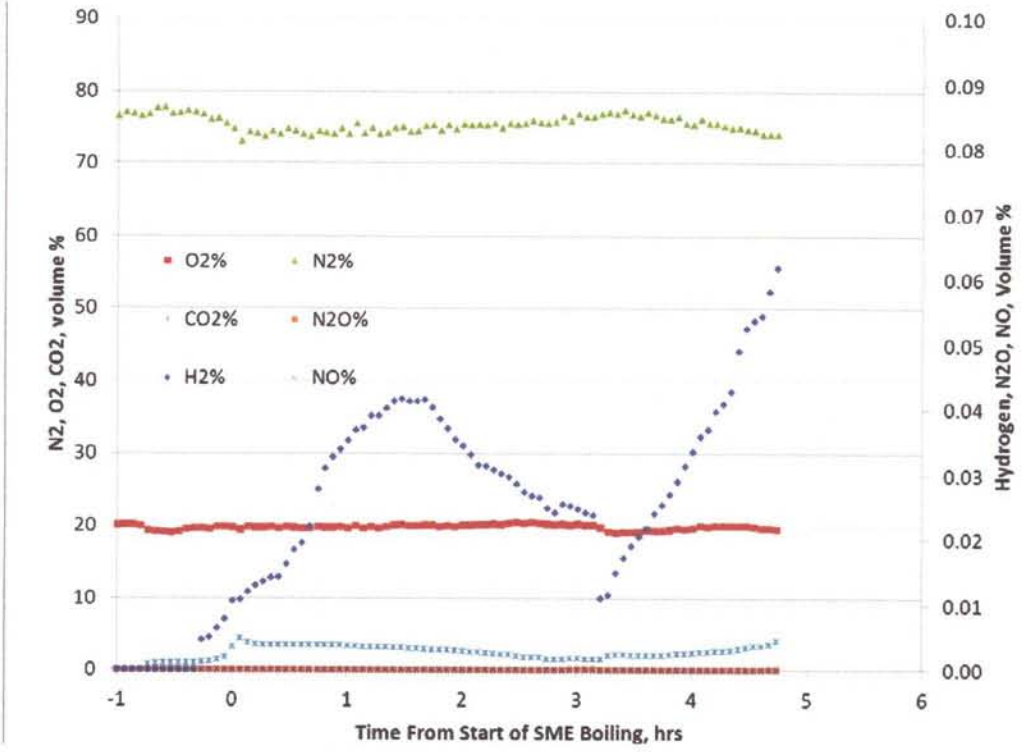

Figure B-16. GF37 SME Off-gas Data

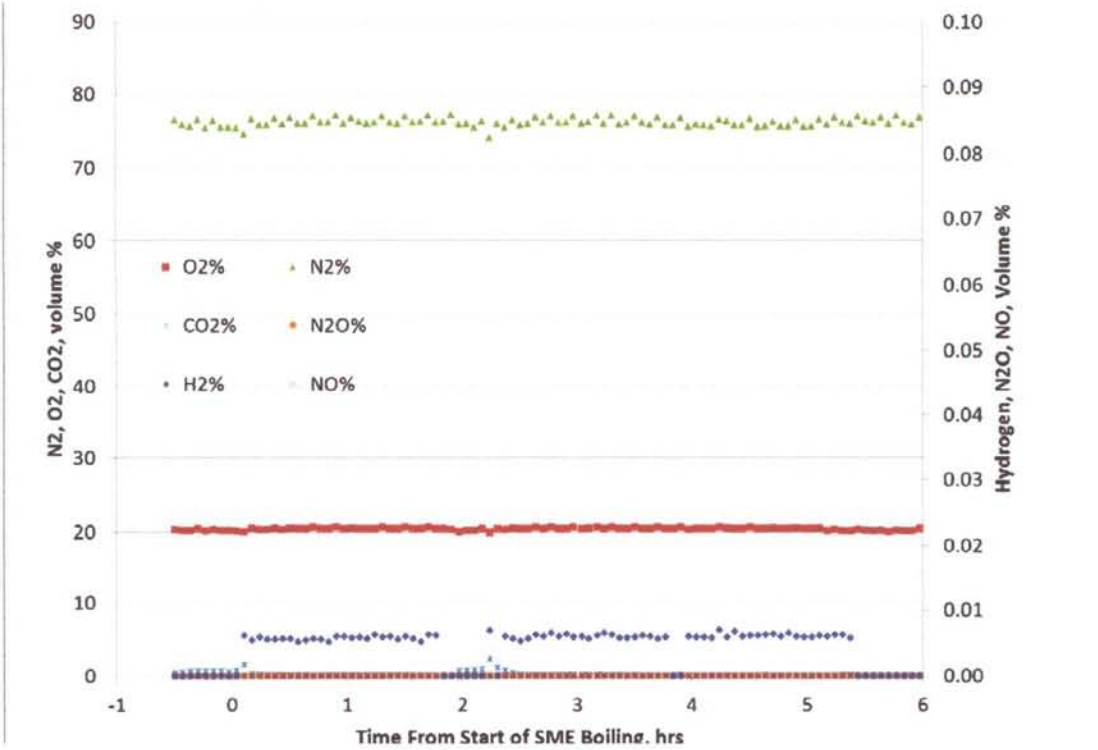

Figure B-17. GF40 SME Off-gas Data

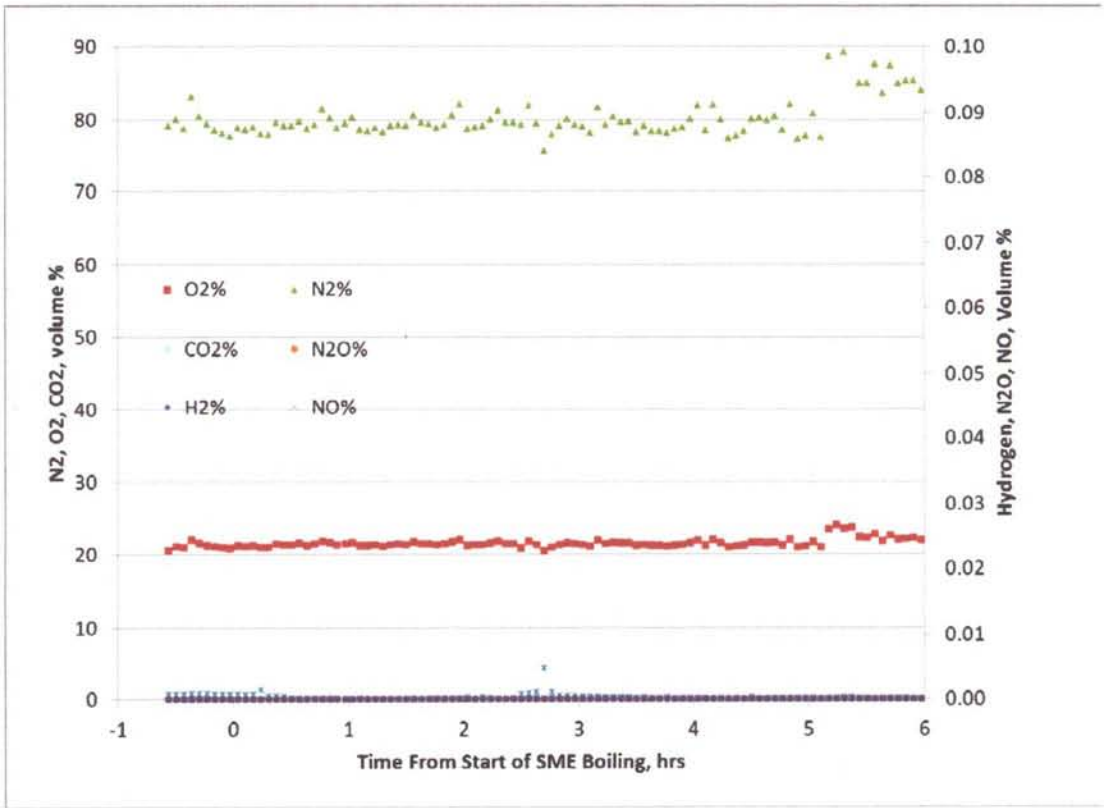

Figure B-18. GF41 SME Off-gas Data

Appendix C. X-ray Defraction (XRD) Results of SRAT and SME Solids and Mercury Solids

This Appendix contains X-ray diffraction data for samples of the crystallized solids that formed post cooling in some SRAT and SME products from the matrix runs.

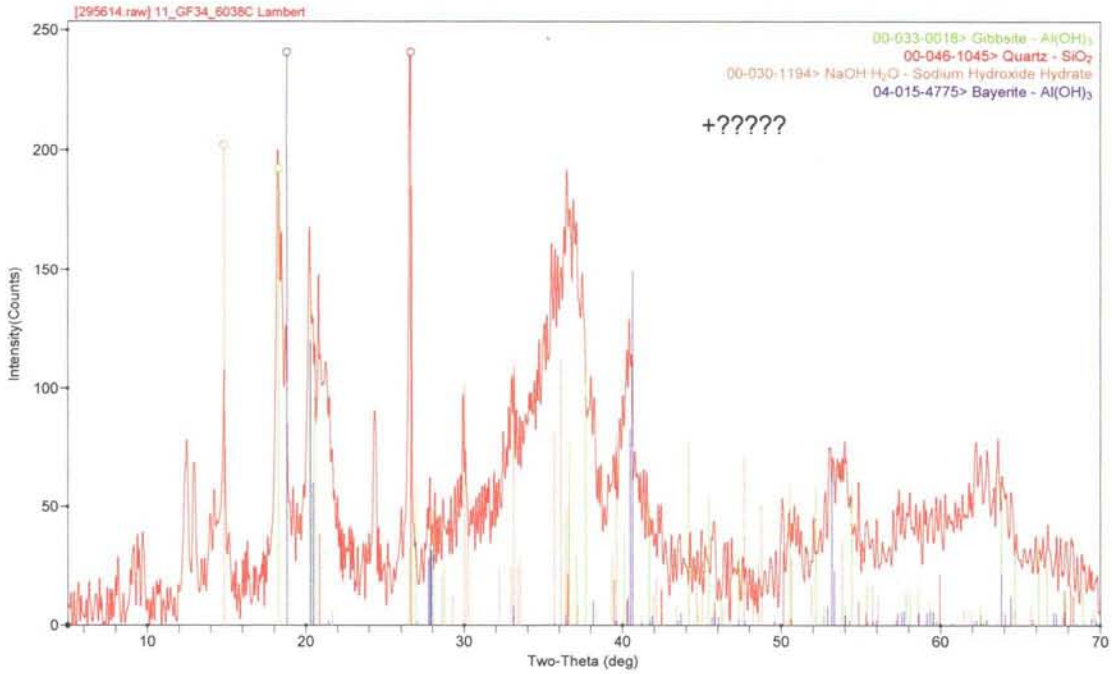

* The NaOH*H2O is questionable. There is a phase in this sample that could not be identified.

Figure C-1. GF34 SRAT Product

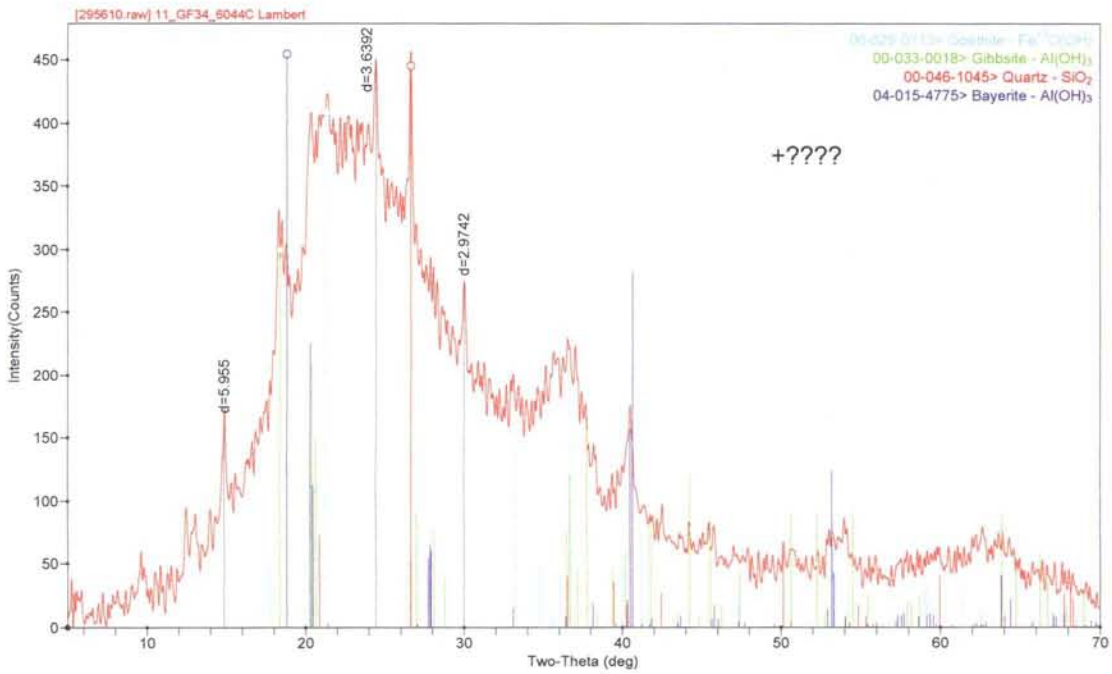

Figure C-2. GF34 SME Product XRD

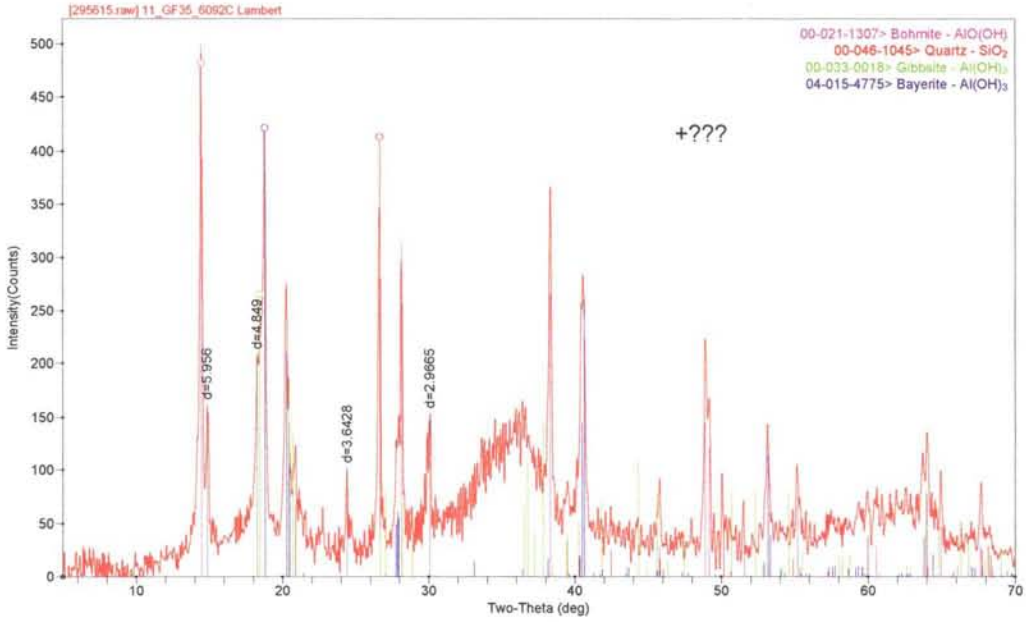

Figure C-3. GF35 SRAT Product XRD

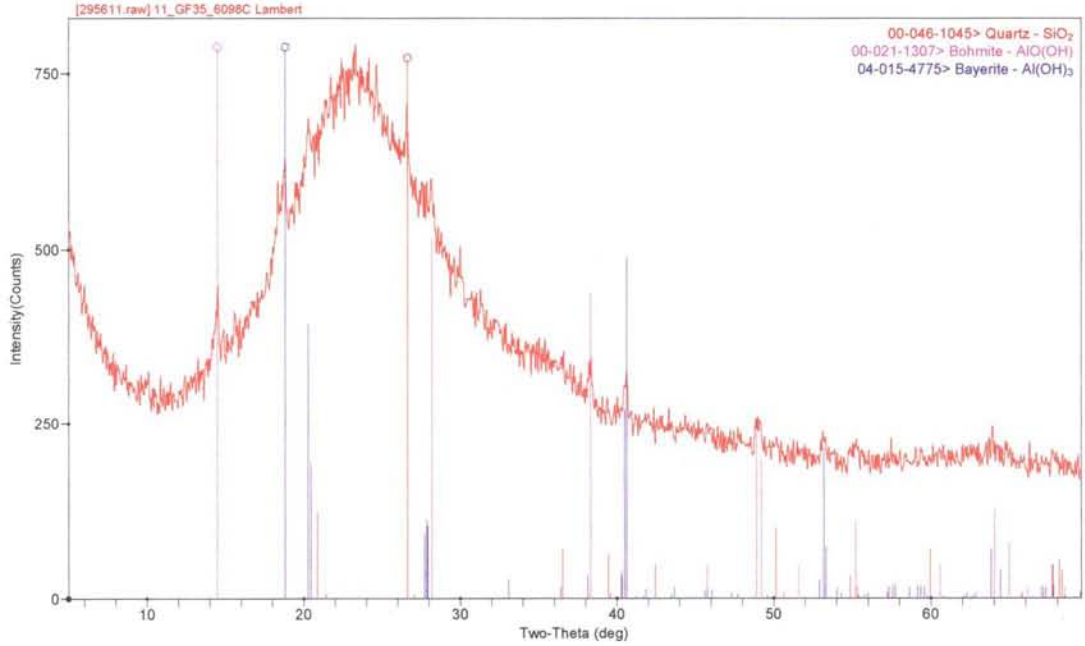

Figure C-4. GF35 SME Product

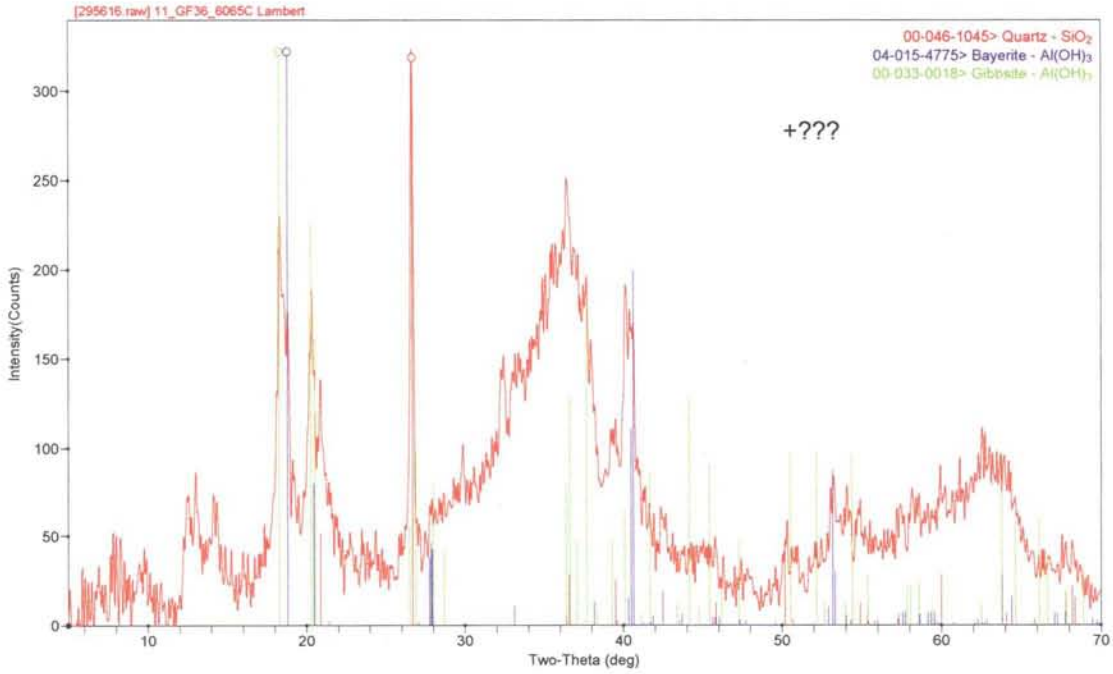

Figure C-5. GF36 SRAT Product

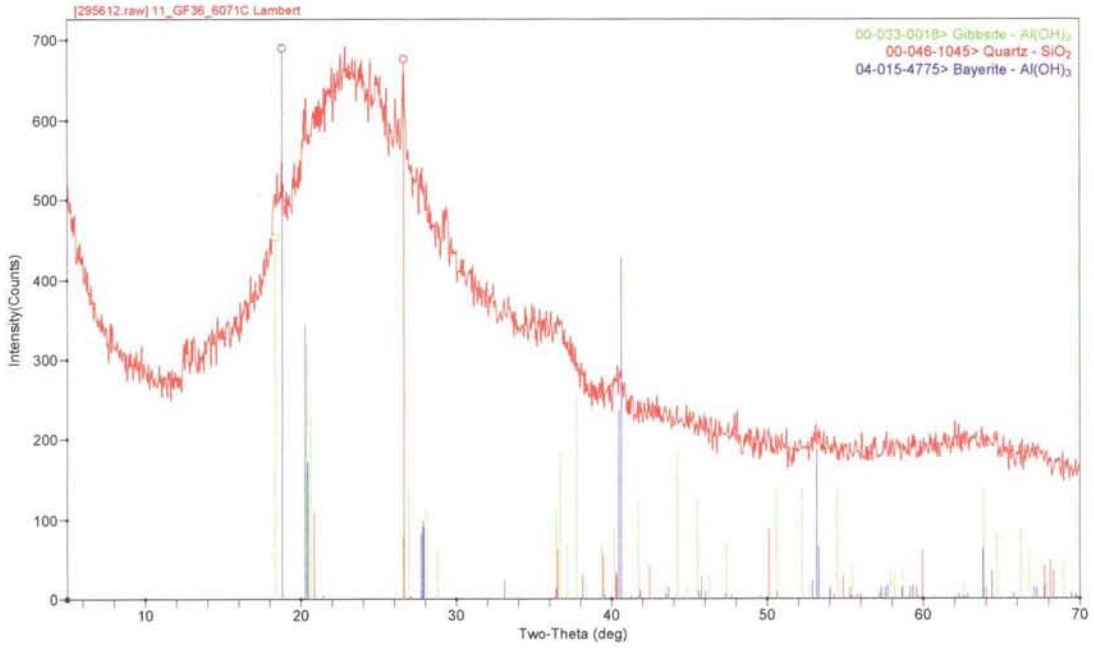

Figure C-6. GF36 SME Product

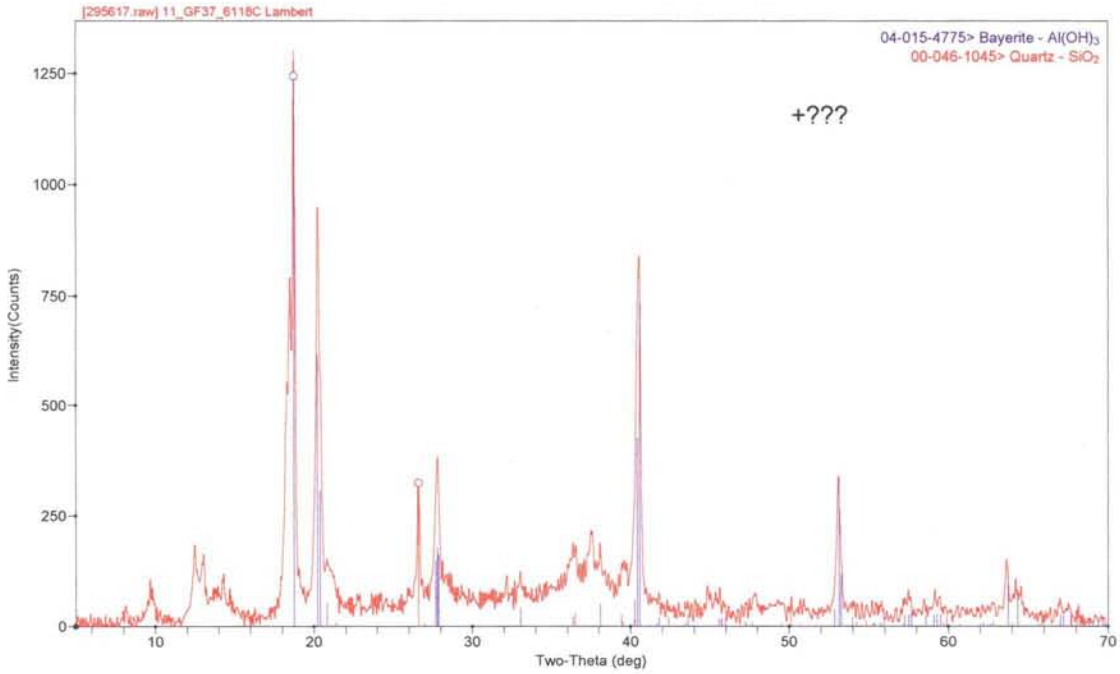

Figure C-7. GF37 SRAT Product

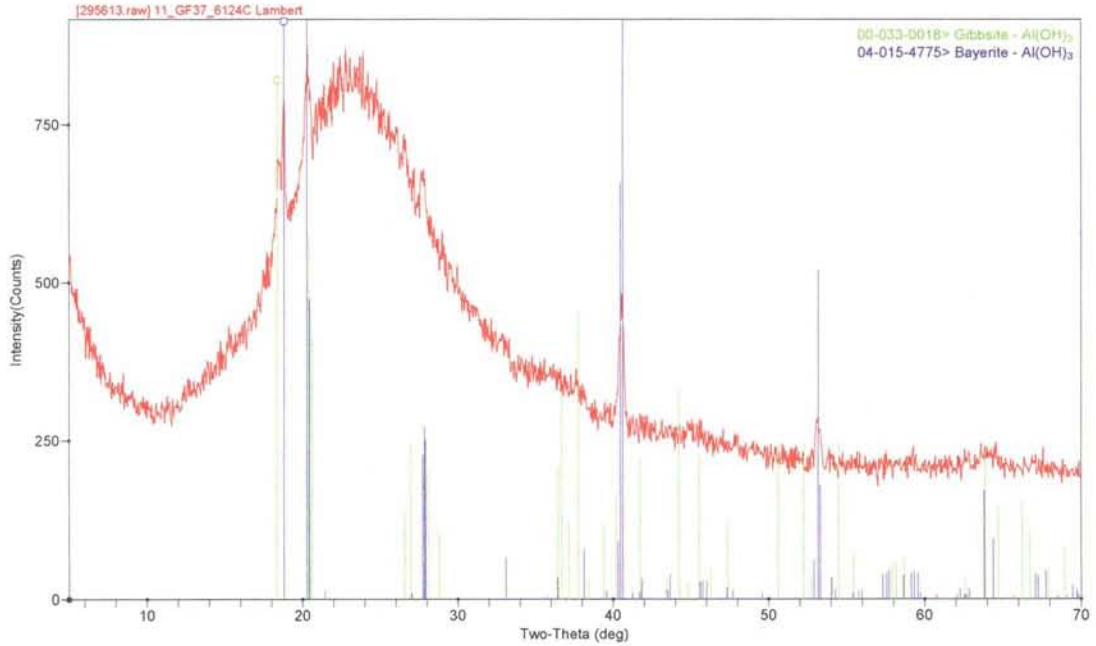

Figure C-8. GF37 SME Product

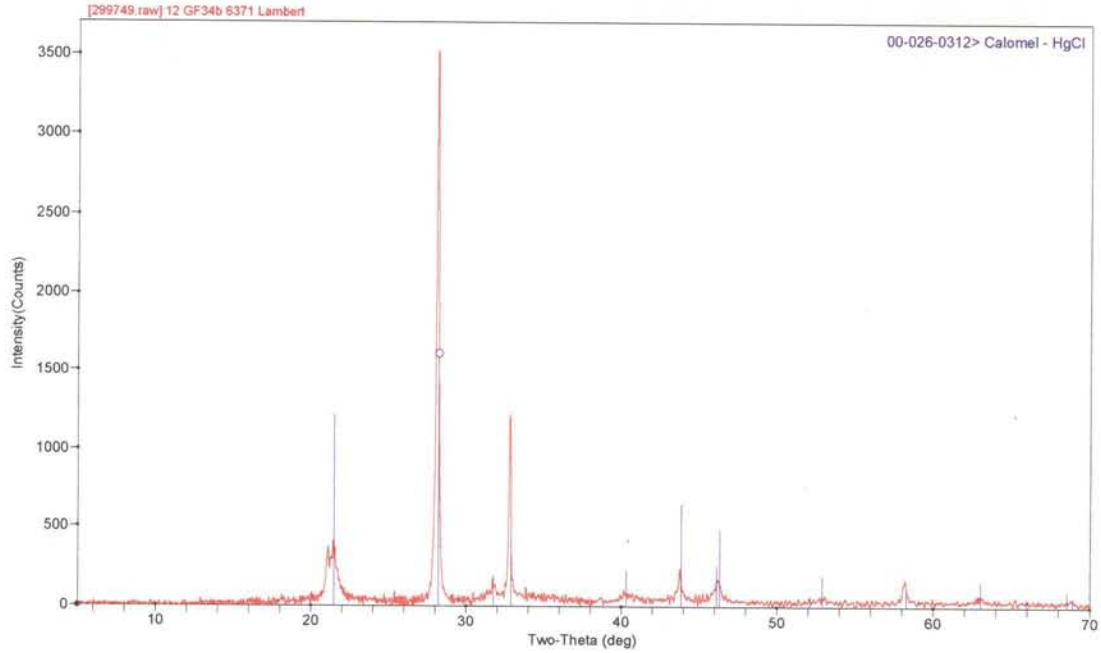

Figure C-9. GF34b MWWT Mercury Product

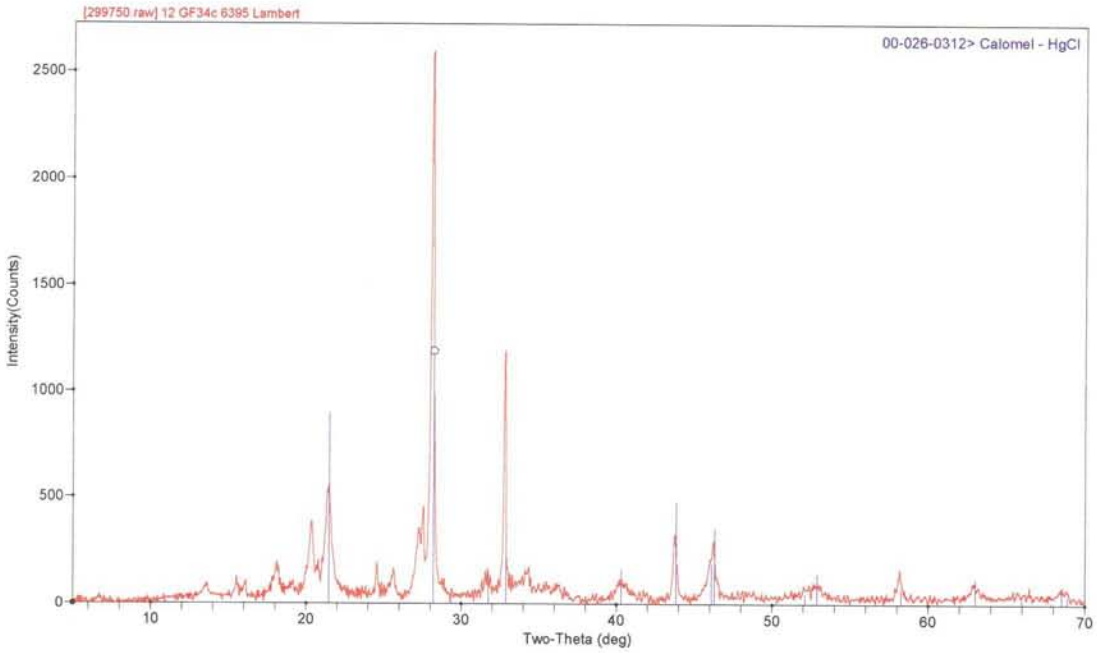

Figure C-10. GF34c MWWT Mercury Product

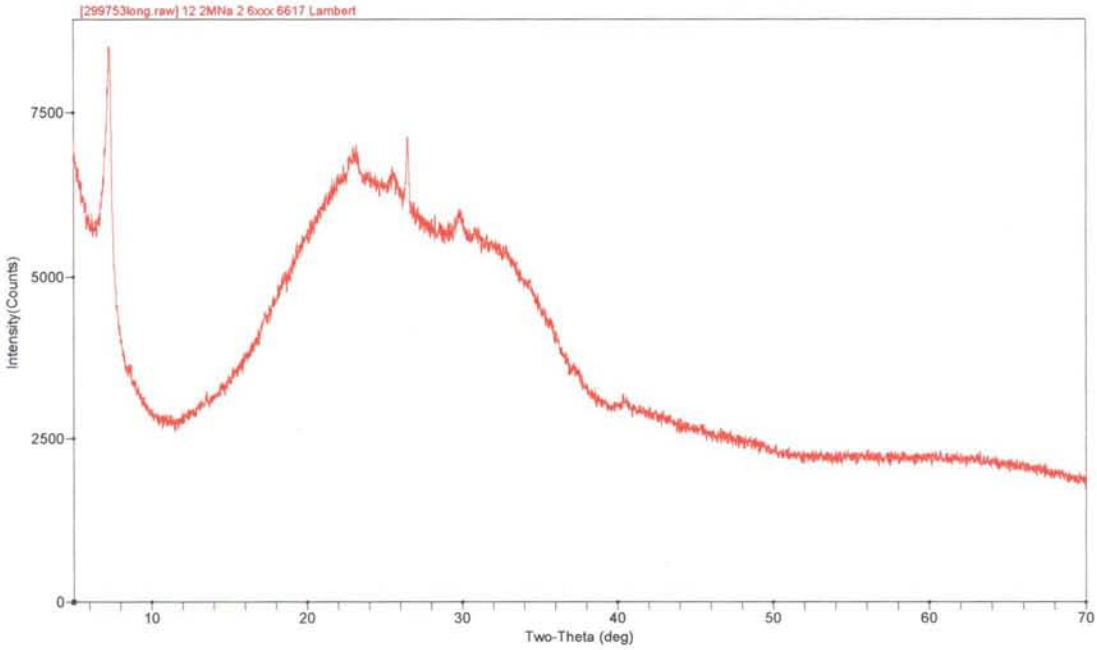

Figure C-11. GF40 MWWT Mercury Product

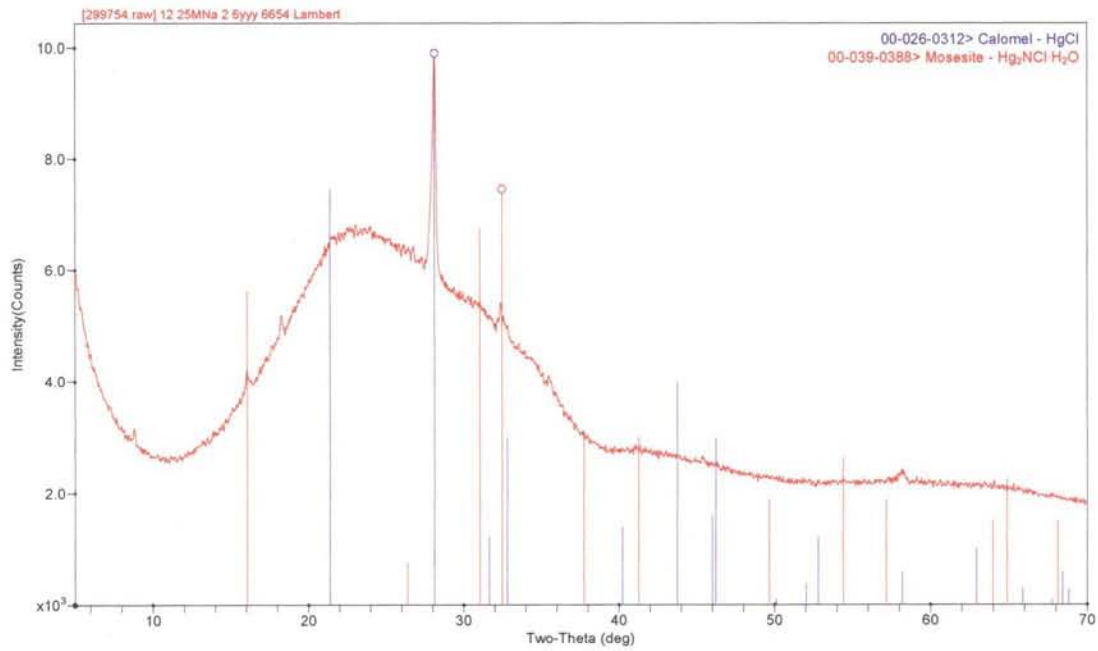

Figure C-12. GF41 MWWT Mercury Product

Appendix D. Supernate Results

This Appendix includes additional data collected from experiments using a supernate simulant instead of sludge as described in Section 3.1.

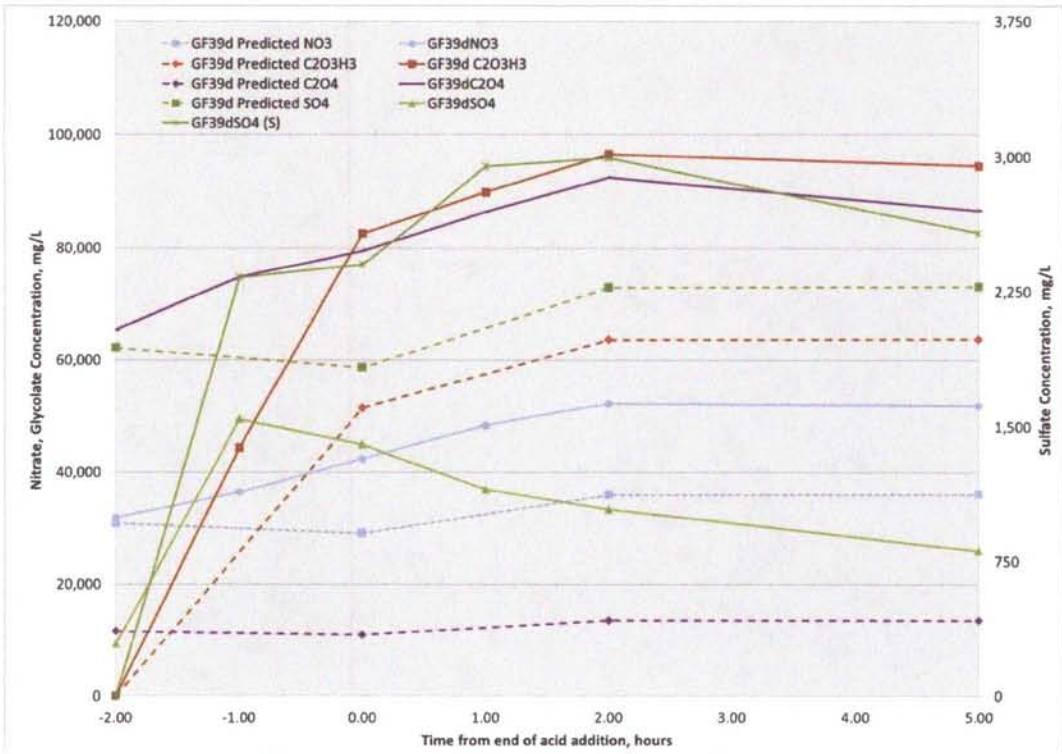

Figure D-1. GF39a Supernate Anion Results

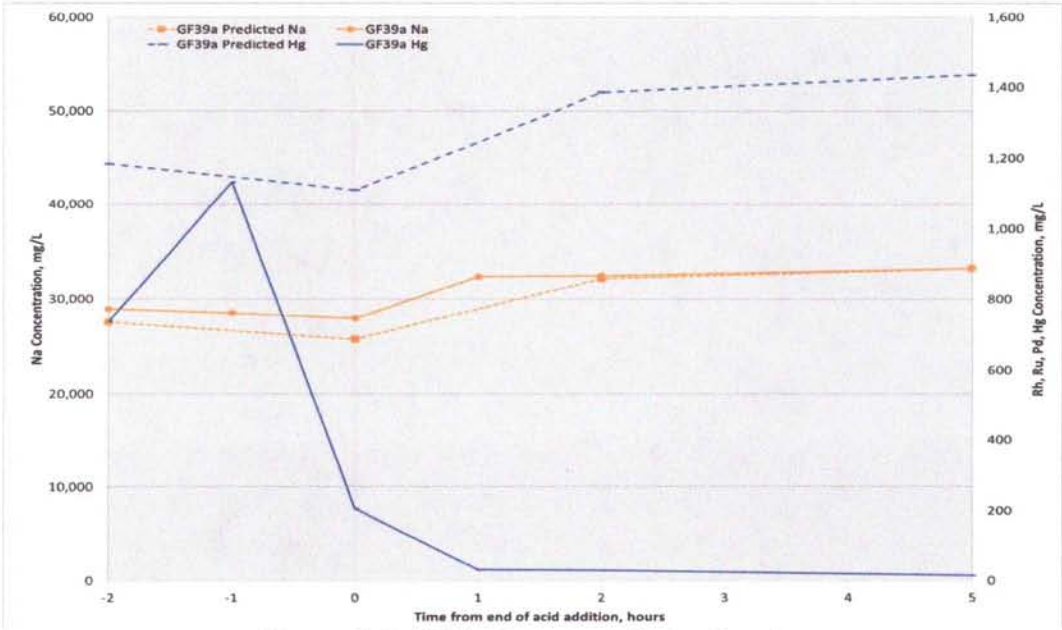

Figure D-2. GF39a Supernate Cation Results

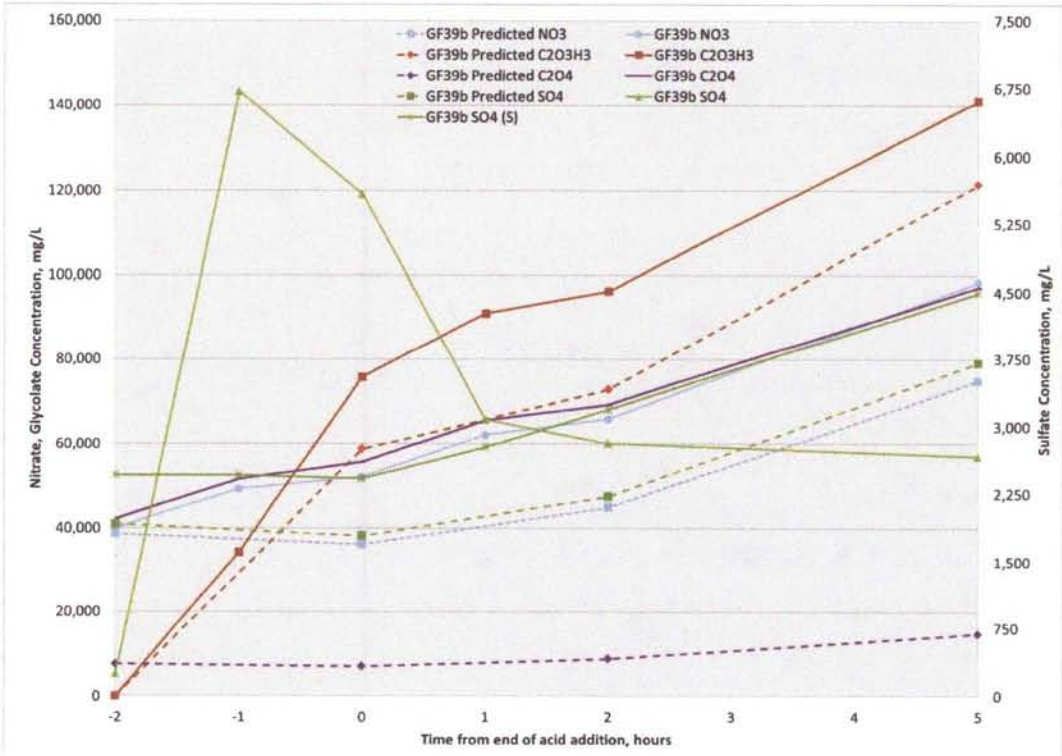

Figure D-3. GF39b Supernate Anion Results

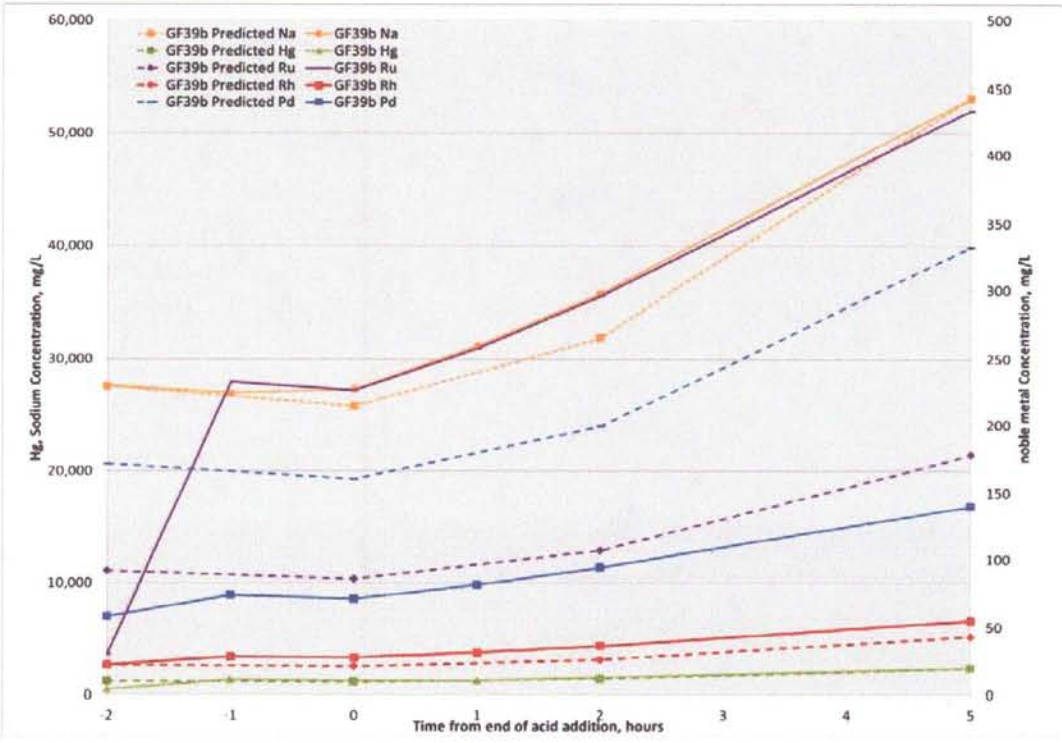

Figure D-4. GF39b Supernate Cation Results

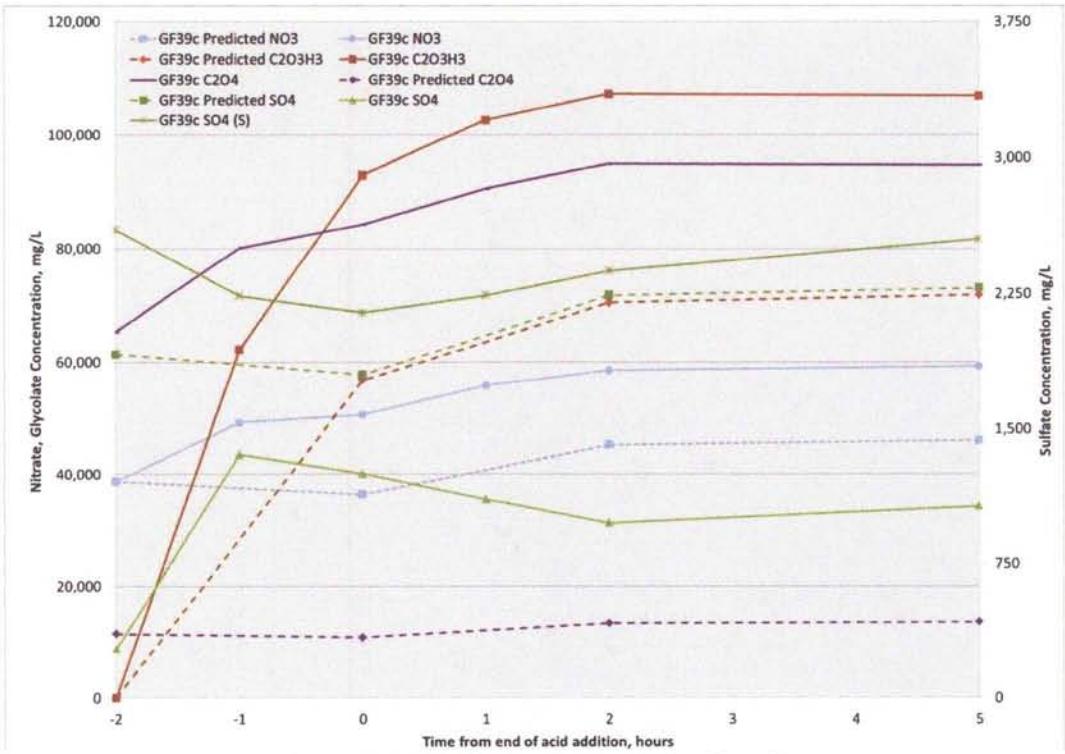

Figure D-5. GF39c Supernate Anion Results

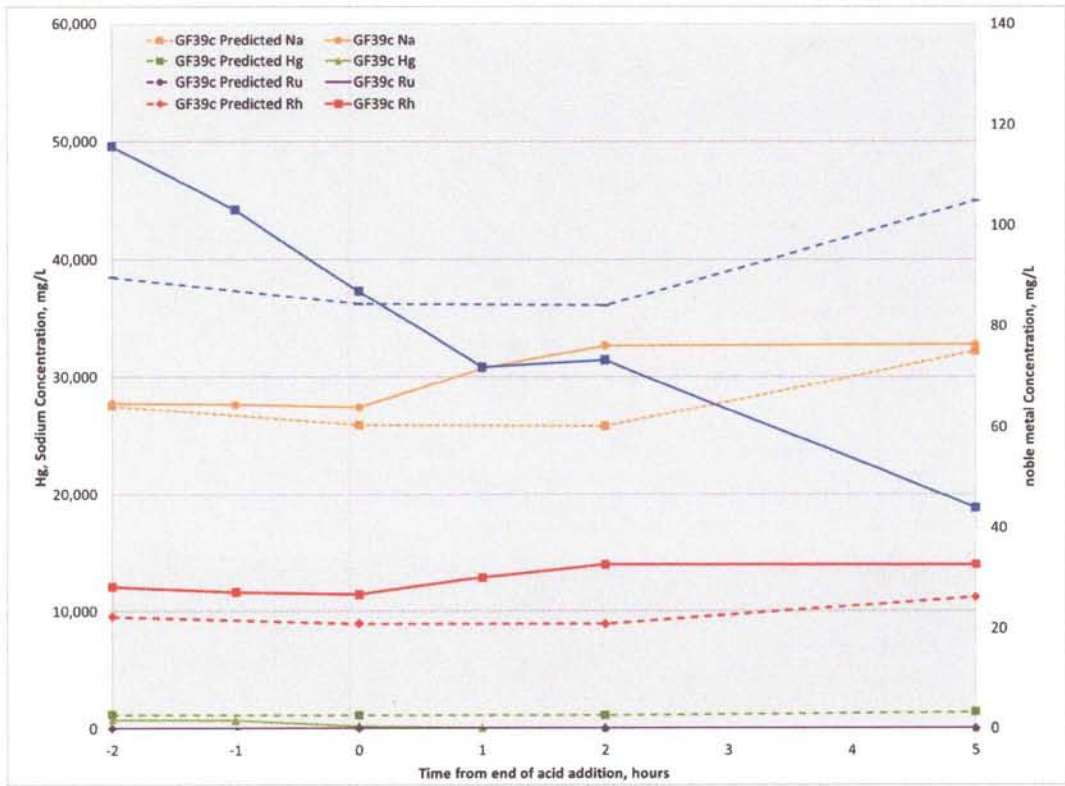

Figure D-6. GF39c Supernate Cation Results

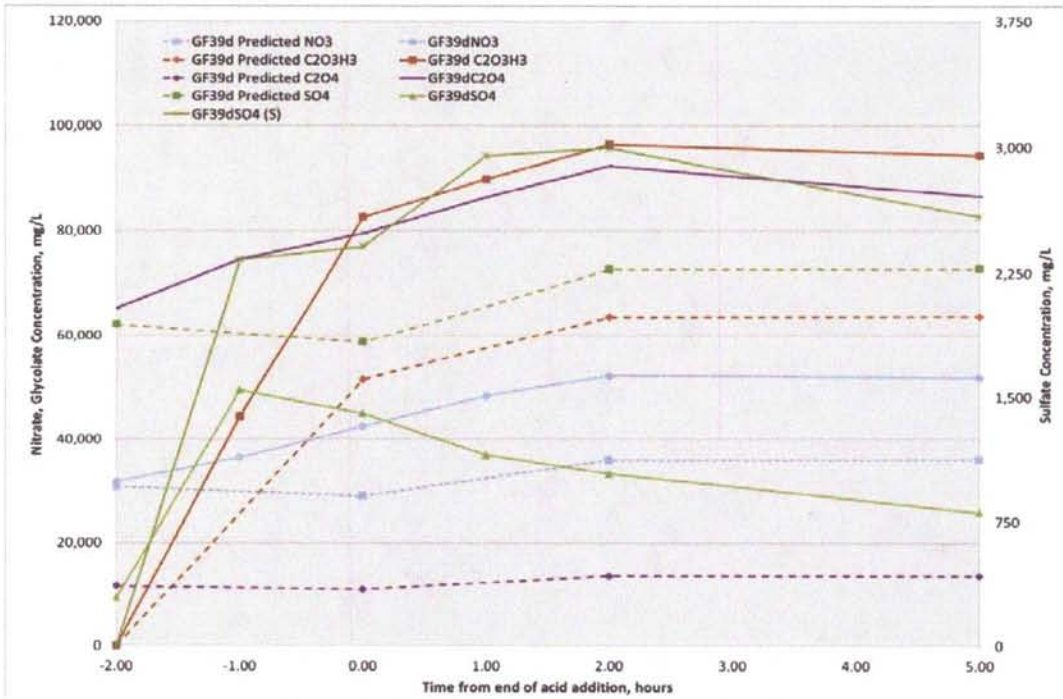

Figure D-7. GF39d Supernate Anion Results

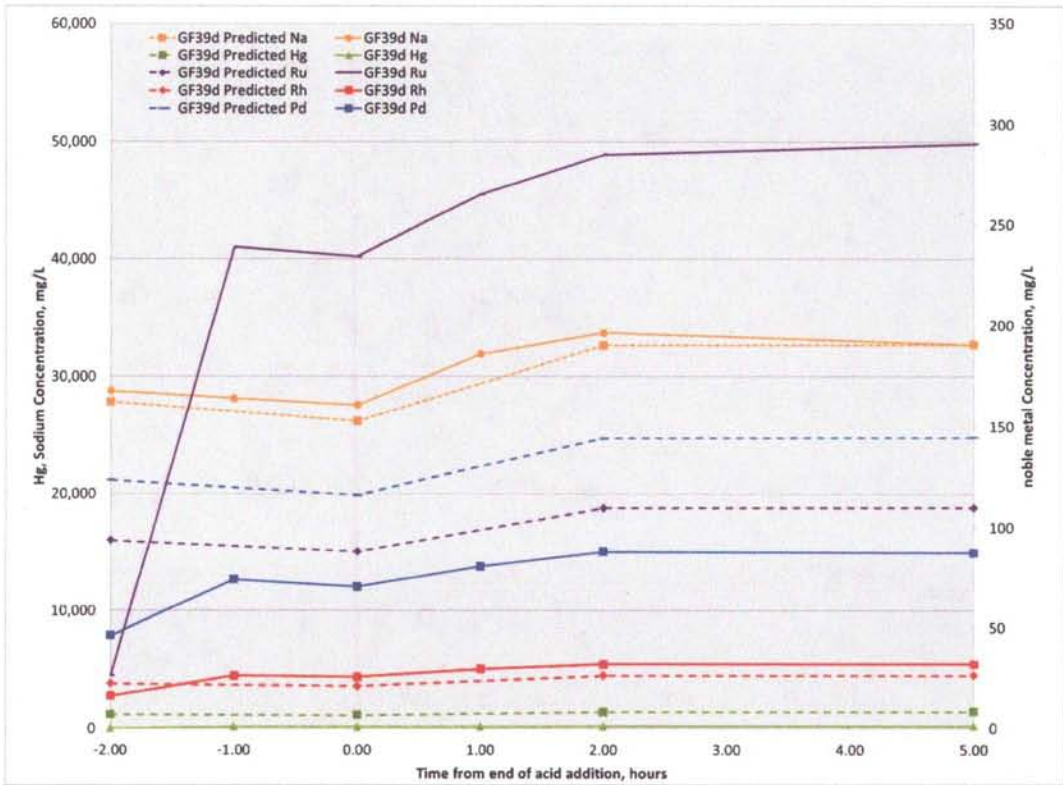

Figure D-8. GF39d Supernate Cation Results

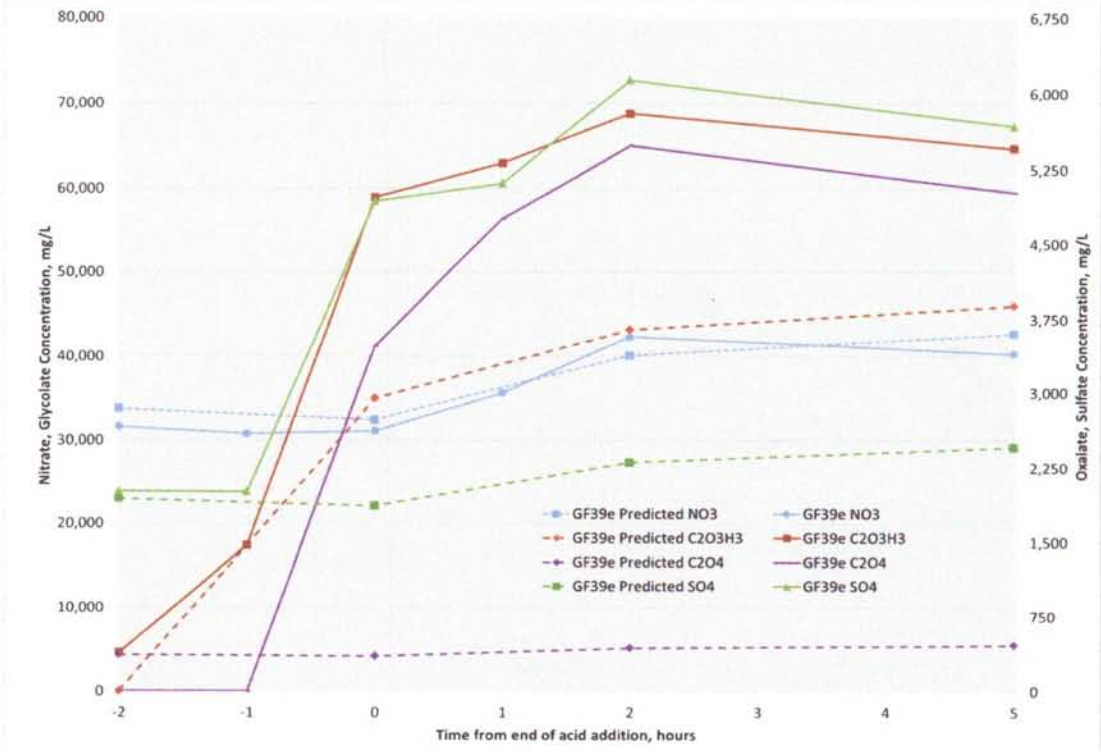

Figure D-9. GF39e Supernate Anion Results

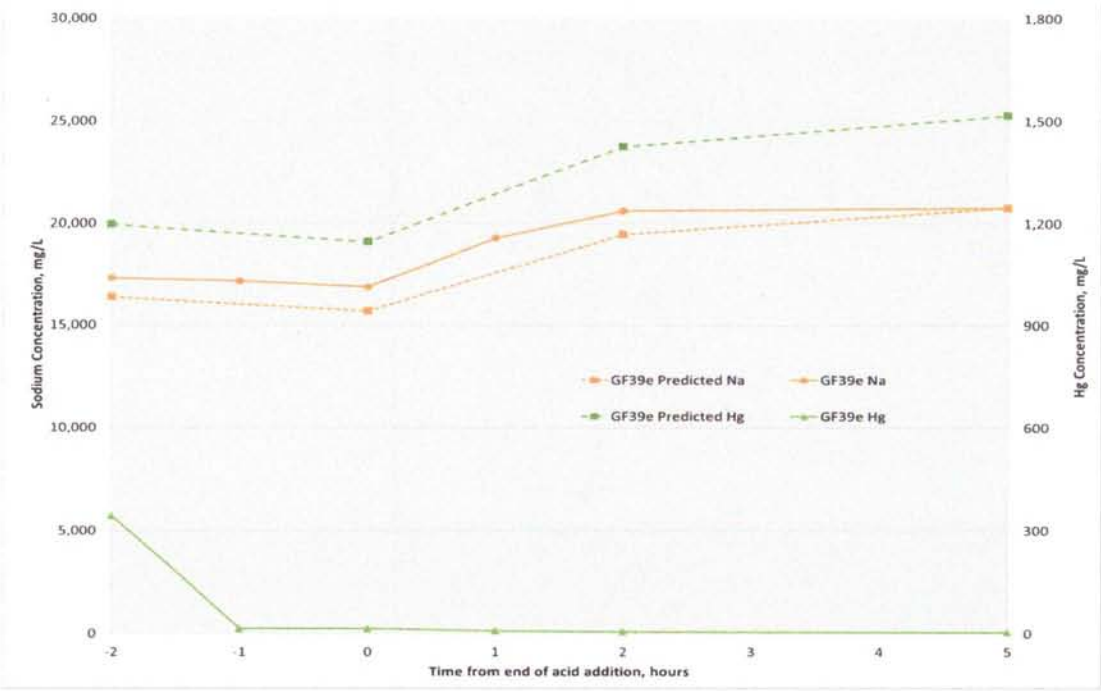

Figure D-10. GF39e Supernate Cation Results

Distribution:

K. M. Fox, 999-W
S. D. Fink, 773-A
B. J. Giddings, 786-5A
C. C. Herman, 999-W
S. L. Marra, 773-A
F. M. Pennebaker, 773-42A
W. R. Wilmarth, 773-A
Records Administration (EDWS)
J. W. Amoroso, 999-W
C. J. Bannochie, 773-42A
J. M. Bricker, 704-27S
D. R. Click, 773-A
T. L. Fellinger, 704-26S
A. Samadi-Dezfouli
J. M. Gillam, 766-H
B. A. Hamm, 766-H
E. W. Holtzscheiter, 704-15S
J. F. Iaukea, 704-30S
P. R. Jackson, DOE-SR, 703-46A
V. Jain, 704-30A
M. T. Keefer, 766-H
D. C. Koopman, 999-W
M. A. Rios-Armstrong, 241-156A
D. W. McIlmoyle, 766-H
T. A. Le, 766-H
J. E. Occhipinti, 704-S
J. M. Pareizs, 773-A
D. K. Peeler, 999-W
J. W. Ray, 704-S
H. B. Shah, 766-H
D. C. Sherburne, 704-S
A. V. Staub, 704-27S
M. E. Stone, 999-W
K. H. Subramanian, 766-H
J. R. Zamecnik, 999-W